EXCITATION OF LOW FREQUENCY TURBULENCE ALONG AURORAL FIELD LINES

by

JAY ROBERT JOHNSON

B.A. Physics, Math, University of Colorado

(1987)

SUBMITTED TO THE DEPARTMENT OF PHYSICS
IN PARTIAL FULFILLMENT OF THE REQUIREMENTS
FOR THE DEGREE OF
DOCTORATE OF PHILOSOPHY IN PHYSICS

at the

MASSACHUSETTS INSTITUTE OF TECHNOLOGY

June, 1992

Signature of Author.......   ⸺..........................
                                                            Department of Physics
            ⸱   ⸱   ⸺   May, 1992

Certified by ....┌────────────────────────┬─────────────────────────..........
            /   Tom Chang, Director
                                       Center for Theoretical Geo/Cosmo Plasma Physics
                                                            Thesis Supervisor

Accepted by.....................⸜   ....
                                                 George F. Koster, Chairman
                                 Graduate Commitee
                                                            Department of Physics

EXCITATION OF LOW FREQUENCY TURBULENCE
ALONG AURORAL FIELD LINES

by Jay Robert Johnson

Submitted to the Department of Physics
in Partial Fulfillment of the Requirements
for the degree of
Doctorate of Philosophy in Physics
May 15, 1992

Abstract

The resonant interaction of low frequency turbulence with oxygen ions has provided a satisfactory explanation for the formation of ion conics at auroral altitudes. These waves, found along closed field lines which emanate from the central plasma sheet, energize ionospheric oxygen to magnetospheric energies and thus provide a major release mechanism for ionospheric oxygen. Although the source of the turbulence is not particularly clear, it is apparently not co–located with ion heating. We have suggested that the turbulence may originate in the equatorial region. Waves generated at frequencies both above and below the equatorial hydrogen cyclotron frequency propagate along field lines to auroral altitudes where they provide substantial ion heating. At low altitudes, where the waves resonant with oxygen, parallel gradients in the magnetic field couple the two propagating cold plasma modes so that right-hand polarized waves exchange energy with the left-hand polarized mode (and vice versa). We determine the transmission coefficients associated with this coupling process analytically by implementing a phase–integral analysis. Moreover, we substantiate these calculations using a numerical technique which involves analytic continuation of the solutions into the complex plane. We determine that wave power generated in the equatorial region of the central plasma sheet contributes substantially to ion heating at auroral altitudes.

Thesis Supervisor: Tom Chang
Title: Director, Center for Theoretical Geoplasma Physics

TABLE OF CONTENTS

CHAPTER 1

INTRODUCTION

I. Ion Conics—Remarkable Agreement with Theory

One of the more interesting phenomena observed in the space environment is the outflow of heavy, gravitationally bound ions from the ionosphere into the magnetosphere. This upflow of ions has been inferred from measurements of ion beams and conics—ions which seem to lie on a cone in velocity space [Klumpar et al., 1986; Burch, 1988]. Conic formation may be easily understood qualitatively in terms of adiabatic folding of perpendicular velocity into parallel velocity in the presence of a parallel magnetic field gradient given an appropriate heating source—typically some form of wave activity which energizes ions through wave-particle interactions [Chang and Coppi, 1981; Crew and Chang, 1989; Lysak, 1986]. One particular variety of conic which has provided remarkable confirmation of theory is that which is observed along closed field lines which emanate from the auroral region into the central plasma sheet (CPS) [Chang et al., 1986]. These conics are generally observed in association with a broadband spectrum of downcoming waves which peaks at low frequencies (Pc1 i.e. $0.2 < f < 5$ Hz) and contains substantial wave energies at the local oxygen cyclotron frequency [Gurnett et al., 1984]. A typical electric field spectral density observation of these waves (which we shall refer to as turbulence) is shown in Figure 1.1. Such wave spectra are observed all along magnetic field lines up to $4R_E$ in
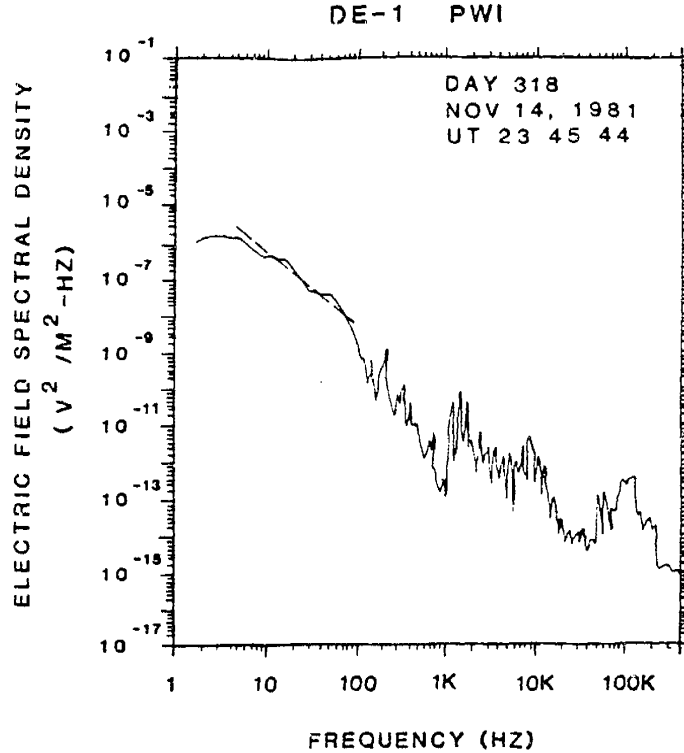
Figure 1.1. Typical electric field spectral density in the central plasma sheet (L = $2.0R_E$) [Chang et al., 1986], courtesy of Gurnett and Mellott.

altitude [Gurnett et al., 1984]. One might naturally suspect that the left-hand circularly polarized (LHCP) component of the observed spectrum might resonate with the ions, thus providing the necessary mechanism for energizing the particles.

In order to understand the relationship between the ions and the broadband electromagnetic spectrum, Chang et al. [1986] considered the behavior of a generic ion situated in an ambient magnetic field, B, under the influence of these waves. For resonant interaction, the net increase of the velocity vector $v_\perp$ in the time δt is

$$\delta v_\perp = \frac{q E_\perp}{m} \delta t \qquad (1.1)$$

where $E_\perp$ is the perpendicular component of the wave electric field in the LHCP mode (the effects of the fluctuating magnetic field are negligible provided that the particle velocities are much smaller than the Alfvèn speed). The net increase in the perpendicular energy of the ion in the time δt is

$$\delta W_\perp = \frac{1}{2}m(v_\perp + \delta v_\perp)^2 - \frac{1}{2}mv_\perp^2 = m\,v_\perp \cdot \delta v_\perp + \frac{1}{2}m(\delta v_\perp)^2 \qquad (1.2)$$

For a gyrotropic ensemble of identical ions, we will find that for each generic ion with velocity $v_\perp$ there is always another ion with equal and opposite velocity $-v_\perp$ so that the first term on the right hand side of equation (1.2) cancels for the two ions. Then for each generic pair of ions the net incremental increase of $W_\perp$ is

$$\delta W_{\perp,res} = \frac{1}{2}\frac{q^2 E_\perp^2}{m}(\delta t)^2 \qquad (1.3)$$

We may relate the perpendicular component of the resonant electric field to the observed wave electric field spectral density at the local cyclotron resonance, $\eta\Sigma^{res}(l)\delta f = E_\perp^2$, for the bandwidth, δf, where η is the fraction of LHCP and l is the field line coordinate. The spectrum is smooth enough near the local gyrofrequency and the Doppler shift small enough to be ignored so that we may rearrange (1.3) to estimate the net heating rate

$$\dot{W}_{\perp,res} = \eta q^2 \Sigma^{res}(l)\delta f\,\delta t/2m \qquad (1.4)$$

where a dot denotes time differentiation. Because the actual spectrum is sufficiently broad in frequency that the resonance time is limited by the correlation time of the incoherent electric field at frequencies near the local gyrofrequency, in effect

$\delta f/\delta t \sim 1$, the heating rate takes the simple form

$$\dot{W}_{\perp,res} = \eta q^2 \Sigma^{res}(l)/2m \tag{1.5}$$

As the ion moves adiabatically along the field line it continues to resonate with that part of the spectral density near the gyrofrequency so that this expression applies continuously. In the guiding center approximation, the evolution for the mean particle motions are

$$\dot{W}_{\perp} = W_{\perp} v_{\parallel} d\ln B/dl + \dot{W}_{\perp,res}$$
$$m\dot{v}_{\parallel} = qE_{\parallel} - W_{\perp} d\ln B/dl \tag{1.6}$$

where $v_{\parallel}$ is the parallel component of the velocity and $E_{\parallel}$ is the field aligned electric field. The effect of the broadband spectrum, then, is to energize the particles in the perpendicular direction. Moreover, the parallel velocity adiabatically increases in the direction of decreasing field strength at the expense of this increasing perpendicular energy. Hence, when a population of particles is enveloped by a broadband electromagnetic field, the particles are energized and flow upwards along the field lines in the form of conics. These results are, of course, obtainable using more rigorous quasilinear arguments [Sagdeev and Galeev, 1969].

When the observations are compared rigorously with this theory there is remarkable agreement [Retterer et al., 1987; Chang et al., 1988; Crew and Chang, 1988; Crew et al., 1990]. The observed distributions may be obtained starting with a thermal distribution at ionospheric altitudes. The particles are allowed to evolve according to a Monte Carlo model in which the particle orbits are periodically perturbed by the
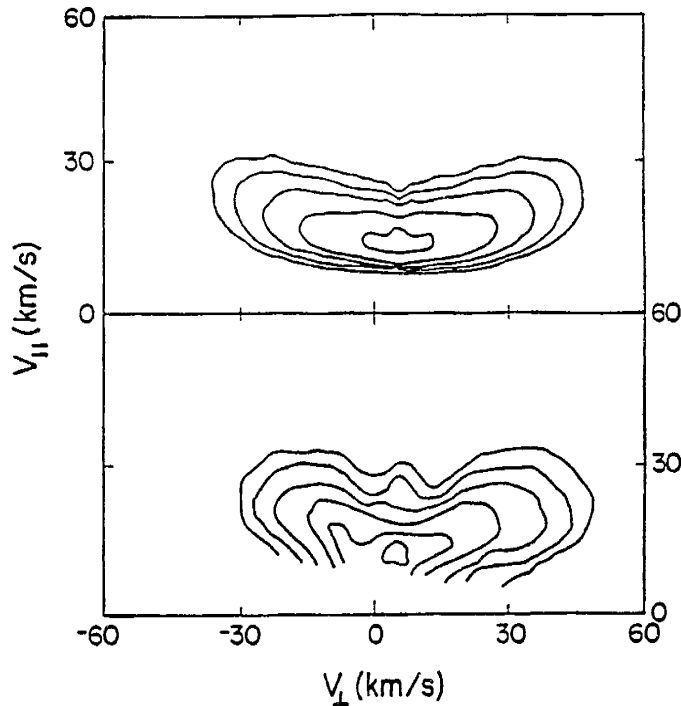
Figure 1.2. The top panel is the result cf a Monte Carlo calculation for the day 81318 oxygen-dominated conic obtained with the HAPI instrument which is displayed in the bottom panel. The contours in both panels are uniformly spaced with an increment of 0.4 in the logarithm of the phase space density.

observed electric field spectral intensity. In Figure 1.2 we show the results of such a Monte Carlo simulation. The upper panel is the result of a Monte Carlo model which is to be compared with the observed ion conic distribution displayed in the lower panel. The results of the Monte Carlo simulation are in remarkable agreement with the observations [Retterer et al., 1987]. The most striking aspect of this calculation is that only one free parameter was required, namely the fraction of LHCP in the spectrum (about 10 percent was sufficient). It is also interesting that the power law nature of the electric field spectrum gives rise to certain scale invariance in the kinetic equations. As a result, the shape of the ion distribution remains the same at all altitudes

along the field line, although the velocities rescale [Chang *et al.*, 1988; Crew and Chang, 1988]. In sum, when the observations are compared rigorously with theory there is remarkable agreement. Nevertheless, certain fundamental questions remain unanswered.

II. Unanswered Questions

Although the mechanism by which the conics are formed seems to be well understood, the origin and nature of the ambient turbulence remain uncertain. Because these conics are observed in a rather quiet region of the magnetosphere the existence of a local source is questionable. Indeed, all of the careful scrutiny of the data to date has failed to reveal the presence of any such source [Chang *et al.*, 1986; Gurnett *et al.*, 1984]. Electron beams and field aligned currents, which in fact do give rise to waves associated with conics in other regions of the magnetosphere, are rather sporadic in both intensity and direction and are therefore an unlikely candidate for the source of the turbulence. Moreover, because these low-frequency waves are Alfvèn-like as the observations suggest [Gurnett *et al.*, 1984], it would be natural to identify them with a large structure which could sustain waves of reasonably long wavelength (the Alfvèn wavelength is of order Earth radii). At present, no such structures have been identified. These considerations strongly suggest that a more global non-local analysis is required to explain the presence of turbulence observed at auroral altitudes. Such an analysis will not only provide important information regarding the nature of the waves, but will also be a significant step towards understanding the coupling between the

magnetosphere and ionosphere.

There are several areas of uncertainty in our present understanding of the nature of the auroral turbulence. In particular, in our theory of ion-cyclotron resonance heated conics, we assumed that a particular portion of the electric field spectrum was LHCP and could therefore contribute to ion conic heating [Chang *et al.*, 1986; Retterer *et al.*, 1987]. It is therefore important to understand the polarization of the observed waves and to determine the fraction of wave energy that will be absorbed near the oxygen resonance.

In light of these questions, we intend to construct a detailed model to explain the origin of the auroral turbulence. Because the magnetosphere is, of course, a very dynamic system with much free energy available to excite all manner of instability, it is not unlikely that the spectrum actually consists of a collage of waves emanating from a number of source regions which could give rise to the observed broadband spectrum. In particular, we will find that energetic distributions of particles in the equatorial region of the central plasma sheet give rise to a variety of instabilities which can generate waves. Having identified a promising source for waves, we will consider the evolution of the waves using a ray tracing analysis. We will find that waves generated in the equatorial region do propagate into the region where ion heating occurs along field lines ranging from 2-5 or more R_E.

Once we have determined that waves are accessible to the auroral region, we will address fundamental questions concerning the nature of the turbulence. In particu-

lar, we will solve the full wave equations near the oxygen resonance, and from these solutions we will determine a definite absorption. In addition, ion-cyclotron waves which are transmitted through an evanescent region will be strongly damped by the thermal component of oxygen. In solving the wave equations near the resonance, we will necessarily address a fundamental phenomenon of basic plasma physics, namely that of the behavior of waves near a minority ion resonance. Our discussion will be such that our method and results may be easily applied to other similar fundamental problems associated with a plasma with several ion species.

In summary, having considered the fundamental questions detailed above, we will have provided a plausible scenario which would explain the origin of the auroral turbulence, and we will have also addressed the relationship between ion heating and the behavior of waves in a plasma medium near a minority resonance.

CHAPTER 2

EQUATORIAL SOURCE OF WAVES

I. Wave Observations

The low frequency, broadband waves (see Figure 1.1) which have been associated with the particular ion conic events described in the previous chapter have been observed continuously across auroral latitudes at radial distances up to 2 R_E [Gurnett et al., 1984] with the DE 1 wave instrument. Other wave measurements at higher altitudes have been associated with similar ion conic events [Crew et al., 1990 and references therein]. The observations seem to indicate that the waves are observed at all latitudes and at longitudes for which data is available. Gurnett et al. [1984] found much support for the notion that the turbulence was electromagnetic and that the waves observed were Alfvèn-like. Because the ratio of the magnetic field to the electric field could be obtained, it was possible to determine the index of refraction for these waves. This data strongly suggested that the waves were were compatible with an Alfvènic rather than an electrostatic model. The polarization of the waves, however, was not determined in this instance. The data from similar broadband waves observed in other regions of the magnetosphere seem to indicate that such waves exhibit varying polarizations ranging anywhere between right-hand polarization (RHCP) to left-hand polarization (LHCP) [Andrè et al., 1990]. These observations would seem to suggest that it is more than likely that both ion-cyclotron and magnetosonic Alfvèn

waves are present. A somewhat more revealing observation was that the Poynting flux, when measurable, was directed earthward [Gurnett et al., 1984]. Although no single mode probably accounts for all of the observations, the modes are apparently constrained to originate at higher altitudes than the observations in the absence of a local source.

Although a subject of debate, careful scrutiny of the data suggests a non-local source [Gurnett et al., 1984; Chang et al., 1986]. As previously mentioned, the lack of correlation between the sporadically observed beams and field aligned currents suggests that the waves are not generated by beams or currents—a major source of turbulence in other regions of the magnetosphere. One might on the other hand suggest that the highly unstable ion conic distributions themselves generate the waves. It should be noted, however, that the ions which are predominately observed are oxygen, and the only source for this oxygen is the ionosphere. Moreover, cold oxygen is gravitationally bound to ionospheric altitudes within a few hundred kilometers of the Earth's surface. The most reasonable mechanism for accelerating the oxygen to magnetospheric energies is the wave-particle interaction discussed in Chapter 1, particularly in light of the absence of strong field aligned potential drops in the central plasma sheet (CPS). Certainly ion conic distributions do excite waves as they relax from their highly anisotropic state; however, the ion conics are observed along field lines up to at least 4 R_E and continue to become more energetic as they are drawn up higher into the magnetosphere [Crew et al., 1990]. Without the waves in the first place, the ions could not be heated to magnetospheric energies. Moreover, if the waves are Alfvènic

as the observations indicate [Gurnett *et al.*, 1984], the local wavelengths are on the order of Earth radii. The size of a local source should probably be the order of the wavelength in which case one might question any suggestion that the waves originating from small scale shears [Ganguli *et al.*, 1985] or higher latitude instabilities associated with electron precipitation [Ashour-Abdalla *et al.*, 1981; Winglee *et al.*, 1987]. We therefore direct our attention to a non-local source for waves observed along field lines which emanate into the CPS.

II. Waves Observations in the Equatorial Region of the CPS

Because the auroral turbulence is observed to have a Poynting flux directed downward along field lines, we are naturally led to look for a source at a higher altitude along that field line. Indeed, the equatorial region of the central plasma sheet contains much free energy in the form of unstable ion distributions. Anisotropic ion distributions are often observed in the nightside equatorial region at geosynchronous orbit [Perraut *et al.*, 1982]. As ions are injected earthward from the magnetotail, they drift adiabatically about the Earth along drift shells. Because the shell on which a particle is constrained to move depends on the equatorial pitch angle, initially isotropic distribution functions tend to develop thermal anisotropies ($T_\perp > T_\parallel$) and acquire anomalous loss cones (significantly enlarged over the ionospheric 3° ionospheric loss cone) [Ashour-Abdalla and Cowley, 1974; Sibeck *et al*, 1987]. In addition, observations reveal that these distributions often contain a large energetic population with 90 degree pitch angle (somewhat like a ring-beam) [Perraut *et al.*, 1982]. Moreover the

proton gyrofrequency near geosynchronous orbit matches the oxygen cyclotron frequency over the range where ion heating occurs. Because anisotropic distributions excite waves near the proton gyrofrequency, both above and below, we have suggested that much or the observed auroral turbulence originates in the equatorial region [Johnson et al., 1989]. Indeed, the observation that waves detected by ground based instruments often have signatures of waves observed to be generated in the equatorial region [Perraut et al., 1984] substantiates such a claim.

Ion distributions with loss-cones or temperature anisotropies excite waves below the proton gyrofrequency [Oscarsson and Andre, 1986]. Indeed, such instabilities have been studied comprehensively in the equatorial region in connection with Pc1 ($0.2 < f < 5$ Hz) wave generation and helium heating [Young et al., 1981]. Waves generated with frequencies below the helium gyrofrequency (typically < 1 Hz) are guided along field lines to the ground [Rauch and Roux, 1982; Perraut et al., 1984]. On the other hand, it is believed that waves generated above the helium gyrofrequency but below the hydrogen cyclotron frequency ($1 < f < 5$ Hz), rather than penetrating directly to the ground, travel between geomagnetic conjugate points near the magnetic equator which correspond to the ion-ion or Buchsbaum frequency. Although the growth rates for these waves are smaller than those for the waves near the helium gyrofrequency, the power in the waves may be comparable because they amplify as they bounce back and forth through the equatorial plane [Rauch and Roux, 1982]. Furthermore, when the concentration of helium is low enough, these waves tunnel through the reflection layer to lower altitudes in the right hand circularly polarized (RHCP) mode (see Figure 6 of

Perraut *et al.* [1984]). In fact, ground based instruments often detect both types of waves. We have therefore suggested that these waves contribute to the auroral turbulence [Johnson *et al.*, 1989].

Propagating waves generated below $f_{cH^+}^{eq}$ may explain a significant part of the wave power observed at auroral altitudes, but much of the wave power has $f > 5$ Hz. Because some of the heating takes place at lower altitudes where the local oxygen cyclotron frequency is larger than Pc1 frequencies it is important to consider the generation and propagation of waves with $f > f_{cH^+}^{eq}$ in the equatorial region. Observations indicate that ion distributions with loss-cone character ($\partial F/\partial v_\perp > 0$) can generate waves at multiples of $f_{cH^+}^{eq}$ [Perraut *et al.*, 1982]. We have investigated instabilities which might arise in such a plasma environment by solving the dispersion relation of linear waves using the WHAMP code [Rönnmark, 1982a,b]. The WHAMP code solves the dispersion relation for a plasma consisting of several species with Maxwellian thermal distributions. By carefully adding and subtracting Maxwellian distributions, we can construct an ion distribution function which retains the characteristics of the observed equatorial distribution function—an enlarged loss cone and a large energetic population with 90 degree pitch angle. Using the WHAMP code, we have found that in addition to electrostatic ion cyclotron harmonic waves, a broad band of oblique electromagnetic modes arises with slightly smaller growth rate [Johnson *et al.*, 1989]. In Figure 2.1 we plot the dispersion surface of the real frequency in a two dimensional wave vector space, and in addition, we indicate the growth rates for this particular mode with shading. The surface corresponds to the magnetosonic-whistler mode, and waves are
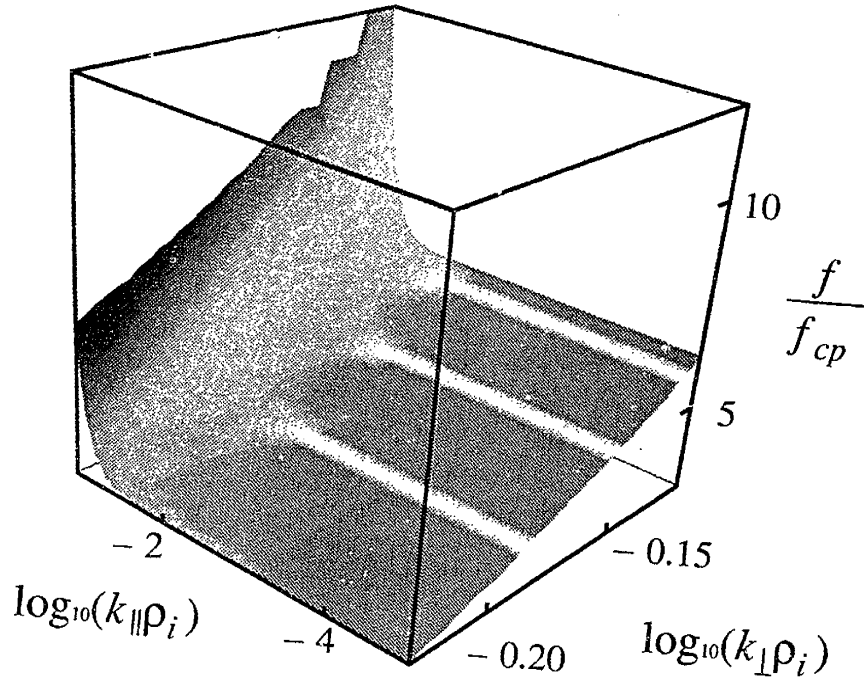
Figure 2.1. Dispersion relation (ω vs. $\log_{10}(k_{\perp}\rho_i)$, $\log_{10}(k_{\parallel}\rho_i)$ where ρ_i is the ion gyroradius) for a sum of Maxwellian distributions which mimic the observations. Shading indicates the growth rates (white for growing, dark for damping) for waves on the surface. Notice that electrostatic waves are generated at multiples of f_{cH^+} which are largest at $k_{\parallel} = 0$ whereas the waves at larger $k_{\parallel}$ tend to be electromagnetic and occupy a much larger region of k-space.

generated at harmonics of the proton gyrofrequency. In Figure 2.2, we take a slice through one of the harmonic bands in Figure 2.1 at fixed $k_{\perp}$. We have plotted one curve which corresponds to maximum growth at $k_{\parallel} = 0$ and another curve slightly offset from the first curve. This figure illustrates that although the maximum growth may be for modes which are electrostatic and propagate perpendicular to the magnetic field, modes with comparable growth rate and group velocity $v_{g\parallel}/v_{g\perp} \sim 1$ are also significant and initially propagate out of the equatorial region. The spatial growth for these modes may be estimated from γ/v_g where v_g is the group velocity (approxi-

$$-- \log_{10}(k_\perp \rho_i) = -0.804 \quad -- \log_{10}(k_\perp \rho_i) = -0.800$$
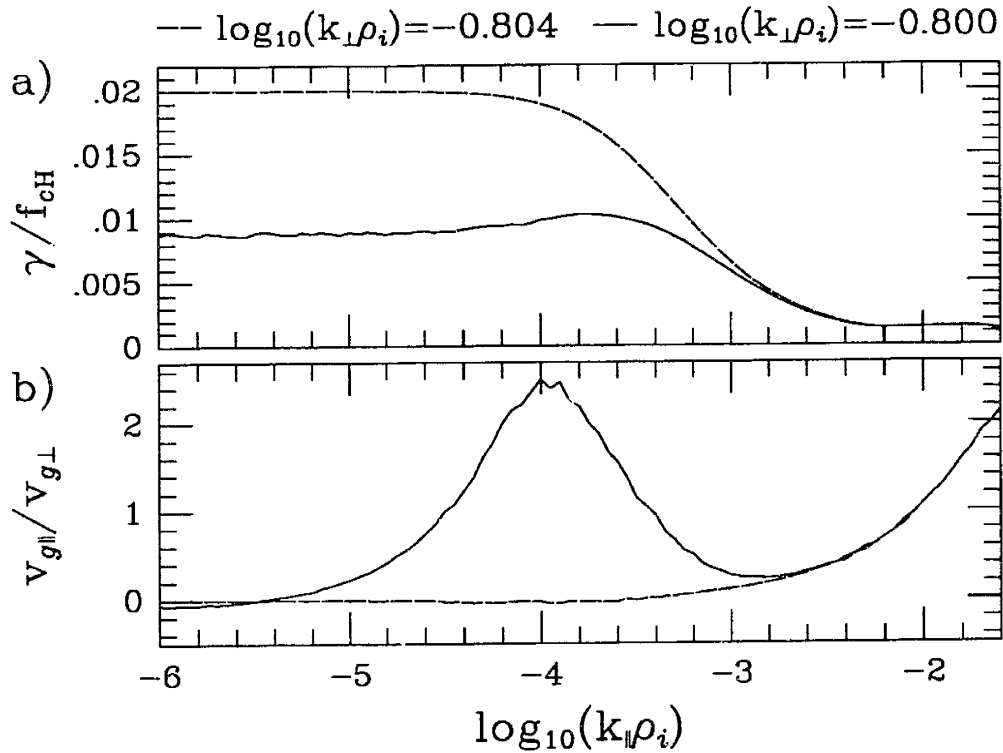

Figure 2.2. Growth rates (a) and group velocity ratio r (b) for a plasma with parameters listed in Table I. The curves are taken at constant $k_\perp \rho_i$ where ρ_i is the ion gyroradius. The dashed curve corresponds to maximum growth for $k_\parallel = 0$ modes near the fourth harmonic of the proton gyrofrequency with κ. The solid curve corresponds to modes with $\log_{10}(k_\perp \rho_i) = -0.800$ which are slightly offset from maximum growth at $k_\parallel = 0$. It is to be noted that these modes have a slightly smaller growth rate, but they also have $v_{g\parallel}/v_{g\perp} > 1$.

mately the Alfvèn velocity). In this case the e-folding distance is the order of $1/10\ R_E$ which is reasonably small compared to the region throughout which the waves grow. Indeed, the observations indicate that waves are generated within a wedge the order of $10°$ with respect to the equatorial plane (that is, the order of R_E) [Young et al., 1981].

If we compare the power in the equatorial and auroral waves using the observed wave amplitudes, we may determine whether the free energy in the equatorial region is a viable source for the turbulence. With the assumptions that the auroral waves are essentially Alfvèn waves and that the WHAMP results accurately reflect the

relationship between the observed magnetic field and the electric field in the equatorial region, we find that the Poynting fluxes are comparable. Clearly if the Poynting flux was substantially less than that flux observed at lower altitudes there would be reason to doubt the relationship between equatorially generated waves and the auroral turbulence. Although detailed ray tracing calculations will be required to confirm the notion that the auroral turbulence originates in the equatorial plane, this simple comparison elicits some confidence.

III. Summary

The low frequency waves observed at auroral altitudes are associated with a downward Poynting flux. In the absence of a local source, we have identified a plausible non-local source for these waves. The equatorial region in the central plasma sheet is characterized by much free energy which gives rise to instabilities along both the ion-cyclotron and magnetosonic branches of the dispersion relation. In the following chapters we will investigate the intricacies involved in determining the accessibility of these equatorial waves to the auroral region.

CHAPTER 3

BASIC CONSIDERATIONS

I. Approach

Having thus identified waves excited in the equatorial region of the magneto-
sphere with frequencies near the local hydrogen gyrofrequency as a plausible source
for the turbulence observed at auroral altitudes, we now turn our attention to the more
relevant questions of whether these waves are, in fact, accessible to lower altitudes
and, if they are, how much wave power will be available to heat ions. In order to get
useful answers to these questions, we must carefully understand the details of the
medium in which the waves propagate and incorporate the relevant aspects into our
analysis.

In a reasonably uniform medium (such as the magnetosphere) wave propagation
is best described in terms of the WKB analysis. In this approach, wave propagation is
described in terms of the evolution of a wave packet which propagates in space
according to the local group velocity while satisfying the local dispersion relation
[Lighthill, 1978; Swanson, 1989]. As a wave packet evolves, it follows a definite tra-
jectory in space and momentum known as a ray. The evolution of an initial wave
packet is described by tracing the position and momentum of the packet along a ray.

In certain regions, however, simple ray tracing does not adequately describe wave propagation. Such is the case near cutoffs where the wavelength of the disturbance typically exceeds the scale length of the relevant plasma parameters, such as density or magnetic field. In addition, the linear dispersion relation occasionally admits two propagating modes with the same frequency and wavelength. When this is the case, mode conversion may occur and the two branches of the dispersion relation exchange energy. Plasma resonances also involve linear mode conversion to some extent. As we consider how waves propagate from regions where the local gyrofrequency matches the hydrogen cyclotron frequency to regions where it matches the oxygen gyrofrequency, we will find that the analysis involves a set of regions where the WKB analysis is adequate and a set of regions which must be analyzed separately from the crude WKB approximation. In regions where the WKB approximations are inadequate, we will carefully solve a suitable approximation of the full wave equations both numerically and analytically. Moreover, the wave equations fail most dramatically in the region where ion heating takes place. Therefore, by carefully solving the wave equations near the cyclotron resonance, we will also obtain information pertaining to ion heating.

II. Dispersion Relations

In order to understand wave propagation and the important mode-conversion processes involved in the present analysis, it is important to understand the relevant dispersion relations. In the crudest approximation, we can ignore all ion species

except hydrogen, which is the dominant species above ionospheric altitudes. In this case, the dispersion relation consists of two modes—the magnetosonic and shear Alfvèn modes, a.k.a. ion-cyclotron waves [Stix, 1962]. These modes remain uncoupled and propagate independently according to the ray equations. At frequencies near the oxygen cyclotron frequency, such an approximation fails to adequately describe wave propagation. Indeed, the topology of the dispersion surfaces changes dramatically with the inclusion of a secondary ion species [Smith and Brice, 1964; Gurnett *et al.*, 1965]. Figures 3.1 and 3.2 contrast the difference between the propagating modes with the inclusion of a heavy ion species (in this case helium). It should be noted that similar effects appear if particles have the same mass but different ionization. For such a plasma, waves near the ion gyrofrequencies are characterized by five important frequencies: the two ion gyrofrequencies, Ω_{c1}, Ω_{c2}; the cutoff frequency, ω_{co}; the crossover frequency, ω_{cr}; and the ion-ion hybrid frequency, ω_{ii}, where

$$\omega_{co} = \frac{n_1\Omega_{c2} + n_2\Omega_{c1}}{n_1 + n_2} \tag{3.1}$$

$$\omega_{cr}^2 = \frac{n_1\Omega_{c2}^2 + n_2\Omega_{c1}^2}{n_1 + n_2} \tag{3.2}$$

$$\omega_{ii}^2 = \omega_{co}\frac{\Omega_{c1}\Omega_{c2}(n_1 + n_2)}{n_1\Omega_{c1} + n_2\Omega_{c2}} \, . \tag{3.3}$$

The structure of the dispersion equations is readily apparent from their algebraic form. In a cold plasma it is well known [Stix, 1962] that for low frequencies the solu-

tions to the dispersion relation are of the form

$$N_{\|\pm}^2 = \frac{R+L}{2} - \frac{N_\perp^2}{2} \pm \left[\left(\frac{R-L}{2} \right)^2 + \frac{N_\perp^4}{4} \right]^{1/2} \tag{3.4}$$

where $N_\|$ and $N_\perp$ are the indices of refraction with respect to the magnetic field and the functions R and L are defined by Stix

$$R = 1 - \sum_s \frac{\omega_{ps}^2}{\omega^2} \frac{\omega}{\omega + \Omega_s} \tag{3.5}$$

$$L = 1 - \sum_s \frac{\omega_{ps}^2}{\omega^2} \frac{\omega}{\omega - \Omega_s} \quad . \tag{3.6}$$

where ω_{ps} and Ω_s are the plasma and cyclotron frequencies for each species s. In the low frequency limit it is most convenient to rescale these indices to the Alfvèn velocity

$$\frac{c^2}{v_A^2} = \sum_{species} \frac{4\pi n_s m_s}{B^2} \tag{3.7}$$

rather than the speed of light. Then the dispersion equation takes the form

$$n_\pm^2 = \frac{r+l}{2} - \frac{\kappa^2}{2} \pm \left[(\frac{r-l}{2})^2 + \frac{\kappa^4}{4} \right]^{1/2} \tag{3.8}$$

where

$$n = N_\| \frac{v_A}{c} \quad , \qquad \kappa = N_\perp \frac{v_A}{c} \tag{3.9}$$

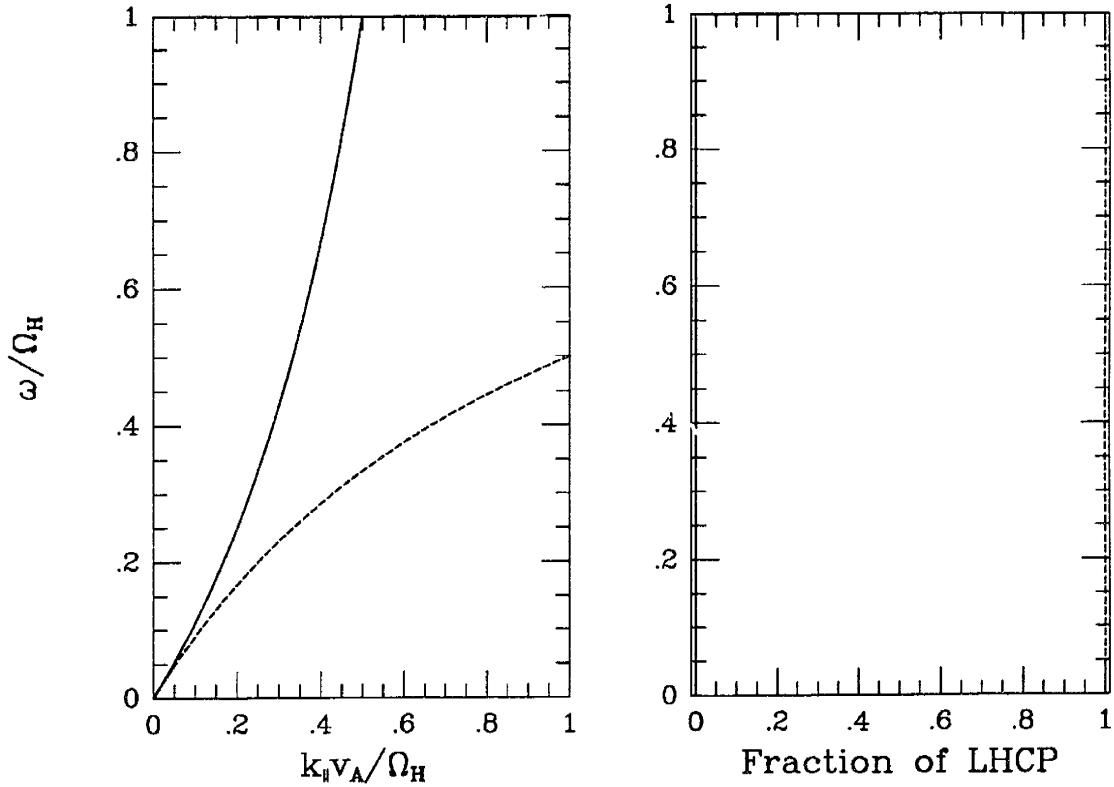and for a two species plasma the analogue of equations (3.5, 3.6) are the normalized

Figure 3.1. Dispersion relation for a cold single ion plasma, with with perpendicular wavevector κ held fixed (κ=0). On the right is the fraction of left-hand circular polarization as a function of frequency.

Stix functions

$$\frac{r}{l} = \pm \frac{\Omega_{c1}\Omega_{c2}}{\omega_{co}} \frac{(\omega \pm \omega_{co})}{(\omega \pm \Omega_{c1})(\omega \pm \Omega_{c2})}$$

(3.10)

The relevance of ion-ion hybrid frequency, ω_{ii} is nested in the sum function

$$s = \frac{r+l}{2} = -\frac{\Omega_{c1}^2\Omega_{c2}^2}{\omega_{ii}^2} \frac{(\omega^2 - \omega_{ii}^2)}{(\omega^2 - \Omega_{c1}^2)(\omega^2 - \Omega_{c2}^2)}$$
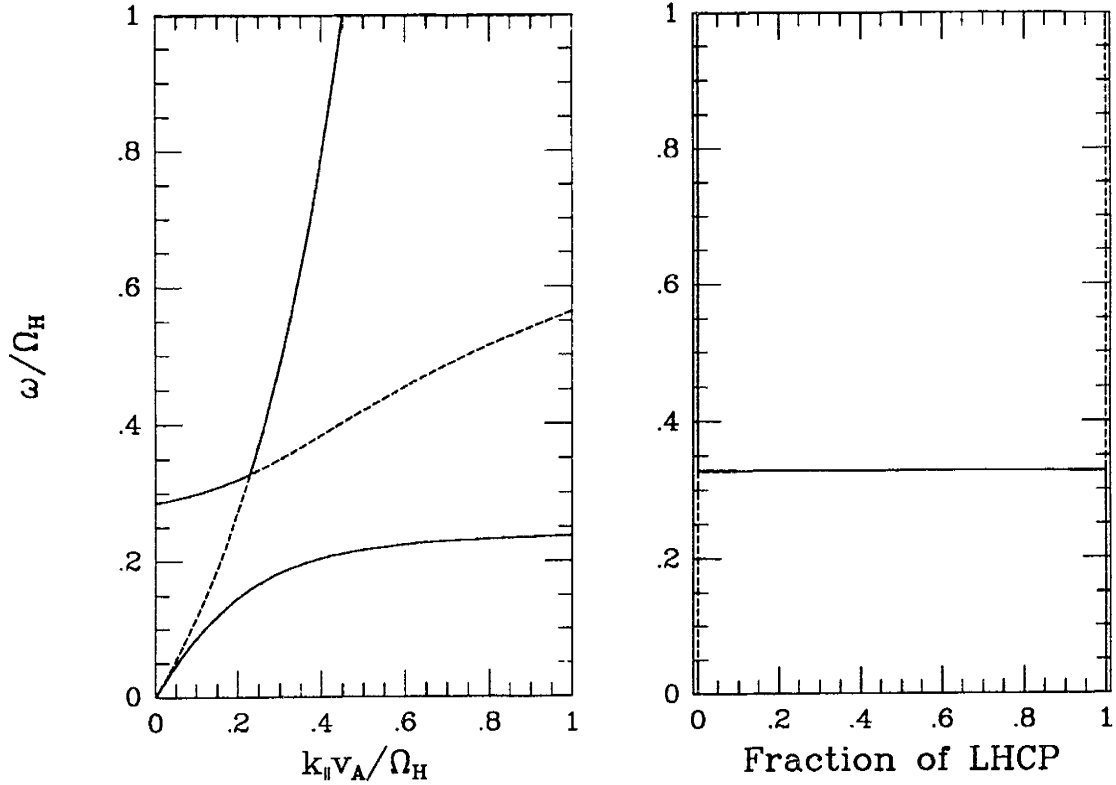
(3.11)

Figure 3.2. Dispersion relation for a cold, two ion species plasma with mass ratio four and density ratio about 0.05 (minority species is the heavy ion). Here we plot frequency vs. wavevector and frequency vs. fraction of LHCP at fixed κ ($\kappa=0$).

while the relevance of the crossover frequency, ω_{cr}, is manifest in the difference function

$$ d = \frac{r-l}{2} = \frac{\Omega_{c1}\Omega_{c2}}{\omega_{co}} \frac{\omega(\omega^2-\omega_{cr}^2)}{(\omega^2-\Omega_{c1}^2)(\omega^2-\Omega_{c2}^2)} \ . \tag{3.12} $$

It is then evident from equation (3.8) that for parallel propagation ($\kappa=0$) the indices reduce to r and l. The mode r remains well behaved and remains virtually independent of the minority ion species. The mode l, on the other hand, is characterized by two resonances and a cutoff. It is also to be noted that the two modes coalesce when
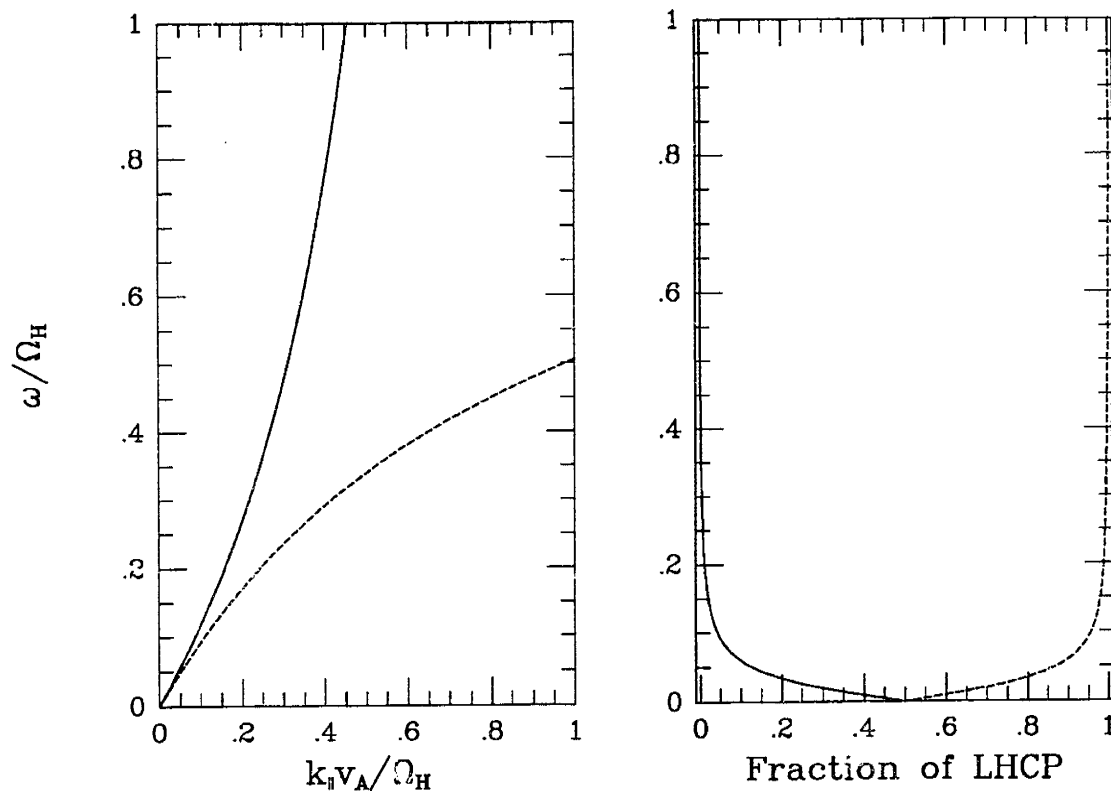
Figure 3.3. Dispersion relation for a cold single ion species. Here we plot frequency vs. wavevector and frequency vs. fraction of LHCP at fixed κ (κ=0.3).

d=0 at the crossover frequency. The importance of ω_{ii} arises for perpendicular propagation ($\kappa \gg d$) in which case the mode n_+ has a cutoff at $s \rightarrow 0$.

In Figures 3.1-8 we plot frequency vs. parallel wave vector at fixed perpendicular wave vector, and in addition we plot the fraction of left-hand circular polarization (LHCP) for the various modes at each frequency. We can make a number of relevant observations concerning the case of two ion species. For nearly parallel propagation the two modes are either strictly right-hand circularly polarized (RHCP) or LHCP, and they cross at the crossover frequency. The LHCP mode resonates with ions at the ion gyrofrequencies and has a cutoff at the cutoff frequency. For non-parallel propagation,
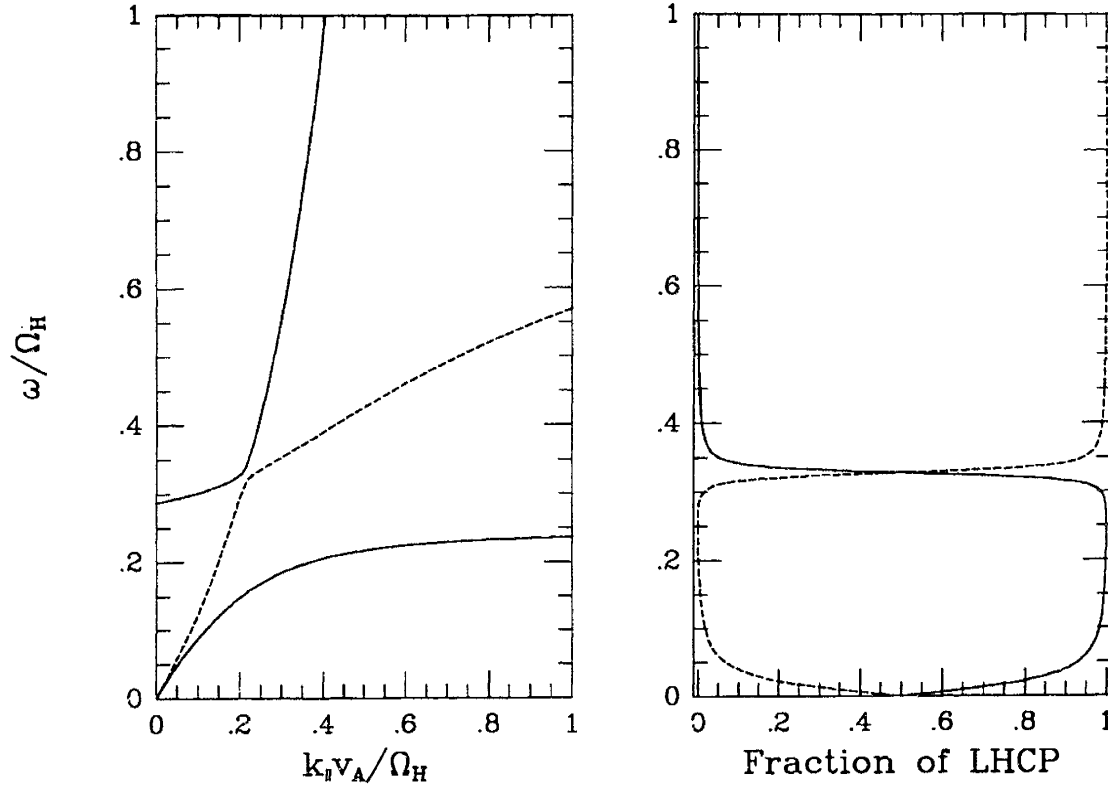
Figure 3.4. Dispersion relation for a cold two ion species plasma. Here we plot frequency vs. wavevector and frequency vs. fraction of LHCP at fixed κ (κ=0.3).

the two modes couple near the crossover frequency so that they no longer cross, and the predominately RHCP mode becomes predominately LHCP across this frequency. For larger angles of propagation the two modes separate substantially, and the magnetosonic mode is cutoff near the lower hybrid frequency

$$\omega_{lh}^2 = |\Omega_{ce}| |\Omega_{cH}| \left[\frac{\omega_{pe}^2 + |\Omega_{ce}| |\Omega_{cH}|}{\omega_{pe}^2 + \Omega_{ce}^2} \right] \tag{3.13}$$

(well above the hydrogen gyrofrequency) so that the only relevant modes are the two downgoing ion-cyclotron branches which have resonances at the two ion gyrofrequen-
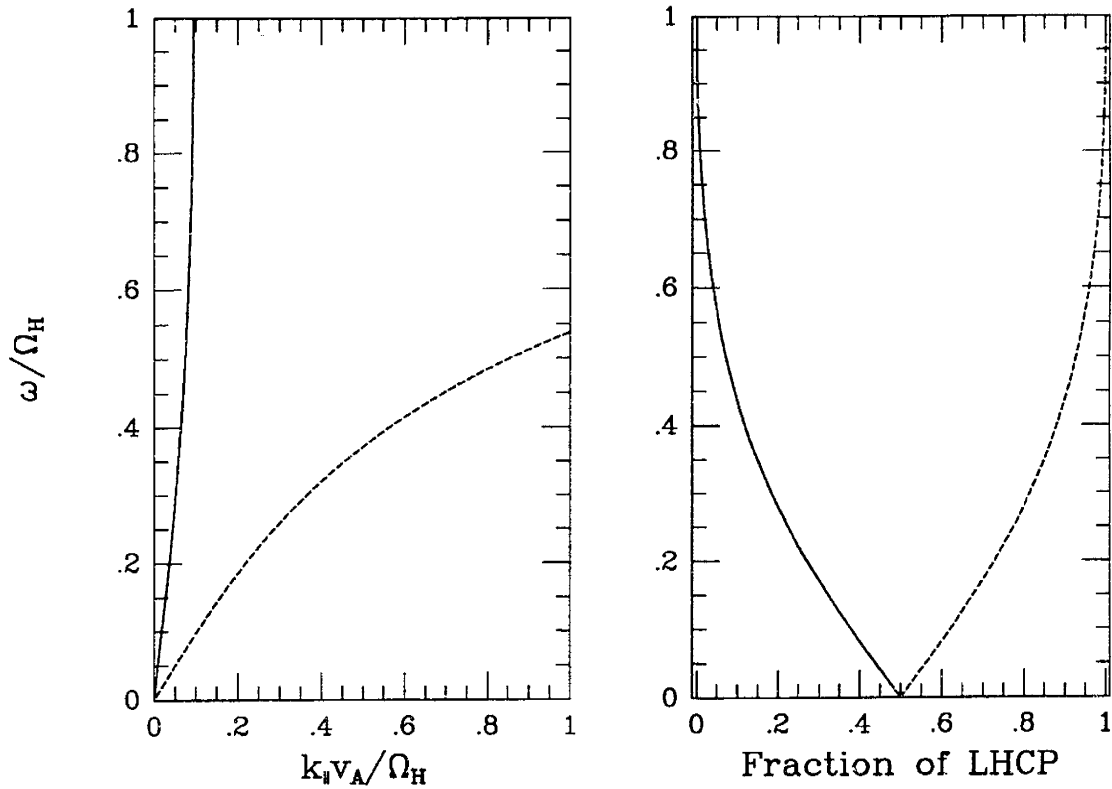
Figure 3.5. Dispersion relation for a cold single ion plasma. Here we plot frequency vs. wavevector and frequency vs. fraction of LHCP at fixed κ (κ=0.9).

cies as shown in Figure 3.8. The mode which is asymptotic to the hydrogen gyrofrequency has a lower cutoff which increases from zero frequency to the ion-ion hybrid frequency as κ increases. For perpendicular propagation, the cutoff is for this mode is the ion-ion hybrid frequency, and a small gap exists between this mode and the mode which is asymptotic to the heavy ion gyrofrequency.

III. Consequences of Dispersion Relations

We may draw a number of conclusions relevant to our analysis from these dispersion relations. First of all, it is clear that the presence of the minority species is
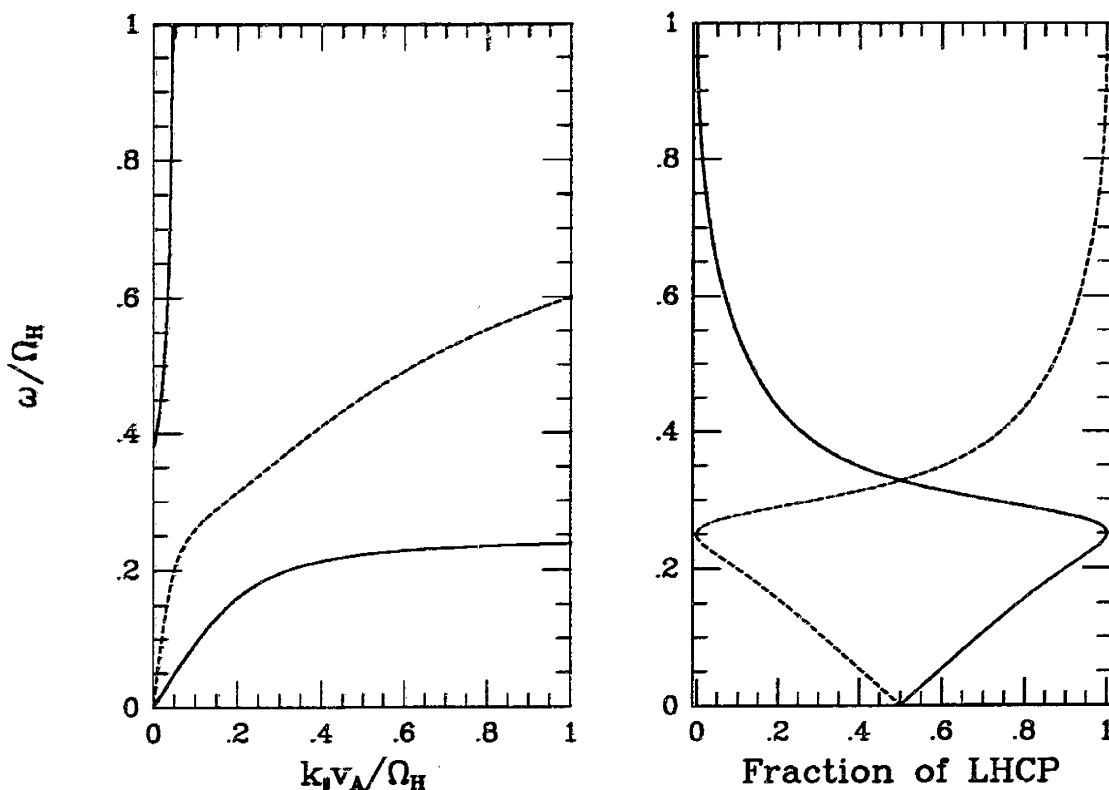
Figure 3.6. Dispersion relation for a cold two ion species plasma. Here we plot frequency vs. wavevector and frequency vs. fraction of LHCP at fixed κ (κ=0.9).

important only near the heavy ion gyrofrequency. As an important consequence, any analysis at frequencies not near the minority cyclotron frequencies need not include the presence of minor species. Thus, in considering the propagation of waves we may, for example, concentrate on the more important aspects of the problem such as field line curvature and density gradients.

A second, more disturbing, implication of the dispersion relation is that even if waves do propagate to regions where their frequencies match the heavy ion gyrofrequency, e.g. from equatorial to auroral regions, there are a number of obstacles in the way of ion heating. Most notably, if ions are incident on the magnetosonic branch at
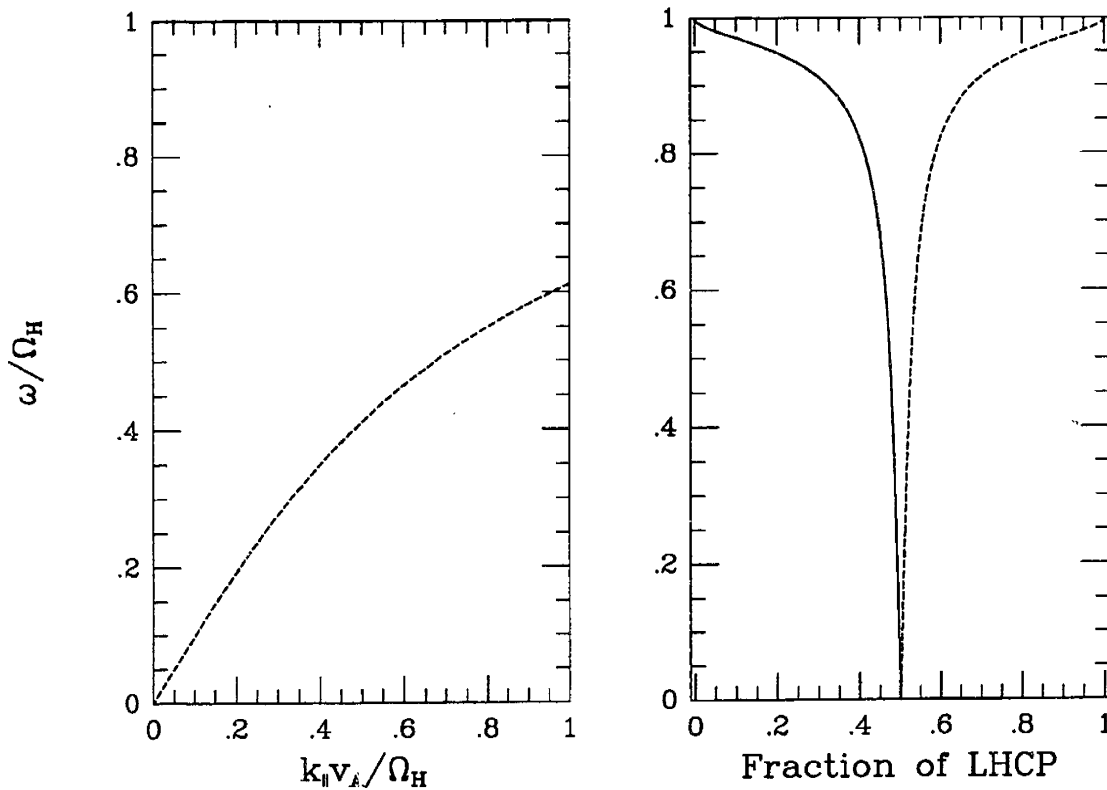
Figure 3.7. Dispersion relation for a cold single ion plasma. Here we plot frequency vs. wavevector and frequency vs. fraction of LHCP at fixed K (K=5.0).

the hydrogen cyclotron frequency, then they will propagate to a point where their frequency matches the local cutoff frequency and be reflected before they can reach altitudes where they can heat ions.

Waves incident on the LHCP ion cyclotron branch appear to have a more profound deficiency. Although they would appear to be accessible to lower altitudes, at the local heavy ion cyclotron frequency they are completely RHCP. However, the heating rate was shown to be directly proportional to the fraction of LHCP. This then means that heating along this branch could only result from thermal effects or via Doppler shift. The plasma in this region is not particularly thermal, so one would
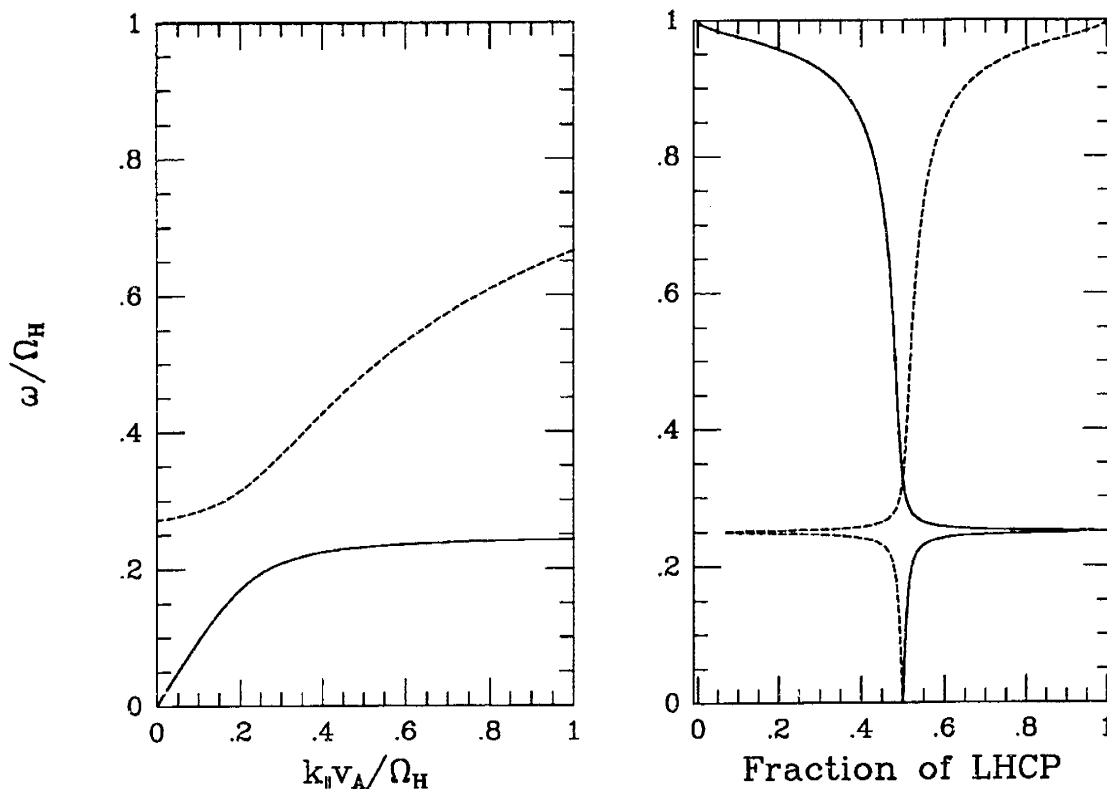
Figure 3.8. Dispersion relation for a cold two ion species plasma. Here we plot frequency vs. wavevector and frequency vs. fraction of LHCP at fixed K (K=5.0).

expect the heating resulting from these waves to be small.

Another salient feature is that for large angle of propagation (large κ) the ion cyclotron wave develops a "gap" or "stop band" between the ion-ion hybrid (Buchsbaum) frequency and the heavy ion resonance. Therefore, in order for perpendicularly propagating ion-cyclotron waves to heat ions, they must tunnel through an evanescent region.

Finally, it is important to note that near the crossover-cutoff-resonance triplet the dispersion relation is not valid and we would expect substantial coupling between the

modes leading perhaps to some absorption and some tunneling to the LHCP ion-cyclotron branch which may then heat ions.

IV. Determination of Accessibility and Heating

After considering the cold plasma dispersion relation it seems clear that the question of wave accessibility to the auroral region naturally lends itself to a twofold analysis. First we shall consider wave propagation from the equatorial region using the well known ray-equations. Presumably, a sizable fraction of these waves will be guided earthward. At some point the waves will encounter a localized region in space where the WKB analysis is no longer valid. In this case we shall solve the electric field equations to determine the behavior of the electric fields across this region. The appropriate boundary conditions will, of course, be the WKB solutions.

It is to be noted that although the equatorial and auroral regions contain much free energy available in the form of unstable distribution functions, the intervening region through which waves propagate in order to reach auroral altitudes (the central plasma sheet) is relatively quiet. In this intervening region, thermal effects are not significant, and the dispersion properties are reasonably described in terms of a cold plasma model. The ray-racing equations therefore imply that energy is conserved, and the fraction of waves which finally reach the auroral region is primarily determined from the behavior of the waves near the heavy ion gyrofrequency where the WKB approximation is inadequate. In the following chapters we will explore whether waves propagate to auroral altitudes using the WKB approximation when applicable. In

regions where the WKB approximation is not appropriate, we will determine the

amount of wave power apportioned in each mode by solving a suitable approximation

of the full wave equations.

CHAPTER 4

RAY TRACING

I. General Theory

In homogeneous media, the solutions to Maxwell's equations are simply plane waves. Such waves are best described in terms of a phase function, $k \cdot x - \omega t$, which remains constant along a wavefront. The wave may then be visualized as a wavefront which travels at a phase velocity, $\frac{\omega}{k}$. In an inhomogeneous medium in which variations in the typical scale lengths of the medium far exceed that of the local wavelength, the waves are best described in terms of eikonals or the WKB approximation [Weinberg, 1962; Stix, 1962; Lighthill, 1978; Swanson, 1989]. In this approach, a wave packet of frequency ω, localized in wavevector and space, then behaves locally as a plane wave while its position and spectrum change according to the ray equations

$$\frac{d\mathbf{x}}{dt} = \frac{\partial \omega}{\partial \mathbf{k}} \tag{4.1}$$

which is the group velocity, and

$$\frac{d\mathbf{k}}{dt} = -\frac{\partial \omega}{\partial \mathbf{x}} \tag{4.2}$$

This represents a simple Hamiltonian system describing the conservation of ω which, in the absence of dissipation, implies conservation of energy.

Ray Tracing

In a plasma, the local properties of the medium are best described by the Fourier transform of Maxwell's equations which takes the form $D_{ij}E_j = 0$ where D_{ij} is the the Dispersion function and E_j is the electric field. The local properties of the medium are then contained in the function $D = \det(D_{ij}) = 0$ which relates the frequency, ω, wavevector, $\mathbf{k}$, and the local values of various quantities at the position $\mathbf{x}$. In a plasma system with an imposed zeroth order magnetic field, it is easiest to evaluate the dispersion equation in a coordinate system in which the magnetic field specifies a preferred direction. In this case, the dispersion relation is of the form,

$$D \ (k_\perp, k_\parallel, \mathbf{x}, \omega) = 0 \tag{4.3}$$

where $k_\parallel = \mathbf{k} \cdot \mathbf{b}$ and $k_\perp = \sqrt{k^2 - k_\parallel^2}$ and $\mathbf{b}$ is the unit vector of the magnetic field. The ray-tracing equations expressed in terms of the dispersion function are then simply

$$\frac{d\mathbf{x}}{dt} = \frac{\partial \omega}{\partial \mathbf{k}} = -\frac{\dfrac{\partial D}{\partial \mathbf{k}}}{\dfrac{\partial D}{\partial \omega}} \tag{4.4}$$

$$\frac{d\mathbf{k}}{dt} = -\frac{\partial \omega}{\partial \mathbf{x}} = \frac{\dfrac{\partial D}{\partial \mathbf{x}}}{\dfrac{\partial D}{\partial \omega}} \tag{4.5}$$

The derivatives of the dispersion function may be expressed in terms of the natural variables, $k_\parallel$, $k_\perp$, $\mathbf{x}$, and ω to be

$$\frac{\partial D}{\partial k_j} = \frac{\partial D}{\partial k_\perp} \frac{(k_j - k_\parallel b_j)}{k_\perp} + \frac{\partial D}{\partial k_\parallel} b_j \tag{4.6}$$

$$\frac{\partial D}{\partial x_j} = \frac{\partial D}{\partial x_j} + \left[\frac{\partial D}{\partial k_\parallel} - \frac{k_\parallel}{k_\perp} \frac{\partial D}{\partial k_\parallel} \right] k_i \frac{\partial b_i}{\partial x_j} \qquad (4.7)$$

where the summation convention is used. The effects of field line curvature are manifest in the last term of Eqn (4.7). Alternatively, we can express the curvature term as

$$k_i \frac{\partial b_i}{\partial x_j} = (k_i - k_\parallel b_i) \frac{1}{B} \frac{\partial B_i}{\partial x_j} = \mathbf{k}_\perp \cdot \mathbb{L}_B^{-1} \qquad (4.8)$$

where $\mathbb{L}_B^{-1}$ is the magnetic scale length tensor. The magnetic field magnitude scale length, L_B, is also simply related to this tensor

$$L_B^{-1} \equiv \frac{1}{B} \frac{\partial B}{\partial x_j} = \mathbf{b} \cdot \mathbb{L}_B^{-1} \qquad (4.9)$$

The above equations adequately describe the evolution of waves in a medium in which the scale length of the relevant plasma quantities is much longer than that of the local wavelet. The details of wave propagation are thus contained in the form of the dispersion function, D which we will now consider.

II. Specific Model

The Central Plasma Sheet (CPS) is a quiescent region characterized by an absence of free energy when compared with the auroral or equatorial regions. Streaming electron beams and field aligned currents which characterize the auroral region are conspicuously absent, and particle distributions in the CPS are more stable than those found in the equatorial region. In the CPS, typical cold ions might have gyroradii the order of meters, and even the most energetic ions might at best have gyroradii the

order of kilometers. In contrast, local wavelengths for low frequency Alfvèn waves tend to be on the order of tens or even hundreds of kilometers. Hence, thermal effects are negligible (except near the resonances which we will not consider using the WKB approximation), and the medium is best described using a cold plasma model.

For a cold plasma, the dispersion relation is well known to be of the form

$$D = \det \begin{vmatrix} S - N_{\parallel}^2 & -iD & N_{\parallel}N_{\perp} \\ iD & S - N^2 & 0 \\ N_{\parallel}N_{\perp} & 0 & P - N_{\perp}^2 \end{vmatrix} \qquad (4.10)$$

where the functions S, D, and P defined by Stix [1962] are

$$S = 1 - \sum_s \frac{\omega_{ps}^2}{\omega^2 - \Omega_s^2} \qquad (4.11)$$

$$D = \sum_s \frac{\Omega_s \omega_{ps}^2}{\omega^2 - \Omega_s^2} \qquad (4.12)$$

$$P = 1 - \sum_s \frac{\omega_{ps}^2}{\omega^2} \qquad (4.13)$$

Here N is the index of refraction, kc/ω, with directions defined with respect to the magnetic field, and the local properties are manifest in the plasma frequency, $\omega_{ps}^2 = 4\pi q_s^2 n_s(x)/m_s$ and gyrofrequency, $\Omega_s = q_s B(x)/m_s c$, for each species s. Clearly wave propagation is then determined entirely by the density and magnetic field models relevant to the region of propagation, and Eqn (4.7) may then be expressed explicitly in terms of the magnetic scale length vectors and the density scale length

$$L_{n_s}^{-1} \equiv \frac{1}{n_s}\frac{\partial n_s}{\partial \mathbf{x}}$$ (4.14)

to be

$$\frac{\partial D}{\partial \mathbf{x}} = \left[\frac{\partial D}{\partial k_\parallel} - \frac{k_\parallel}{k_\perp}\frac{\partial D}{\partial k_\parallel}\right]\mathbf{k_\perp} \cdot \mathbb{I}_B^{-1} + \sum_s \omega_{ps}^2 \frac{\partial D}{\partial \omega_{ps}^2}\mathbf{L}_{n_s}^{-1} + \sum_s \Omega_s \frac{\partial D}{\partial \Omega_s}\mathbf{L}_B^{-1}$$ (4.15)

The magnetic field of the Earth is to first approximation a dipole. As the solar wind flows past the Earth, however, the field is stretched and distorted into an elongated tail-like configuration which can be rather dynamic: superquiet, quiet, disturbed, superdisturbed. The magnetic field has been carefully classified empirically by, for example, Mead and Fairfield [1975]. Nevertheless, within 7 or 8 L of the Earth, where L is the equatorial crossing of a particular magnetic field line in Earth radii (that field line is referred to as an "L-shell") a dipole field adequately describes the Earth's magnetic field. For our present purposes, then, it seems reasonable to model the magnetic field as a dipole with

$$\mathbf{B} = B_0 \frac{3\hat{z}\cdot\hat{r}\hat{r}-\hat{z}}{r^3}$$ (4.16)

where r is measured in Earth radii and B_0 = 0.35 gauss is the approximate field strength at equatorial latitudes near the Earth.

The density profile, on the other hand, remains somewhat more uncertain. As discussed by Moore et al. [1987], the only reliable data for low energy "core" plasma at present is in regions of high density such as the plasmasphere. Measurements of electron density appear to be more reliable and at least give reasonable estimates of the

cold ion density although no information concerning the proportion of species can be known for certain. Most measurements of ion composition instead concentrate on energetic ion populations which are easier to measure and are perhaps more interesting in that they provide evidence in the perennial question of the origin of thermal plasma—"from the solar wind or the ionosphere?". However, it is apparent that these thermal populations throughout most of the region of interest constitute less than 1 percent of ion species [Olsen et al., 1987; Strangeway et al., 1986], and such information is not particularly useful except for understanding instabilities associated with the origin of waves. The most striking feature of the density profile is, of course, the existence of a plasmapause around 4.5 R_E. Plasma measurements although somewhat uncertain seem to indicate plasma falloff as r^{-p}, where $p \sim 3\text{-}4$ near the Earth, that is, within the plasmasphere (although closer to the Earth there is an apparent trough of decreased density) [Moore et al., 1987; Olsen et al., 1987; and references therein]. At the edge of the plasmasphere, the plasma density falls off exponentially from the plasma density in the plasmasphere to the plasma density in the central plasma sheet. Except near the Earth, the plasma density appears to remain essentially constant along field lines and the abrupt gradients occur mainly across field lines.

In light of these considerations, a natural density model, suitable for a qualitatively correct theoretical analysis, would be a profile in which the density depends primarily on L-shell. Because the waves that are of interest in this analysis interact most strongly with the boundary of the plasmasphere rather than with the plasmasphere itself, it is most convenient to take a model in which density variations inside the

plasmasphere are ignored. An appropriate model for the density is

$$n(x) = \frac{1}{2}(n_{ps} - n_{cps})\left[1 - \tanh\left[\frac{L(x) - L_0}{\alpha}\right]\right] + n_{cps} \qquad (4.17)$$

where n_{ps} is the plasma sphere density, n_{cps} is the central plasma sheet density, L_0 is the L-shell of the plasma pause, and α is the gradient scale length. The L-shell is related to the dipole coordinates through the field line equation

$$L(x) = \frac{r}{\sin^2(\theta)} \qquad (4.18)$$

where θ is the angle with respect to the dipole axis. In Figure 4.1 we plot such a profile for typical values of the parameters. It should be noted that the value of densities in the plasmasphere and plasma sheet, location of the plasmapause, scale length of the density falloff may vary substantially depending on the magnetic activity, i.e. whether there is a substorm or a quiet period. It is, however, fair to say that the qualitative aspects of the density configuration should remain essentially the same [Carpenter and Park, 1973].

III. Qualitative Discussion

The general characteristics of wave propagation in our model may be understood heuristically in terms of the approximate dispersion relations for low frequency waves. For a cold proton-electron plasma two propagating modes exist at low frequencies— shear Alfvèn waves a.k.a. ion-cyclotron waves, and compressional magnetosonic waves. Shear Alfvèn waves are characterized by the approximate dispersion relation
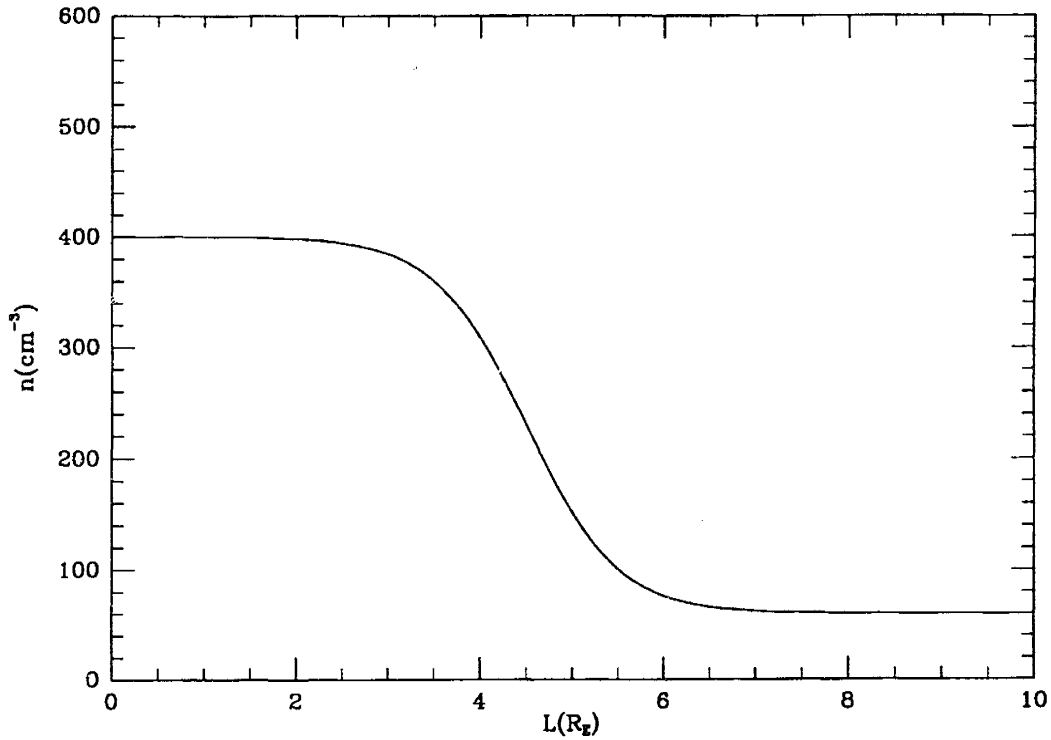
Figure 4.1. Density as a function of L-shell for the density model (4.17). This density profile mimics the plasma falloff at the edge of the plasmasphere. The density is assumed to be constant along each L-shell as shown in Figure 4.2.

$$\omega \approx k_{\|} v_A \tag{4.19}$$

where the Alfvèn velocity varies as $Bn^{-1/2}$. The appropriate ray equations (4.4, 4.5) then take the form

$$\frac{d\mathbf{x}}{dt} = v_A \, \mathbf{b} \tag{4.20}$$

$$\frac{d\mathbf{k}}{dt} = -\omega \left[\mathbf{L}_B^{-1} - \frac{1}{2} \mathbf{L}_n^{-1} \right] \tag{4.21}$$

These equations clearly describe rays which travel along a field line because the group velocity is always along the magnetic field direction, and as they travel along the field

line they refract according to equation (4.21). It should be clear that the waves refract

out of regions of larger magnetic field and into regions of larger density. Thus, as

shear Alfvèn waves propagate earthward, we expect them to remain tied to a field line,

and we expect the direction of the wavevector to be determined by a delicate balance

of the magnetic field and density gradients. It is easy to conceptualize this balance

from Figure 4.1 in which we plot lines of constant magnetic field and lines of constant

density "L-shells." In our model, the density gradient is largest near $L_0 \approx 4.5$. Waves

generated in the equatorial region have $L \gg L_0$ so that we can expect the effects of the
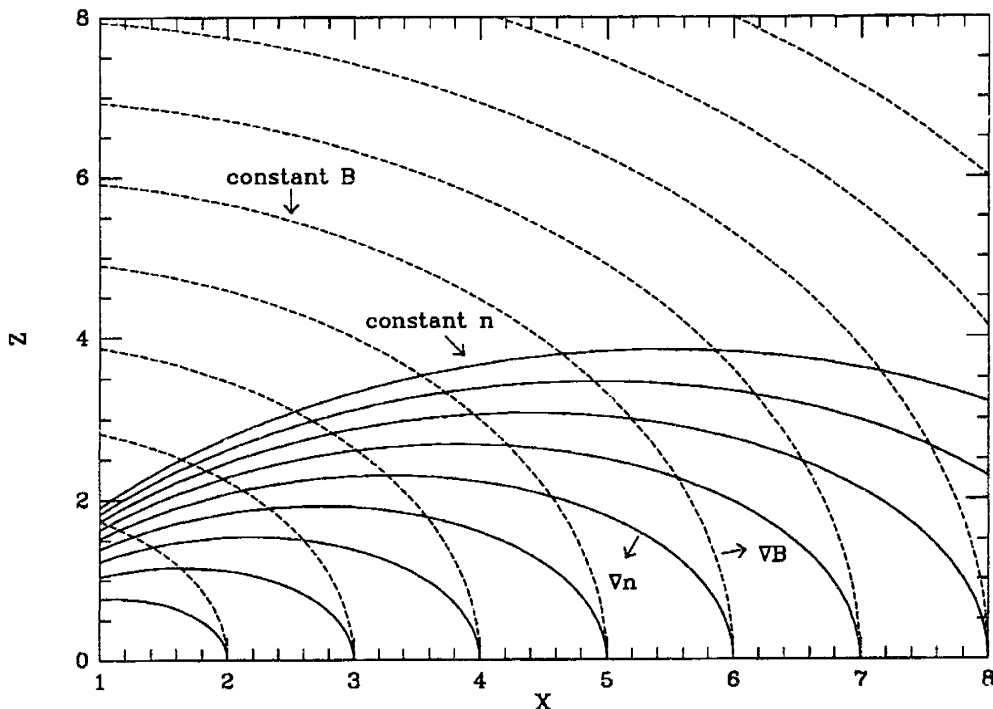
Figure 4.2. Lines of constant density and magnetic field for our model. The z-axis is along the dipole field while the x-axis extends tailward. Density is taken to be constant along magnetic field lines—L-shells. The gradients are perpendicular to the constant surfaces as indicated. The magnetic field gradient tends to expel the waves while the density gradient draws them earthward.

density gradients to be negligible as the waves propagate earthward.

On the other hand, magnetosonic waves obey the approximate dispersion relation

$$\omega \simeq k v_A \qquad (4.22)$$

and the ray equations (4.4, 4.5) are of the form

$$\frac{dx}{dt} = v_A \hat{k} \qquad (4.23)$$

$$\frac{dk}{dt} = -\omega \left[L_B^{-1} - \frac{1}{2} L_n^{-1} \right] \qquad (4.24)$$

In contrast to ion-cyclotron waves, the group velocity of magnetosonic waves is directed along the direction of the wavevector rather than the magnetic field which implies that magnetosonic waves propagate and refract in the same direction. If we ignore density gradients it is clear that magnetosonic waves are repulsed from regions of large magnetic field, in which case it is not possible for those waves to reach auroral altitudes in that they refract tailward and propagate into the region of smaller magnetic field. This behavior can be inferred from Figure 4.2 if we realize that ray trajectories follow magnetic field gradients and propagate perpendicular to surfaces of constant magnetic field. On the other hand, we see that density gradients oppose the magnetic field to some extent everywhere. In particular, the density gradient is directed earthward at the equator and near auroral altitudes the density gradient is directed downward toward the equator. The waves that we have identified in the equatorial region which are generated above the proton gyrofrequency propagate earthward

with wavevector oblique to the magnetic field. These waves may in fact reach the boundary of the plasmasphere in which case the density gradients may balance the magnetic field gradient and essentially "guide" the waves along the edge of the plasmapause boundary to auroral altitudes.

IV. Results

In order to investigate the ray paths of the waves of interest, we solve the ray-tracing equations (4.4, 4.5) numerically using various integration codes. In particular we have used three different integrators based upon the Bulirsch-Stoer, Runge-Kutta and predictor-corrector methods [Press et al., 1986]. The predictor-corrector method is much more efficient in that it requires the least number of function evaluations. The results from all three integrators agree to acceptable precision, and as an additional check, ray paths may be traced backwards to determine the validity of the integration procedure. All results are correct to within acceptable numerical accuracy.

A. LHCP Waves Guided by Magnetic Field

It is well known that LHCP ion-cyclotron waves are guided along field lines as indicated in our heuristic analysis. Indeed, a number of studies have contributed to our understanding of the propagation of this variety of wave along dipolar field lines. The seminal work of Rauch and Roux [1982] clearly demonstrated the guiding effects of the magnetic field on ion-cyclotron waves. In their analysis, they determined that waves of this variety, generated near the helium gyrofrequency or the hydrogen gyrofrequency are guided along field lines. Their results clearly showed that LHCP

waves are accessible to auroral altitudes where they contribute to ion heating. On the other hand, their calculations were inadequate in that the waves that they traced reflected at lower altitudes and thus bounced back and forth between conjugate points in the two hemispheres. The analysis inadequately treated the behavior of the waves at the reflection point near the plasma resonances where mode coupling occurs and substantial wave power tunnels through the "stop gap" which occurs when the wave frequency is the order of the local heavy ion gyrofrequencies. We shall discuss the proper treatment of this problem in detail in the following chapters.

In this section we present a brief review of the predictions of our model, which we expect to be similar to the analysis of Rauch and Roux [1982], and we also discuss and critique some of the recent work concerning tracing of LHCP waves in the area between the plasmapause boundary and the magnetotail.

In the following figures we present ray paths for waves incident in the LHCP mode propagating toward auroral altitudes. In all the figures z is taken to be the coordinate along the dipole axis of the magnetic field while x is taken as an equatorial coordinate. In addition, we also superimpose the field lines to more easily indicate the location of wave packets. Waves are launched in the equatorial region tailward of the plasmapause boundary. The waves propagate earthward to lower altitudes where they presumably contribute to ion-heating. We terminate ray-tracing when the eikonal approximation becomes suspect and/or the presence of multiple ion species becomes important.
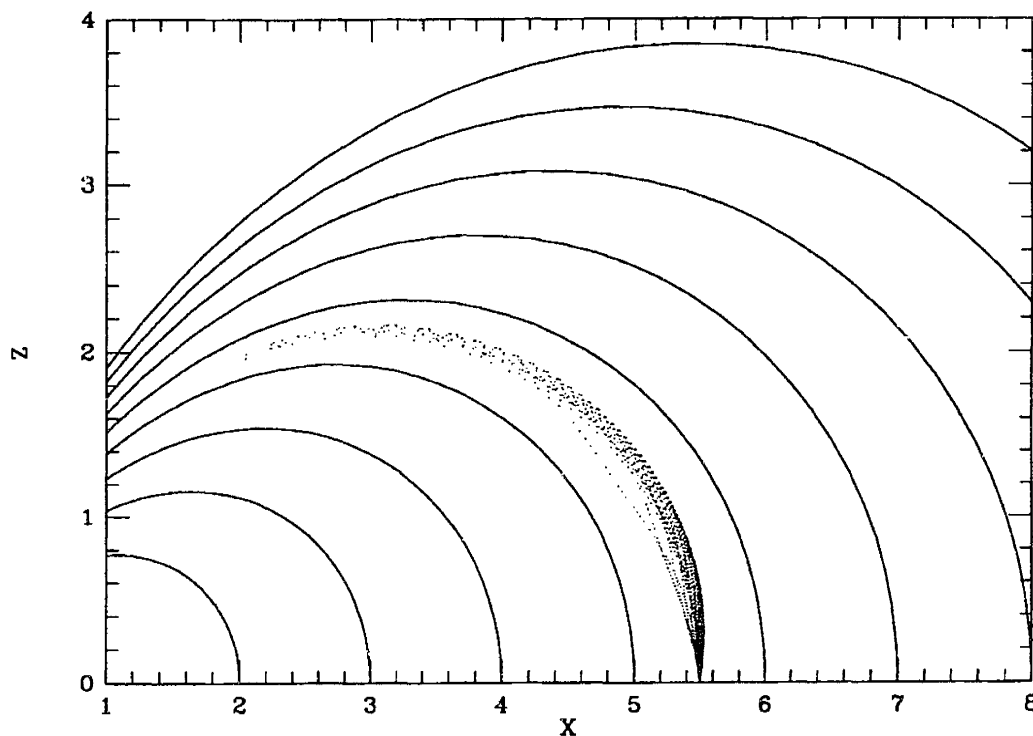
Figure 4.3. Ray paths for ion-cyclotron waves with a constant density model. Wave packets follow rays indicated by dots. The spacing of the dots indicates the velocity of the wave packet along the ray path.

In these figures we plot the paths of waves which originate at a particular location in the equatorial region. In this instance all waves are launched at 5.5 R_E. The paths differ according to the angle of the initial wavevector. We increment the angle of the wavevector with respect to the magnetic field by $\pi/20$ thus investigating all initial wavevectors between ±90 degrees with respect to the magnetic field direction, $\hat{z}$. In Figure 4.3 we have assumed a constant density model and the dipole field model. It is clear that the waves are guided along the field lines to auroral altitudes. Moreover, the spread about the field line resulting from different initial wavevector is negligible. On the other hand, in Figure 4.4, we take the density to fall off according to the model
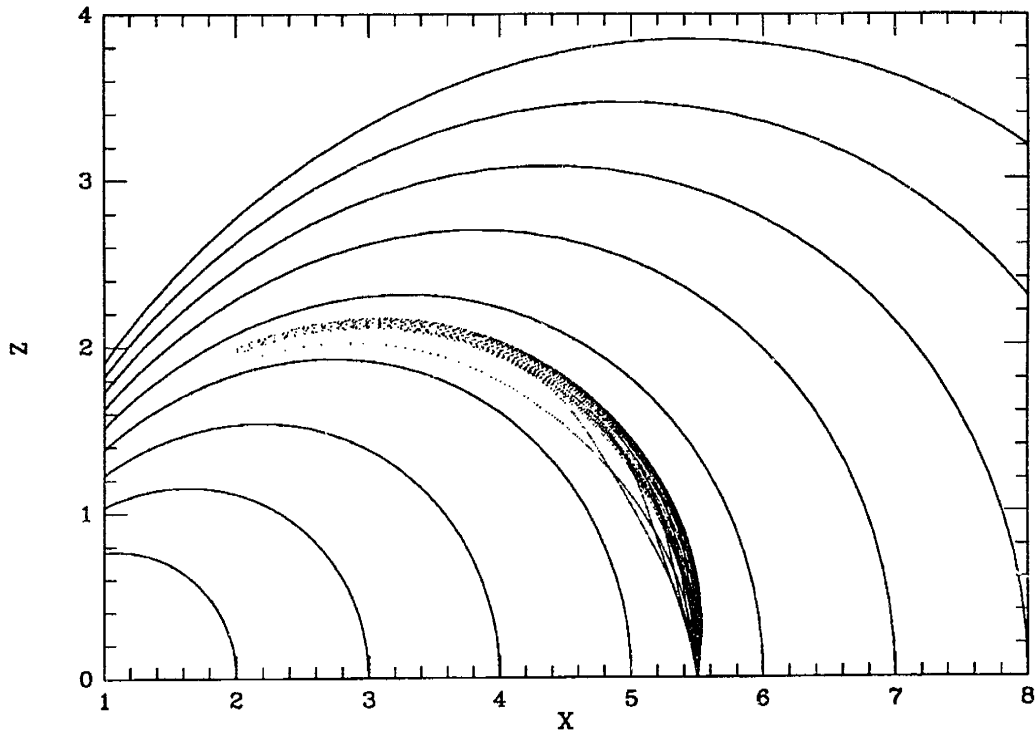
Figure 4.4. Ray paths for ion-cyclotron waves with a density model which mimics the den-
sity gradients at the plasmapause boundary.

given by equation (4.17). We have investigated this model taking as typical ranges for

the parameters [Carpenter and Park, 1973; Moore et al., 1987; Olsen et al., 1987; and

references therein]

$$\alpha = 1\text{--}2$$
$$L_0 = 4\text{--}5$$
$$n_{ps} = 200\text{--}2000 cm^{-3}$$ \hfill (4.25)
$$n_{cps} = 20\text{--}100 cm^{-3}$$

In the case of Figure 4.4 we have taken $\alpha = 2$, $L_0 = 4$, $n_{ps} = 2000$ and $n_{cps} = 60$.

The results are not strongly dependent on these numbers and provide a reasonably

representative qualitative as well as quantitative description of waves incident from the
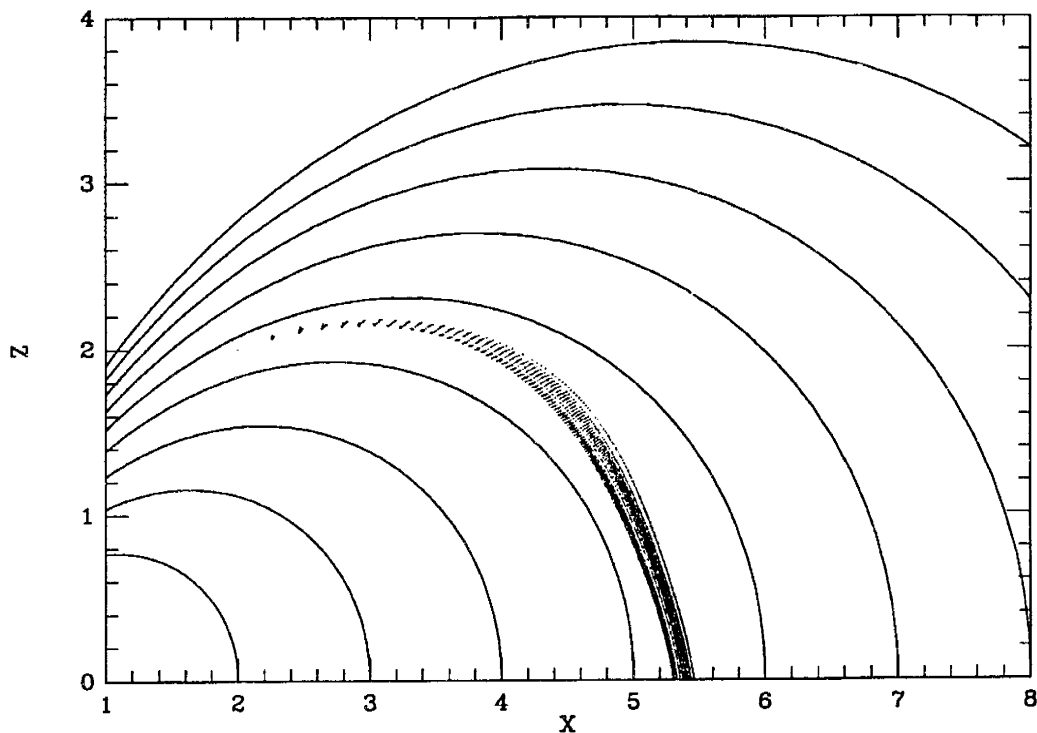
Figure 4.5. Ray paths for ion-cyclotron waves traced backwards from the auroral region. Note that the source for the waves is restricted to a narrow spatial range in the equatorial region.

equatorial region. As is readily apparent, density gradients do not affect the ray path substantially. As expected, the wavevectors refract so that they are more oblique to the magnetic field [Rauch and Roux, 1982]. In Figure 4.5, we trace backward from a point in the auroral region to determine the location of the source for such waves. In this case, initial conditions are specified in the auroral region. As before, we sample all wavevector directions from $\hat{z}$ to $-\hat{z}$. It is clear that the source for LHCP waves is a very localized source tailward of the plasmasphere. From these results it is obvious that LHCP generated in the equatorial region propagate to altitudes where the WKB solutions are inadequate. At these altitudes, we must leave the primitive WKB solu-
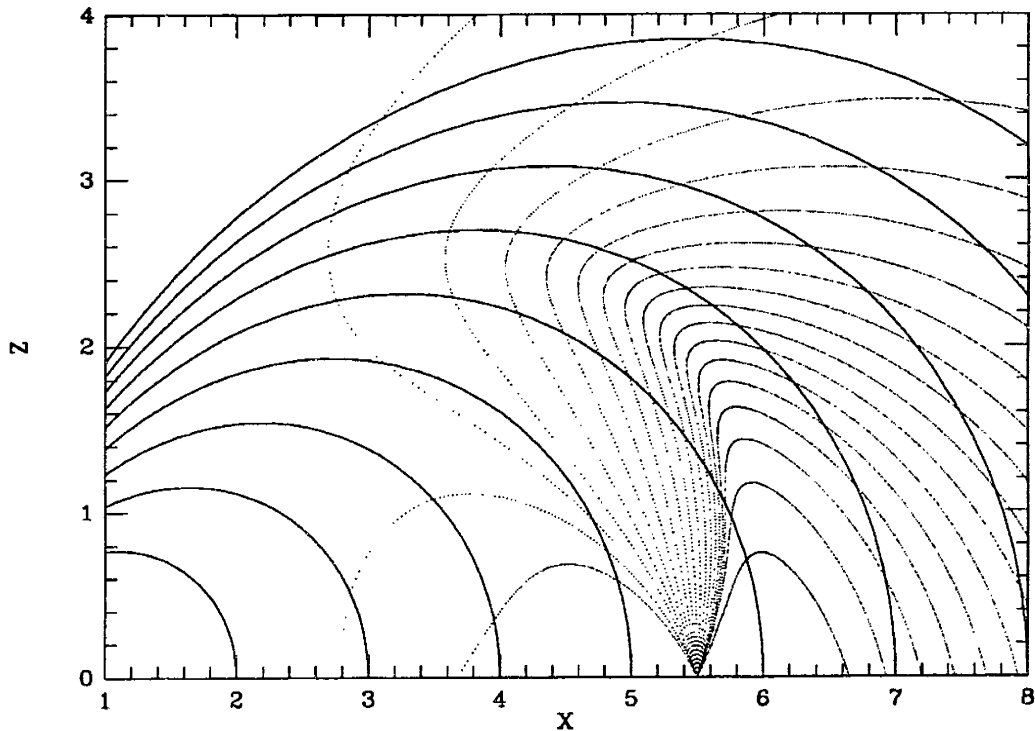
Figure 4.6. Ray paths for magnetosonic waves with a constant density model. The waves are launched at 5.5 Earth radii. Note that the waves tend to be unguided.

tions behind and address the question of accessibility by considering the asymptotic solutions to a suitable approximation to the full wave equations.

In recent work which stems from our suggestion that waves generated in the equatorial region are the source of waves observed at auroral altitudes, Rönnmark and André [1991] have investigated the focusing of waves due to the effects of the converging field line geometry. Their calculation is based upon the conservation of a distribution function of waves from which the spectral density may be obtained. This wave distribution function is conserved along ray paths and thus provides an effective tool for comparing real satellite data at different altitudes along the ray path. They
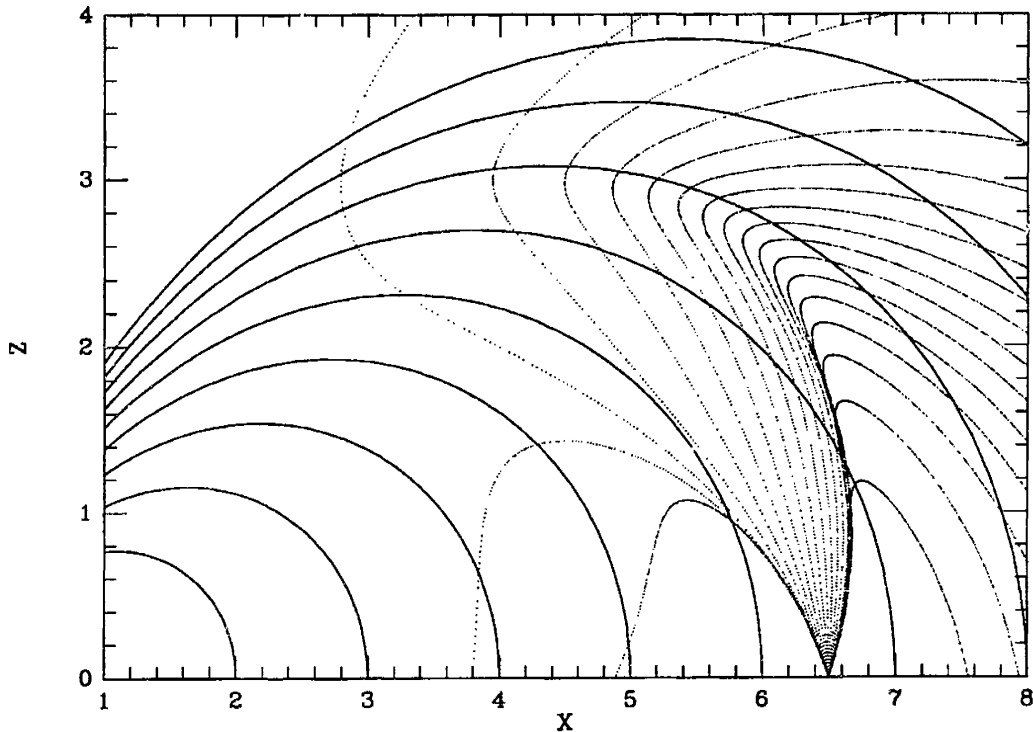
Figure 4.7. Ray paths for magnetosonic waves with a constant density model. The waves are launched at 6.5 Earth radii.

determined that as waves propagate down along field lines that the spectral density increases by a factor of approximately 10.

Numerous other ray-tracing calculations have indicated a similar behavior for LHCP waves in a thermal plasma. Unfortunately, simple ray tracing near the ion gyrofrequencies and even near the harmonics of those cyclotron frequencies are conspicuously deficient in that the amplitudes of those waves changes rapidly in stark contrast to the assumptions of the WKB approximation. Thus any ray tracing code which predicts strong absorption or reflection must be considered suspect [Horne and Thorne, 1990]. Indeed, any such analysis which traces waves through the crossover frequency

Figure 4.8. Ray paths for magnetosonic waves with a density model which mimics the density gradients at the plasmapause boundary. The waves are launched at 5.5 Earth radii. A much larger range of initial wavevectors are directed along field lines towards the auroral region.

where substantial mode conversion occurs is simply wrong [Mei, *et al.*, 1992].

B. Magnetosonic Waves Ducted by Density Gradients

Magnetosonic waves, on the other hand, have generally been assumed to not reach auroral altitudes because the refract away from field lines [Rauch and Roux, 1982]. It is useful, however, to consider the analogy of whistler waves. Whistler waves are simply related to magnetosonic waves in that they are the same mode, but at a lower frequency. Because they obey a similar dispersion relation, they should have similar properties of propagation. Whistlers are well known to be ducted along field
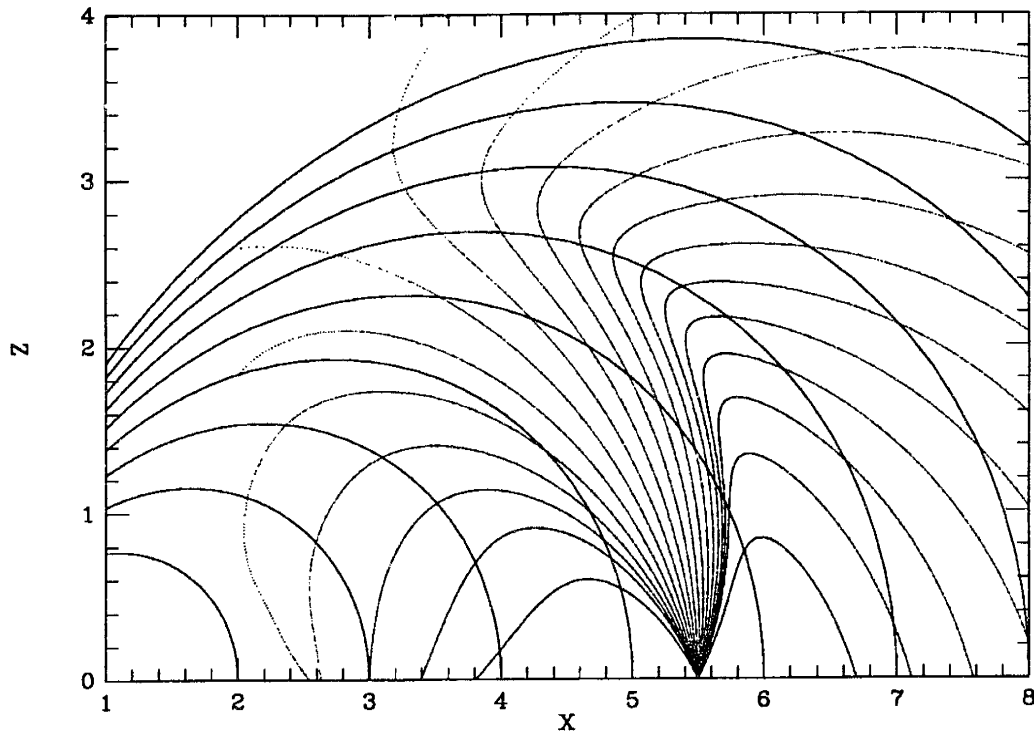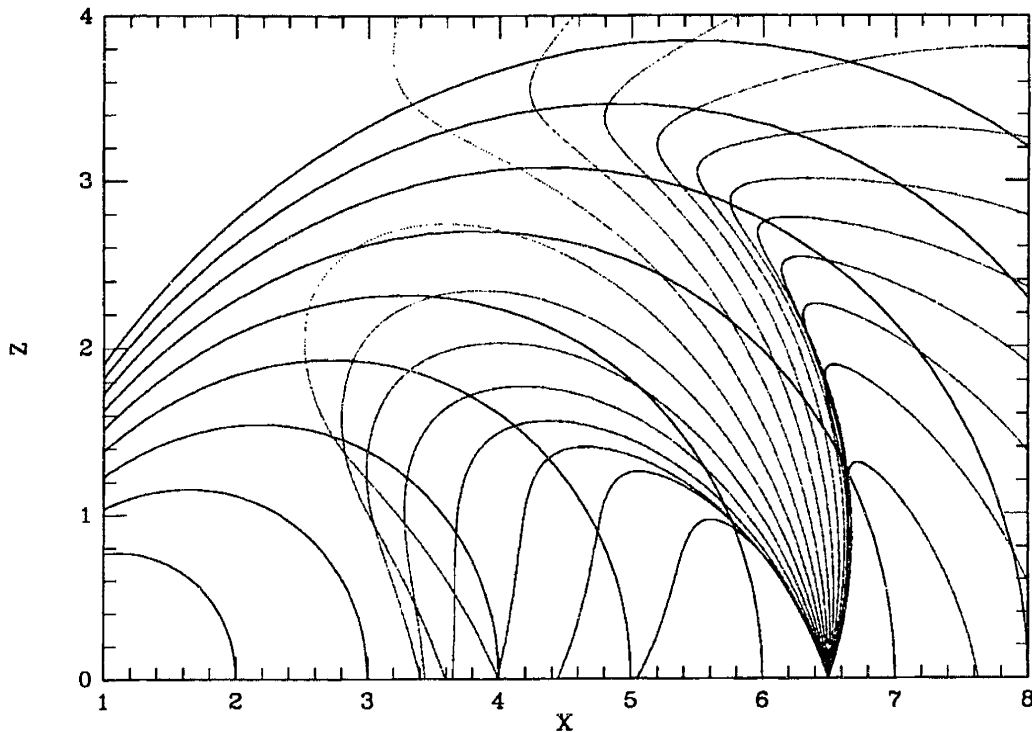
Figure 4.9. Ray paths for magnetosonic waves with a density model which mimics the density gradients at the plasmapause boundary. The waves are launched at 6.5 Earth radii.

lines between opposite hemisphere particularly after lightning [Helliwell, 1965; Al'pert, 1990]. However, whister waves behave in the same manner as magnetosonic waves in that they are not guided along magnetic field lines and instead are refracted into regions of smaller magnetic field. Nevertheless, because whisters propagate along the boundary at the outer edge of the CPS, they are subject to a phenomenon termed ducting in which the density gradients in fact duct or guide the waves along the edge of a density boundary. Such ducting is easy to imagine if we consider equations (4.23, 4.24). Waves are clearly refracted into regions of large densities. As they try to escape from a region of large density, they encounter a negative density gradient and are thus refracted back into the region of large density (providing the density gradient
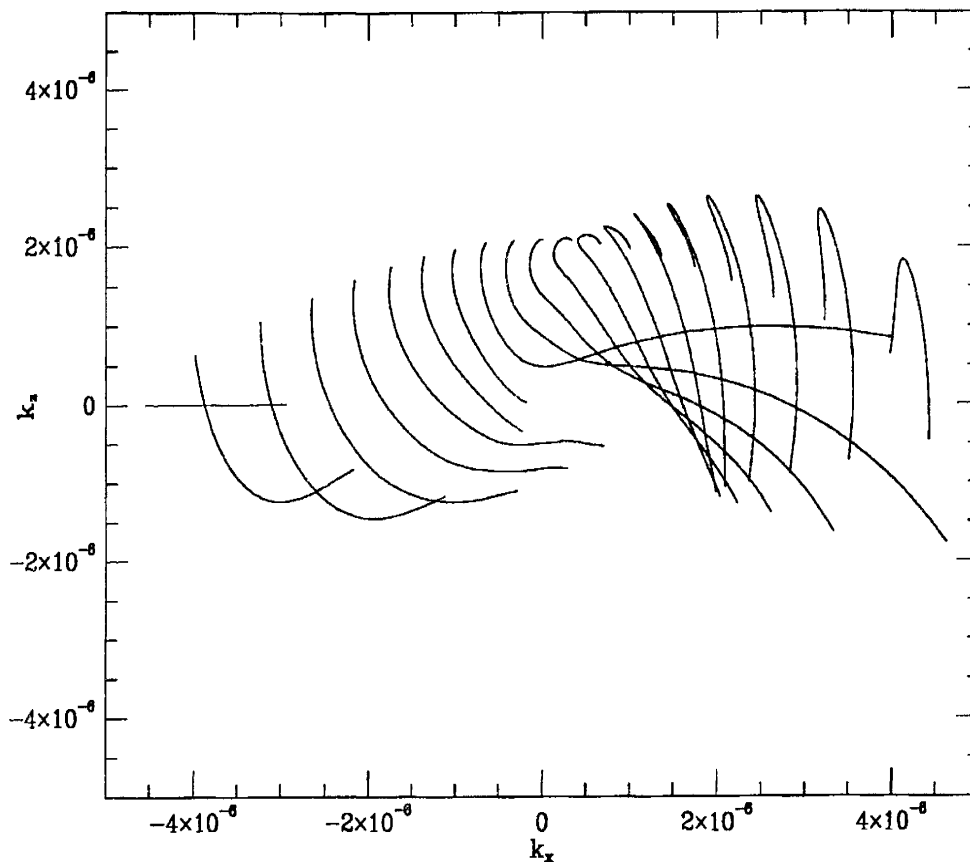
Figure 4.10. Evolution of the wavevector along ray paths associated with Figure 4.8. Note the correspondence between the direction of wavevector and the direction of wave propagation. Zeros of the components of the wavevector correspond to reflection in the x or z direction.

is sufficient to overcome the magnetic field gradient). In this manner, whistler waves are ducted along field lines.

In an analogous manner, we expect to find that near another plasma boundary, namely at the plasmapause interface between the plasmasphere and the central plasma sheet, RHCP waves may again be ducted. In the following plots we establish that perpendicularly propagating modes generated in the equatorial region are to some degree accessible to auroral altitudes and clearly accessible to altitudes where they can

Figure 4.11. Wave paths for magnetosonic waves traced backwards from the auroral region. Note that the source for the waves encompasses a substantial region outside of the plasmapause boundary. The scale length α is taken to be 2.

undergo mode conversion to LHCP waves at the helium gyrofrequency.

In Figures 4.6-9 we consider ray paths for waves which can propagate to auroral altitudes. In Figures 4.6 and 4.7 we plot ray paths for waves in the absence of density gradients. These two cases differ in that the waves are launched from 5.5 and 6.5 R_E respectively. It is clear that the waves are somewhat guided for the first R_E and then suffer strong refraction and are lost to the magnetotail [Rauch and Roux, 1982]. The reason that the waves are somewhat guided initially is that wave normal surface is actually an ellipse rather than a sphere as in the heuristic model (4.22). In Figures 4.8 and 4.9 we include the effects of density gradients taking typical parameters as for the
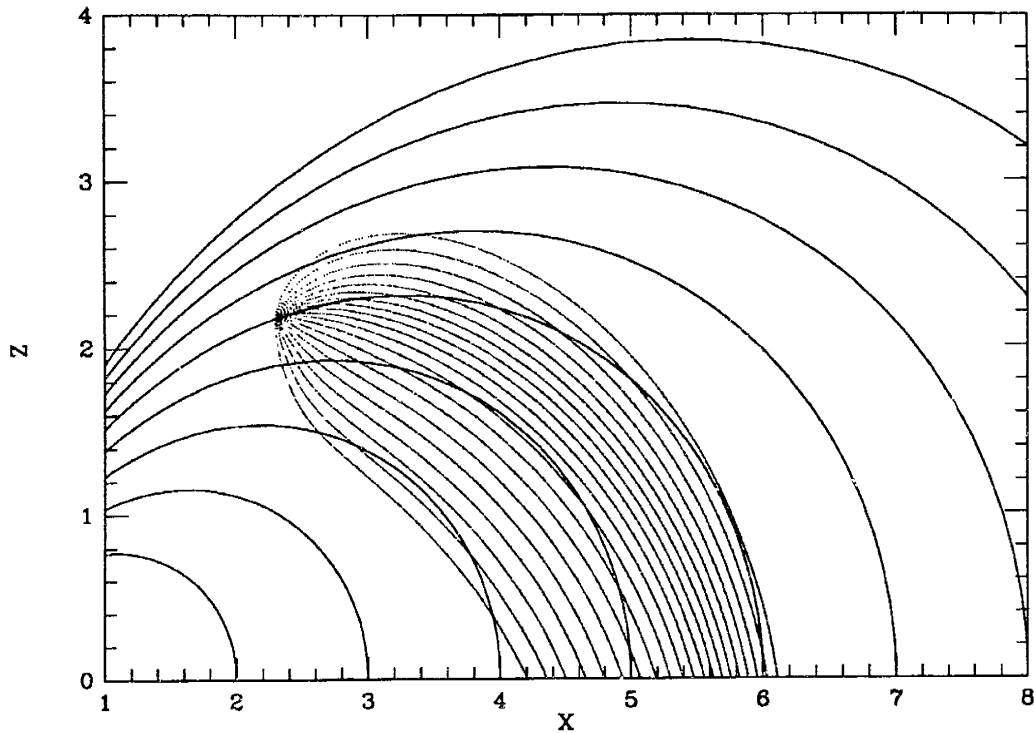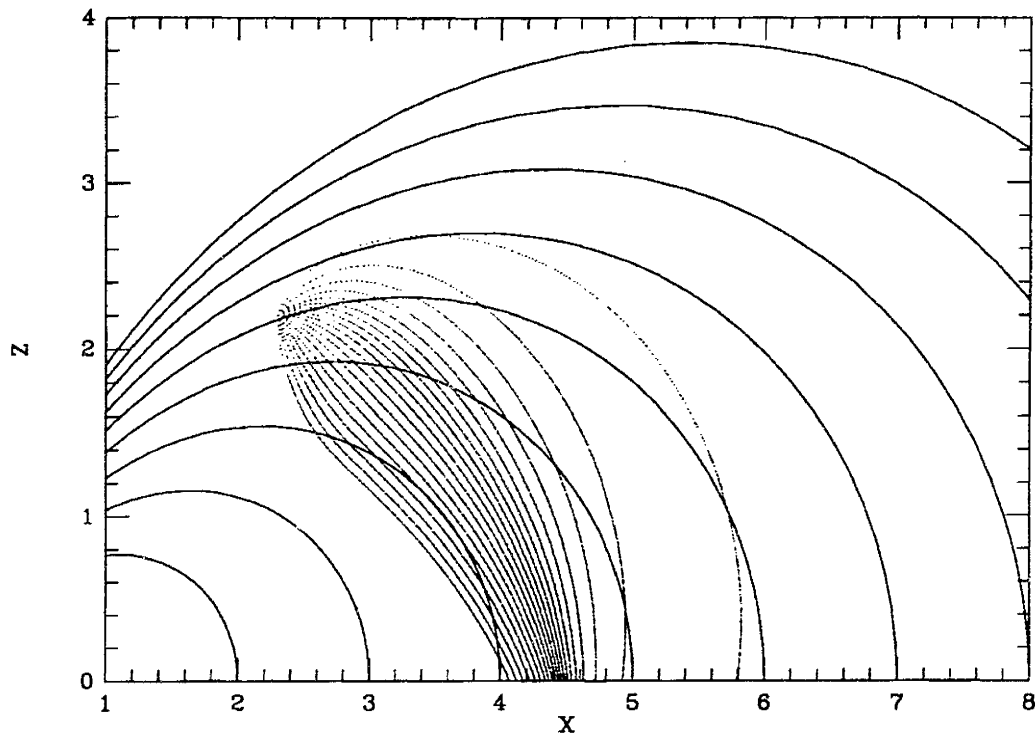
Figure 4.12. Wave paths for magnetosonic waves traced backwards from the auroral region. Note that the source for the waves encompasses a substantial region outside of the plasmapause boundary. The scale length α is taken to be 1.

ion-cyclotron case (4.25). It is apparent that waves with a much larger range of initial

angles penetrate deeper into the auroral region of the CPS than without the gradients.

In Figure 4.10, we plot the behavior of the wavevector associated with Figure 4.8.

The initial wavevectors lie on the wave normal surface at the equator which is an

ellipse. The components of the wavevectors are in the directions x and z. The

wavevectors with an initial negative k_x are associated with the leftmost contours of

Figure 4.8. As the waves evolve, the group velocity tends to be in the direction of the

wavevector. It is interesting to note the relationship between the the spatial turning

points for the ray paths in Figure 4.8 and the zeroes in the components of the

wavevector in Figure 4.10. This relationship confirms the heuristic argument that the group velocity lies along the direction of the wavevector.

In Figures 4.11 and 4.12 we trace waves backwards from a location in the auroral region to determine the source. Figures 4.11 and 4.12 differ in the value of the scale length of the density gradient. Increasing the ratio of n_{ps} to n_{cps} has a similar effect to decreasing the scale length. As is the case for ion-cyclotron waves, the source appears to be in the region outside of the plasmapause. Decreasing the scale length, α, leads to a much more defined source outside of the plasmapause. In contrast to Figure 4.5, we see that the source would appear to be a more extensive area of the equatorial region. Indeed, this elicits some confidence that some of the waves at auroral altitudes may be RHCP waves. Nevertheless, this result should be tempered by the observation that it is only oblique modes which are guided to auroral altitudes (waves which are generated with wavevectors aligned to the field still tend to be pushed into the tail by the magnetic field gradient), however, we should keep in mind that it is also the perpendicular modes which are primarily generated in the equatorial region, and, indeed, the equatorial region provides a large source from which to focus energy to auroral altitudes.

The waves observed at auroral altitudes tend to be broadband in frequency. If waves are generated in the equatorial region near the harmonics of the hydrogen gyrofrequency, then sources ranging over several R_E would vary substantially in frequency. As a result one would expect that such an admixture of waves would result in broadband spectrum. In contrast, ion-cyclotron waves generated by the ion-cyclotron

instability tend to be excited in a small range of frequencies. Because waves in the equatorial region are strongly tied to field lines, one would not expect to find as broad a spectrum as is observed.

C. Summary

In this chapter we have discussed ray-tracing at some length, and we have investigated whether waves generated in the equatorial region are accessible to auroral altitudes in light of a well approximated cold plasma model which retains magnetic field curvature and the essential features in the density profile at the plasmapause boundary. It is quite clear that LHCP waves, regardless of density profiles, propagate to auroral altitudes. This behavior is easily understood from the guiding influence of the magnetic field because the group velocity for these waves tends to be field aligned. On the other hand, we have also demonstrated that although RHCP waves at first glance appear to not be guided along field lines, they may be ducted by means of density gradients. We have studied a simple model which retains the essential features of the plasmapause boundary, and we have found that the effect of such a boundary is to cancel the competing effects of the magnetic field gradient so that waves generated in the magnetosonic mode may, in fact, be found at lower altitudes.

We have thus established that much wave power is available in both the LHCP and RHCP modes all along auroral field lines and can contribute to ion heating. The determination of accessibility of waves and determination of wave power available to heat ions then boils down to a detailed consideration of what happens as waves pro-

pagate into regions where their frequency matches the heavy ion gyrofrequencies. It is

this subject to which we shall direct our attention in the following chapters.

CHAPTER 5

MODE CONVERSION—ANALYTICAL CONSIDERATIONS

I. Inadequacies of Ray Tracing

In the previous chapter we have demonstrated that waves generated along both the ion-cyclotron and the magnetosonic branches of the dispersion relation propagate to altitudes where they may, in fact, be responsible for ion heating to some extent. The questions regarding accessibility, however, remain uncertain in that the preceding analysis did not consider the presence of a minority ion species. Indeed, it is impossible to study the detailed behavior of such waves in the vicinity of the ion resonances using the eikonal approximation. The existence of a cutoff most certainly indicates that the local scale of the disturbance far exceeds the scale length of the magnetic field. Moreover, the presence of a resonance generally indicates that the four propagating modes couple to some extent and that significant wave energy may be transferred between the modes [Gurnett, *et al.*, 1965]. This energy transfer may be quantified by determining the coefficients of the various propagating modes on either side of the region where the WKB approximation is inadequate. Unless these coefficients indicate either the absence of energy transfer or complete energy transfer, it is neither useful nor correct to trace ray paths through these frequencies. Such has been the case in a number of recent studies of low frequency wave behavior in multispecies plasma. As we shall see, there are regimes in which the coefficients are such

that ray-tracing may be proper; however, to a large extent the admixture of energy between the modes can be rather complicated and somewhat non-intuitive.

In regions where ray-tracing is unacceptable we must instead solve the full wave equations for the solution [Swanson, 1989]. The boundary conditions for this solution will, of course, be the wave solutions described by the WKB analysis. In the next two chapters we will consider carefully the full wave equations both analytically and numerically, and we will thus obtain reasonable estimates of the power apportioned to each of the WKB solutions on either side of the resonance.

In order to understand more completely the processes which we are examining, consider the dispersion relation of Figure 5.1 (for a full review of the dispersion relations associated with this problem see Chapter 3). This dispersion relation is characterized by three separate modes which we have labeled I, II, and III. Mode I is the magnetosonic branch and is predominately right-hand circularly polarized at high frequency whereas mode II, which is the hydrogen ion-cyclotron branch, is predominately LHCP. Below the oxygen cyclotron frequency mode II continues to propagate as the RHCP magnetosonic branch and mode III represents the LHCP ion-cyclotron branch. Near the crossover frequency, modes I and II couple and exchange energy. Mode I also suffers a cutoff at the cutoff frequency and is separated from mode III by an evanescent region. As waves move into regions of larger magnetic field they move "down" along the dispersion curves according to the WKB approximation in that they satisfy the local dispersion relation. The scenario in which waves propagate earthward into a region of larger magnetic field (as is the case for waves propagating from the
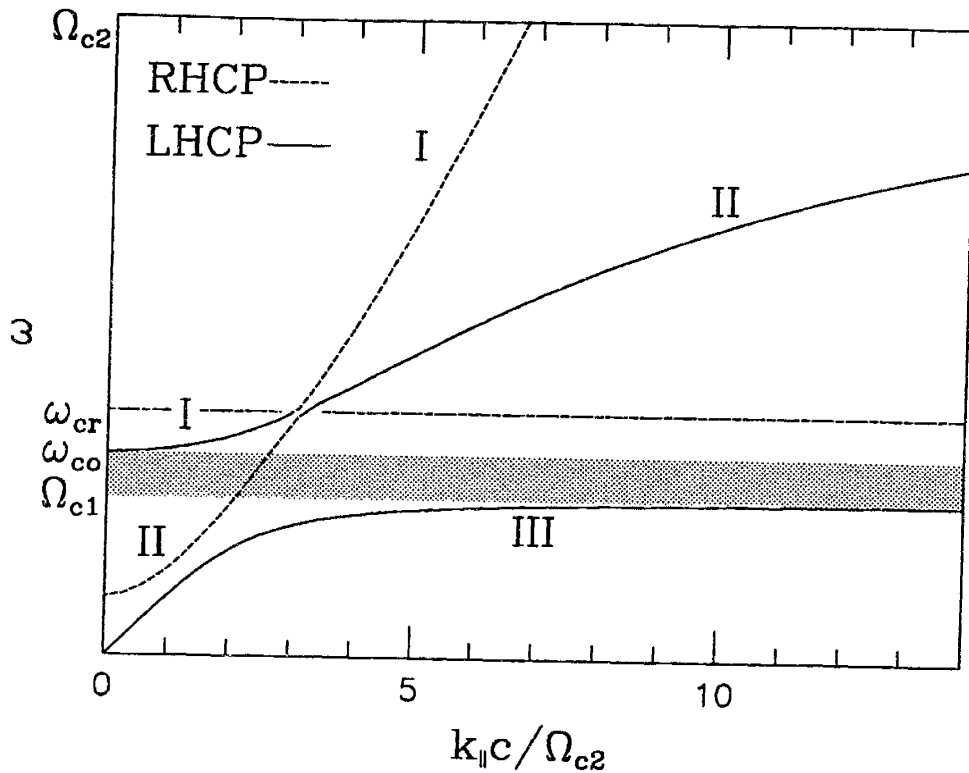
Figure 5.1. Dispersion relation for a cold two ion component plasma for nonparallel propagation. The various branches are labeled according to their predominate polarization with RHCP dashed and LHCP solid. Coupling occurs at the crossover frequency (ω_{cr}) where the polarization of branches I and II switches abruptly [Smith and Brice, 1964]. Tunneling occurs across the shaded "gap" between the cutoff frequency (ω_{co}) and the heavy ion gyrofrequency (Ω_{c1}).

equatorial region to the auroral region) corresponds to waves incident from "above" the coupling-evanescent region. Some of the incident wave power is then reflected back along branches I and II, some wave power is transmitted along branches II and III "below" the heavy ion cyclotron frequency, and some wave power is absorbed in the evanescent region. Particle heating may result from ion-cyclotron damping of branch III (for a thermal plasma) and from the calculated absorption which typically corresponds to mode conversion to a thermal plasma wave which is strongly damped.

II. Relevant Equations

Our goal is to describe the behavior of low frequency waves near the series of crossover cutoff and resonance frequencies found in a multispecies plasma. The essential feature that we wish to retain, then, is the variation of the magnetic field strength along field lines (density gradients do not affect the location of the resonances and only density ratios affect the location of the other special frequencies). The differential equations are most tractable and still retain the essential features which we wish to incorporate into our analysis if we consider a plasma in which the mode conversion processes are dominated by the variation in the strength of the magnetic field along one dimension and the density is taken to be constant.

At low altitudes where the heating and mode conversion processes are presumed to occur, the primary variation in the magnetic field strength is along the direction of the magnetic field (see Figure 4.2) thus we will assume that the only magnetic field variations are along the field line, and we will neglect the variations perpendicular to the field line. In doing so, we also neglect the effects of curvature which were critical for ray-tracing. Such an approximation is reasonable if the conversion process is localized in some sense with respect to the scale length of the magnetic field. Indeed, the scale over which the mode conversion occurs is asymptotically small compared with variations in the magnetic field so that such an approximation is valid.

Maxwell's equations combined with the momentum transfer equations describe wave propagation in a plasma medium [Stix, 1962]. In light of the approximations

detailed above, these equations reduce to a set of coupled ordinary differential equations for the components of the electric field [Försterling, 1942]. For low frequencies, the electric field parallel to the magnetic field becomes negligible [Stix, 1962] so that the equations for the circularly polarized electric field components perpendicular to the magnetic field

$$E_{\pm} = E_x \pm iE_y \qquad (5.1)$$

take the simple form

$$\varepsilon^2 \frac{d^2 E_-}{dz^2} - (\frac{\kappa^2}{2} - r)E_- = -\frac{\kappa^2}{2}E_+$$

$$\varepsilon^2 \frac{d^2 E_+}{dz^2} - (\frac{\kappa^2}{2} - l)E_+ = -\frac{\kappa^2}{2}E_- \qquad (5.2)$$

with

$$\varepsilon \equiv \frac{1}{k_A L_B} \quad , \quad \kappa \equiv k_\perp / k_A \quad ,$$

$$k_A \equiv \omega / v_A \quad , \quad L_B \equiv \frac{1}{B}\frac{dB}{dz} \quad , \qquad (5.3)$$

The rescaled Stix functions take the form

$$\begin{matrix} r \\ l \end{matrix} = \pm \frac{\Omega_{c1}\Omega_{c2}}{\omega_{co}} \frac{(\omega \pm \omega_{co})}{(\omega \pm \Omega_{c1})(\omega \pm \Omega_{c2})} \qquad (5.4)$$

and the Alfven velocity v_A has been defined previously. We have taken the Fourier transform in the direction perpendicular to the magnetic field. In addition, we have rescaled the coordinate variable to some length scale L_B which appropriately describes the scale length of the magnetic field.

These equations are related to the dispersion relation discussed in Chapter 3 and are related to the Fourier transform of the matrix equation (4.10). Indeed, the substitution $i\varepsilon d/dz \rightarrow n$ recovers the related dispersion relations

$$n_\pm^2 = \frac{r+l}{2} - \frac{\kappa^2}{2} \pm \left[\left(\frac{r-l}{2} \right)^2 + \frac{\kappa^4}{4} \right]^{\frac{1}{2}} \qquad (5.5)$$

These dispersion relations have been discussed at length in Chapter 3.

We can make a number of observations concerning the differential equations (5.2). These equations are primarily characterized by the quantities ε, κ, and the relative spacing of the cyclotron frequencies and the cutoff. The essence of the WKB approximation is contained in the parameter ε. For small ε the WKB solutions most nearly approximate the correct solution in the regions where r and l are well behaved. The parameter κ, on the other hand characterizes the coupling between the two modes. Indeed, from equations (5.2) it is obvious that for $\kappa = 0$, the two equations are completely uncoupled and each mode may be described separately. In this case, the equations simply describe the parallel propagating r and l modes.

The functional dependence of r and l on the altitude, z, which is shown in Figure 5.2, also greatly influences the behavior of the solutions. The function r is well behaved at low frequencies and varies slowly over the range of z for which the coupling occurs. The function, r, is well approximated by a linear function or even a constant. On the other hand, the function l is characterized by a pole at the cyclotron frequencies and a zero at the cutoff frequency. A suitable approximation for the func-
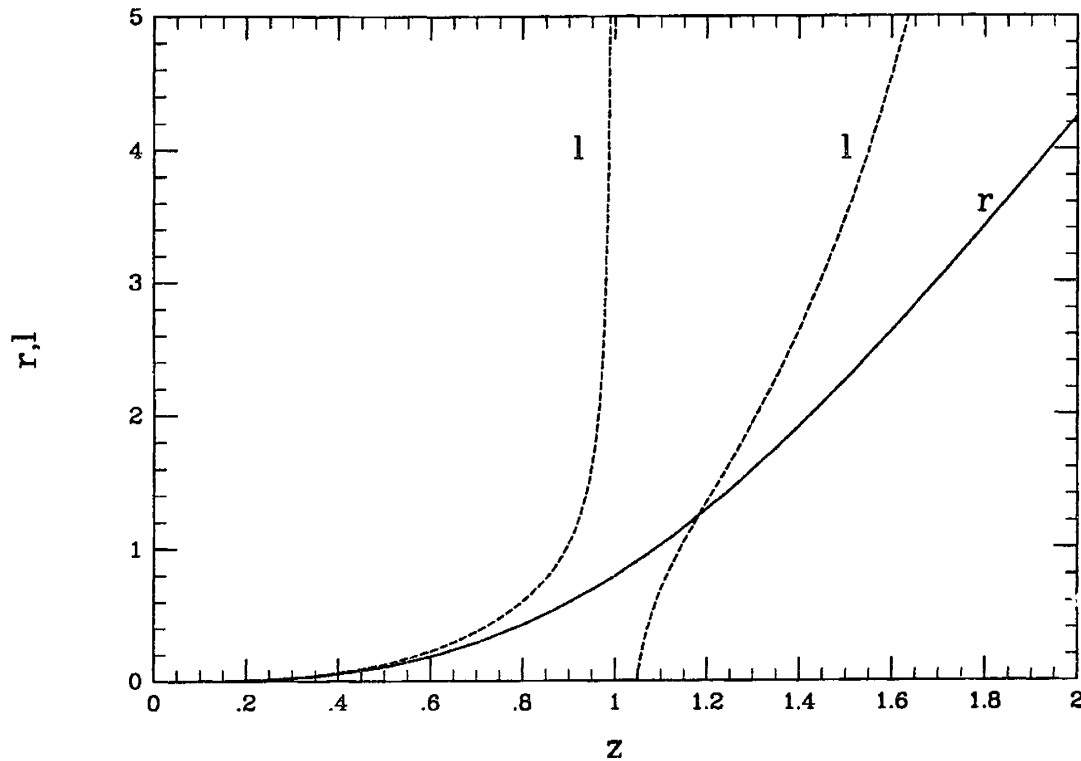
Figure 5.2. The functional dependence of r and l as a function of altitude. The coordinate is scaled so that $z=1$ corresponds to the oxygen resonance.

tion l must include the pole at the gyrofrequency as well as the zero at the cutoff frequency.

III. Analytical Considerations

A. General Discussion of Mode Conversion

Mode conversion is generally characterized by the coalescence of two propagating modes [Budden, 1965; Fuchs et al., 1981; Swanson, 1989]. In a region where mode conversion occurs, the propagating modes which coalesce may, in fact, exchange substantial energy. The local properties of a medium in one dimension are characterized by the dispersion relation

$$D(k,z) = 0 \qquad (5.6)$$

Saddle points of the dispersion relation where at least two roots coalesce are given by

$$\frac{\partial D}{\partial k} = 0 \qquad (5.7)$$

Equation (5.7) is satisfied for the mapping $k = k_c(z)$ which clearly depends upon the spatial coordinate, z. To see that at least two modes coalesce along the saddle point contours, expand the dispersion function about some $k = k_c$ which satisfies equation (5.7).

$$D(k,z) = D(k_c,z) + \frac{\partial D}{\partial k}(k-k_c) + \frac{1}{2}\frac{\partial^2 D}{\partial k^2}(k-k_c)^2 + O[(k-k_c)^3] \qquad (5.8)$$

Then at a point, z_b, where the dispersion relation is satisfied $k_c(z_b)$ becomes a double root of the dispersion relation. The point, z_b, is referred to as a branch point. Near the coupling point, the dispersion equation may be described in terms of an embedded dispersion relation

$$D(k_c,z) + \frac{1}{2}(k-k_c)^2 D_{kk}(k_c,z) = 0 \qquad (5.9)$$

Then a differential equation describing the two mode coupling may be obtained from the Fourier transform in k so that

$$\psi''(z) + Q(z)\psi = 0 \qquad (5.10)$$

where

$$Q(z) = -2\frac{D(k_c,z)}{D_{kk}(k_c,z)} \tag{5.11}$$

By definition, the potential Q vanishes at branch points z_b where $D = 0$. When coupling points are well separated, the embedded equation contains sufficient information to describe the coupling between the embedded modes. Such coupling is typically very strong if the coupling point z_b occurs close to the real axis and is weak if the coupling point is far from the real axis.

The particular dispersion relation that we are considering for low frequency waves may be obtained from the Fourier transform of equations (5.2) which is then of the form

$$D(k,z) = (k^2-r)(k^2-l)+\kappa^2(k^2-\frac{r+l}{2}) \tag{5.12}$$

where it is understood that r and l are explicit functions of z. The saddle points where the waves may be strongly coupled are located along contours for which

$$D_k(k,z) = 2k(2k^2-(r+l)+\kappa^2) = 0 \tag{5.13}$$

Saddle points lie along the contours

$$k_c(z) = 0, \frac{1}{2}(r+l-\kappa^2) \tag{5.14}$$

The branch points in space related to these saddle points may be obtained by solving the dispersion relation (5.12) along the saddle point contours, $k_c(z)$. For the coupling point at $k_c = 0$ we find the cutoff condition

$$rl = \frac{\kappa^2}{2}(r+l) \tag{5.15}$$

which occurs at the position at which the magnetic field satisfies the condition

$$\omega^2 = \omega_{co}^2 \omega_{ii}^2 \frac{1 - \dfrac{\kappa^2}{2}}{\omega_{ii}^2 - \dfrac{\kappa^2}{2}\omega_{co}^2} \tag{5.16}$$

This is simply the cutoff condition for the dispersion relation. For small values of κ, this cutoff occurs at the cutoff frequency, ω_{co}, which for parallel propagation is the cutoff of the LHCP L-mode. As κ increases this frequency increases as is clear if we write it in the form

$$\omega^2 = \omega_{co}^2 \frac{1 - \dfrac{\kappa^2}{2}}{1 - \dfrac{\kappa^2}{2}\dfrac{\omega_{co}^2}{\omega_{ii}^2}} \tag{5.17}$$

where $\omega_{co} > \omega_{ii}$—the numerator is always larger than the denominator for $\kappa \leq \sqrt{2}$. Near $\kappa^2 = 2$ the denominator diverges. (Actually the root approaches the lower hybrid frequency, but our approximations, suitable for low frequencies do not adequately describe this.) On the other hand, for $\kappa > \sqrt{2}$ a cutoff appears at low frequencies which increases as a function of κ up to the ion-ion resonance. This can be clearly seen if we express equation (5.16) in the form

$$\omega^2 = \omega_{ii}^2 \frac{1 - \dfrac{2}{\kappa^2}}{1 - \dfrac{2}{\kappa^2}\dfrac{\omega_{ii}^2}{\omega_{co}^2}}$$ (5.18)

where the numerator is smaller than the denominator. At some critical κ the cutoff passes through the resonance.

The coupling point $k_c = \frac{1}{2}(r + l - \kappa^2)$, when substituted into the dispersion relation, yields the coupling point condition

$$d^2 + \frac{\kappa^4}{4} = 0$$ (5.19)

where d is the difference function discussed in Chapter 3 and takes the form

$$d = \frac{r - l}{2} = \frac{\Omega_{c1}\Omega_{c2}}{\omega_{co}} \frac{\omega(\omega^2 - \omega_{cr}^2)}{(\omega^2 - \Omega_{c1}^2)(\omega^2 - \Omega_{c2}^2)}$$ (5.20)

This condition simply corresponds to a double root of the dispersion relation for the modes given in equation (5.5). For $\kappa = 0$, this condition is satisfied at the cutoff and crossover frequencies which are the zeros of the function d. As $\kappa \to \infty$, this condition may only be satisfied near the ion gyrofrequencies. For $\kappa \neq 0$ it is clear that this condition may be satisfied only for values of complex d which correspond to complex values of the magnetic field in which case the branch points, z_b, are complex. It should also be clear from the complex conjugate of equation (5.19) that the complex branch points always occur in complex conjugate pairs. In Figure 5.3 we plot values of the complex frequency along which equation (5.19) is satisfied. Equation (5.19) is
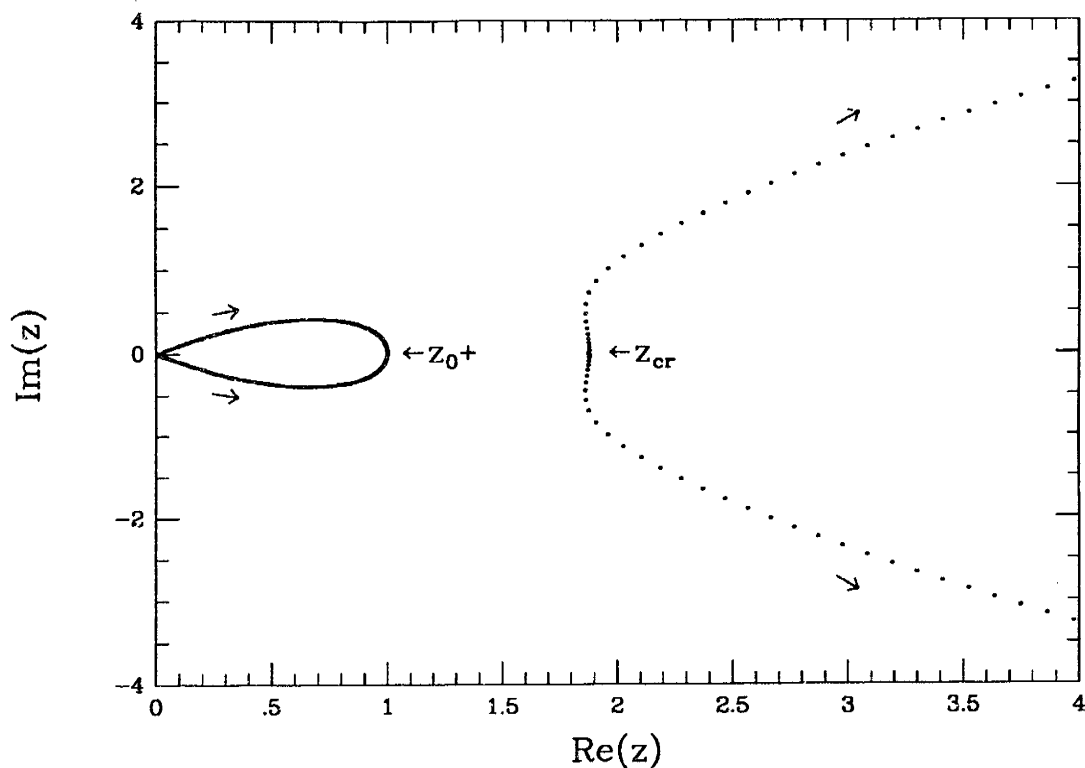
Figure 5.3. The locus of solutions to equation (5.19) for varying κ. The coordinate z corresponds to the ratio ω/Ω_{c1}. For $\kappa = 0$, the condition is satisfied at crossover frequency and at zero frequency while for large values of κ the condition is satisfied near the oxygen resonances and the hydrogen resonance (not shown). The arrows indicate the direction of increasing κ. For very small densities (less than 0.2%) the topology changes and the crossover frequency is connected to the oxygen gyrofrequency whereas the zero frequency solution is connected to the hydrogen gyrofrequency.

an eighth order equation in frequency with four complex conjugate pair solutions except at $\kappa = 0$ and $\kappa \to \infty$ where the modes coalesce into a pair of real double roots. For reasonable ionospheric values of the oxygen density, the crossover frequency connects to the oxygen cyclotron frequency and the double root at $\omega = 0$ connects to the heavy ion gyrofrequency. From the topology, we expect coupling to be largest when the coupling points lie near the real axis. In this sense, we see that the largest coupling takes place for small values of κ near the crossover frequency and near the $\omega = 0$ root (which corresponds physically to very low altitudes). On the other hand,

for large values of κ the coupling occurs near the two gyrofrequencies (the other gyrofrequency at $z = 16$ is not shown in Figure 5.3).

In the following sections we will carefully consider the problem at hand, and using suitable approximations, we will extract the behavior of the coupling coefficients analytically. Finally, we will solve the differential equations (5.2) numerically and obtain coefficients valid for all relevant κ.

B. Mode Coupling at Crossover Frequency

For $\kappa \ll 1$, the two modes coalesce near the crossover frequency and couple strongly. We may describe this coupling in a number of ways. In doing so, we shall demonstrate that a substantial amount of energy will be exchanged between the two propagating modes near the crossover frequency for $\kappa \ll 1$. For $\kappa > 1$ the magnetosonic mode is cut off at the lower hybrid frequency which lies above the light ion cyclotron frequency so that only two modes propagate near the heavy ion gyrofrequency. The character of the problem therefore changes as the value of κ changes across some critical value. In this section, we will concentrate on values of κ below this critical value such that four modes propagate in the vicinity of the heavy ion gyroresonance. In a later section, we address propagation for larger values of κ.

One way in which to understand coupling near the crossover frequency is to consider a perturbation about parallel propagation [Budden, 1965]. Such an analysis is particularly insightful because it is then quite clear that the coupling results from the presence of finite κ. Indeed, the coupling between the two modes is found from

equations (5.2) to be of order κ^2.

For small κ the fields may be expanded in the parameter κ

$$E_\pm = E_\pm^{(0)} + \kappa^2 E_\pm^{(1)} + \cdots \qquad (5.21)$$

To zeroth order in κ, the equations (5.2) take the form

$$\varepsilon^2 \frac{d^2 E_-^{(0)}}{dz^2} + r\, E_-^{(0)} = 0$$

$$\varepsilon^2 \frac{d^2 E_+^{(0)}}{dz^2} + l\, E_+^{(0)} = 0 \qquad (5.22)$$

The functions r and l vary slowly in altitude (in particular near the crossover frequency), so that we may apply the WKB analysis, which is valid for $\varepsilon \ll 1$, to solve the zeroth order equations. The zero order electric fields are then simply the r and l modes with

$$E_-^{(0)} = E^0 [r(z)]^{-1/4} \exp\left(-\frac{i}{\varepsilon} \int_h^z [r(s)]^{1/2} ds \right) \qquad (5.23)$$

$$E_+^{(0)} = E^0 [l(z)]^{-1/4} \exp\left(-\frac{i}{\varepsilon} \int_h^z [l(s)]^{1/2} ds \right) \qquad (5.24)$$

where h is a suitably chosen reference altitude. The parameter κ couples the two parallel propagating modes so that we may solve for the electric field perturbatively. To first order in κ, the coupled equations for the electric fields are

$$\varepsilon^2 \frac{d^2 E_-^{(1)}}{dz^2} + r(z) E_-^{(1)} = \frac{1}{2}(E_-^{(0)} - E_+^{(0)})$$

$$\varepsilon^2 \frac{d^2 E_+^{(1)}}{dz^2} + l(z) E_+^{(1)} = \frac{1}{2}(E_+^{(0)} - E_-^{(0)})$$

(5.25)

The solution to the homogeneous part of these differential equations is indeed, just the WKB solutions

$$\phi_\pm^L(z) = E^0 [l(z)]^{-1/4} \exp\left(\pm \frac{i}{\varepsilon} \int_h^z [l(s)]^{1/2} ds\right)$$

(5.26)

for $E_+^{(1)}$ and

$$\phi_\pm^R(z) = E^0 [r(z)]^{-1/4} \exp\left(\pm \frac{i}{\varepsilon} \int_h^z [r(s)]^{1/2} ds\right)$$

(5.27)

for $E_-^{(1)}$. The particular solutions for the first order equations are then of the form

$$E_-^{(1)} = A_+^R \phi_+^R + A_-^R \phi_-^R$$

(5.28)

and

$$E_+^{(1)} = A_+^L \phi_+^L + A_-^L \phi_-^L$$

(5.29)

where

$$A_\pm^R = \int_h^z \frac{r.h.s.\,(5.25a) \times \phi_\mp^R}{W[\phi_+^R, \phi_\pm^R]}$$

(5.30)

and

$$A_\pm^L = \int_h^z \frac{r.h.s.\,(5.25b) \times \phi_\mp^L}{W[\phi_+^L, \phi_\pm^L]}$$

(5.31)

and W is the Wronskian of the homogeneous solutions.

For the case of downcoming RHCP magnetosonic waves, the zero order electric fields are of the form

$$E_+^{(0)} = 0 \quad , E_-^{(0)} \neq 0 \tag{5.32}$$

whereas for the case of downcoming ion-cyclotron waves, the zero order electric fields are of the form

$$E_+^{(0)} \neq 0 \quad , E_-^{(0)} = 0 \tag{5.33}$$

In the following analysis, we will concentrate on downcoming magnetosonic waves consistent with the zero order fields (5.32). Coupling to the LHCP ion-cyclotron wave, E_+, is first order in κ^2 and may be determined by evaluating the coefficients

$$A_\pm^L(z) = \frac{1}{4i\varepsilon} \int_h^z ds \; [l(s)r(s)]^{-1/4} \times$$
$$\exp\left(-\frac{i}{\varepsilon} \int_h^z \left([r(q)]^{1/2} \pm [l(q)]^{1/2} \right) dq \right) \tag{5.34}$$

The amplitudes of the downgoing coupled waves $A_\pm^L$ involve integrals over rapidly oscillating functions with scale length ε. The integral over such a function is asymptotically small except in the region where the oscillations become stationary. Therefore, coupling between the modes is negligible except at the stationary point where the integrand in the exponential vanishes. The function, A_+^L, has no stationary point in the region of interest so that there is no reflected LHCP wave to first order. On the other hand, the function, A_-^L, has a a stationary point at the crossover frequency, ω_{cr} where

$d \equiv (r-l)/2 = 0$. Because the contribution to the overall integral in (5.34) is exponentially small except near the stationary point, we may expand the integral in the integrand of (5.34) about the stationary point and evaluate it using the standard methods of stationary phase [Bender and Orszag, 1978]. The overall integration may then be extended to $+\infty$ which introduces only exponentially small errors. Then we find that the coupling coefficient, up to an unimportant phase, is given by

$$A_{-}^{L}(-\infty) = \frac{1}{4\varepsilon\,[r\,(\omega_{cr})]^{1/2}} \int_{-\infty}^{+\infty} ds \exp\left(\frac{-i\ d'(\omega_{cr})\ s^2}{2\ \varepsilon[r\,(\omega_{cr})]^{1/2}} \right) \tag{5.35}$$

where

$$d'(\omega = \omega_{cr}) = \frac{2\omega_{cr}^3 \Omega_{c1}\Omega_{c2}}{\omega_{co}(\Omega_{c1}^2 - \Omega_{c2}^2)^2} \frac{(n_1 + n_2)^2}{n_1 n_2} \tag{5.36}$$

The integral may then be rotated in the complex plane in which case it becomes a trivial Gaussian integral. We have thus obtained, to first order in κ the asymptotic form of the coupling to the LHCP mode.

By comparing the Poynting flux along the magnetic field

$$\hat{z} \cdot \mathbf{S} \sim \hat{z} \cdot \mathbf{E} \times \mathbf{B} \sim \mathrm{Im}(E_{+}^{*}E_{+}' + E_{-}^{*}E_{-}') \tag{5.37}$$

of the incident wave above the coupling region to that of the coupled wave below the coupling region we may obtain the coupling coefficient

$$C \equiv \left| \frac{\hat{z} \cdot \mathbf{S}_{below}}{\hat{z} \cdot \mathbf{S}_{above}} \right| = \frac{\pi}{8\varepsilon} \frac{\kappa^4}{\sqrt{r}\,d'} \bigg|_{\omega = \omega_{cr}} \sim \frac{k_{\perp}^4}{k_{\parallel}^4} L_B\ k_{\parallel} \tag{5.38}$$

It is also obvious from the preceding equations that the coupling between an incident

LHCP wave and a coupled RHCP is described by the same coupling coefficient, C. Although less straightforward, by keeping terms to second order in κ (recall that the Poynting flux involves the square of the wave amplitudes) we may also show that the wave energy which remains on the incident branch is found to be $1-C$.

As is clear from the preceding analysis, the coupling occurs as the result of finite κ and increases rapidly for small angles of propagation. For infinite magnetic field scale length $\varepsilon \rightarrow 0$ so that coupling only occurs at $\kappa = 0$ and the modes are well separated for all other κ. In that sense, then, it is not acceptable to trace waves through the crossover frequency for those κ for which $C \leq 1$ in which case coupling is strongly dependent upon the angle of propagation.

This result may, indeed, be naturally extended to larger values of κ if we consider the embedded dispersion relation discussed in equation (5.12). The coupling which occurs at the crossover frequency arises from the branch point which is the solution to equation

$$d^2 + \frac{\kappa^4}{4} = 0 \qquad (5.19)$$

As discussed previously, two of the solutions to this equation correspond to two complex conjugate roots which occur near the crossover frequency. Moreover, the coupling may be described in terms of the embedded equation (5.10) with

$$D(k_c, z) = -d^2 - \frac{\kappa^4}{4} \qquad (5.39)$$

and

$$D_{kk}(k_c, z) = 4(2s - \kappa^2) \qquad (5.40)$$

so that

$$Q(z) = \frac{1}{2} \frac{d^2 + \frac{\kappa^4}{4}}{2s - \kappa^2} \qquad (5.41)$$

The function d has a zero at the crossover frequency, so that locally

$$d = d_{cr} + d_{cr}'\xi \qquad (5.42)$$

where $d_{cr} = 0$. The coupling is described by the potential equation

$$\psi''(\xi) + \frac{1}{2} \frac{d_{cr}'^2\xi^2 + \frac{\kappa^4}{4}}{2s_{cr} - \kappa^2}\psi = 0 \qquad (5.43)$$

where the sum function has been evaluated at the crossover frequency (the shape of the potential is not affected too much by the expansion of s, and in particular the complex turning points are independent of the form of s). With the appropriate substitution

$$k_0^2 = \frac{d_{cr}'^2}{s_{cr} - \kappa^2/2} \qquad (5.44)$$

$$\beta^2 = \frac{\kappa^4}{16d_{cr}'^2} \qquad (5.45)$$

equation (5.43) takes the form of a Weber equation

$$\psi''(z) + k_0^2 \left(\frac{z^2}{4} + \beta^2\right)\psi = 0 \qquad (5.46)$$

The transmission coefficient for this equation is well known [Heading, 1962; Fuchs *et al.*, 1985; Lashmore-Davies *et al.*, 1985] and takes the form

$$T = \exp\left[-\frac{\pi}{8\varepsilon}\frac{\kappa^4}{d'_{cr}\sqrt{s_{cr} - \kappa^2/2}}\right] \qquad (5.47)$$

For small values of κ

$$T \simeq 1 - \frac{\pi}{8\varepsilon}\frac{\kappa^4}{d'_{cr}\sqrt{s_{cr} - \kappa^2/2}} \qquad (5.48)$$

so that

$$C \equiv 1 - T \simeq \frac{\pi}{8\varepsilon}\frac{\kappa^4}{d'_{cr}\sqrt{r_{cr}}} \qquad (5.49)$$

as obtained in equation (5.38).

C. Tunneling Phenomena

1. Budden's Equation

The dispersion relations for the propagating modes of the differential equation (5.2) are characterized by various cutoffs ($k \rightarrow 0$) and in particular by a cutoff-resonance gap. For parallel propagation, the modes are uncoupled and the LHCP ion-cyclotron exhibits the characteristics of the "gap" while the RHCP magnetosonic branch remains essentially constant. The LHCP branch is characterized essentially by the dispersion relation $n_- = l$ where l has a zero at the cutoff frequency, ω_{co}, and a

resonance at the heavy ion gyrofrequency, Ω_{c1}. For non-parallel propagation the situation is more complex in that the refraction indices

$$n_{\pm}^{2}=\frac{r+l}{2}-\frac{\kappa^{2}}{2}\pm\left[\left[\frac{r-l}{2}\right]^{2}+\frac{\kappa^{4}}{4}\right]^{\frac{1}{2}} \tag{5.5}$$

suffer a discontinuity at the gyrofrequency where l diverges. Across this discontinuity, l varies as $\dfrac{1}{\omega-\Omega_{c1}}$ which changes sign. Hence, although the magnetosonic solution appears to be continuous across the resonance, there is in fact a change in branch $n_{\pm}\rightarrow n_{\mp}$. The existence of such a discontinuity signals one of the most critical aspects of the problem which we are considering to which we shall return many times. Namely, the solution is not continuous, is multivalued, and is characterized by a branch cut. We must work to carefully understand both the physics and mathematics involved in the multivalued nature of the solution and realize that the proper choice of the branch of this solution is essential to our analysis. The proper continuation of the dispersion relation is such that the magnetosonic branch is **not** continuous across the resonance. Hence, although the ion-cyclotron branch apparently mode converts into the magnetosonic branch, the asymptotic behavior of the ion-cyclotron branch below the resonance is determined primarily by the asymptotic behavior of the ion-cyclotron branch above the resonance.

The existence of a "gap" in the dispersion relation indicates that the WKB solutions for a particular mode are cut off and are decaying exponentials over some region of space. In general, the solutions of the dispersion relation across this "gap" decay

such that only exponentially small amplitude may be found on the other side of the "gap." In such a case, the mode will have been reflected. However, if the "gap" is sufficiently small such that it is only a fraction of a wavelength in size, substantial tunneling may occur in which case large wave amplitude will be found on the other side [Budden, 1965].

One particular example of the Budden equation in which a cutoff-resonance occurs is the case of parallel propagation ($\kappa = 0$) for the differential equation (5.2) in which case the lower component of that equation

$$\varepsilon^2 \frac{d^2 E_+}{dz^2} + l\, E_+ = 0 \tag{5.50}$$

adequately describes the behavior of this mode. The function l may be expanded about the resonance as

$$\Omega_1 = \Omega_1^0 (1-z) \quad , \quad \Omega_1^0 = \omega \tag{5.51}$$

Then

$$\frac{d^2 E_+}{dz^2} + k_0^2 (1 - \frac{a}{z}) E_+ = 0 \tag{5.52}$$

where

$$k_0^2 = \frac{1}{\varepsilon^2} \frac{\omega_{co}}{\Omega_{c1}} \quad , \quad a = \frac{\omega_{co} - \Omega_{c1}}{\Omega_{c1}} = \eta_1 \frac{(m_1 - m_2)}{m_2} \tag{5.53}$$

where η_s is the concentration, n_s/n_{total}, of a particular species. This is the well known Budden equation [Budden, 1965].

It will be useful at this juncture to review the Budden equation. Although the solutions to the Budden equation are well tabulated, we will present an alternative method for obtaining the asymptotic properties of the the Budden equation which requires no information with regard to the exact solution. It will become clear that although the Budden equation itself has a complicated solution, substantial information may be garnered from the asymptotic behavior of its solutions which may indeed be applied to the fourth order equation under consideration. Moreover, the Budden equation involves the concept of "missing" wave flux which is apparently absorbed by the medium. It will be of substantial interest for us to understand the concept of "missing" wave energy, how it relates to the physics of the problem and how it may be applied to the behavior of the fourth order equation that we are investigating.

Budden first solved this problem when considering the behavior of plasma waves near a resonance. The existence of a pole in the differential equation is troublesome in that it is not physically correct, and, in addition, it involves the complications of a regular singular point which generally leads to multivalued solutions of a differential equation except under extraordinary circumstances. As far as physical correctness is concerned, it is obvious that a higher order expansion of the Z-functions in terms of the thermal velocity will introduce corrections to the dispersion relation that will remove the singularity (the Z-functions are well defined at the plasma resonance, hence the corresponding differential equation is also well defined). These corrections arise in the form of a higher order terms in the differential equation which contain the essentials of the physics. Physically, the pole corresponds to dissipation which may be

understood in terms of strong ion cyclotron damping. In order to understand this, consider the conserved function which is the Poynting flux

$$J = i(\psi\psi'^* - \psi^*\psi') \tag{5.54}$$

For a differential equation of the form (5.10) we find

$$J' = i(Q - Q^*)\psi\psi^* \tag{5.55}$$

where $'$ denotes real derivatives along a contour with fixed imaginary part (recall that $d\psi^*/dz \neq (d\psi/dz)^*$ except along a line, $z = x + i\gamma$, with γ fixed). The conserved quantity J, however corresponds identically to the flux of wave energy in the system. The function

$$Q = k_0^2\left[1 - \frac{a}{z}\right] \tag{5.56}$$

is real along the real axis so that J takes a constant value along the real axis on either side of the pole at $z = 0$. Equation (5.55) is not well defined at the point $z = 0$ so that it is not clear that the conserved quantity J takes the same value on either side of the real axis. Indeed, as it shall become clear, the total energy flow undergoes a discontinuous change Δ across the branch point $z = 0$. (The pole in the differential equations turns out to be a branch point of the multivalued solution to the differential equation (5.52).)

Near the gyrofrequencies, the cold plasma dispersion relations exhibit an unphysical resonance. If we were to incorporate more physical considerations into our analysis, such as the thermal effects, we would find that the solution to the dispersion

relation near the gyrofrequencies is of the form $\omega \approx \Omega_{c1} - i\gamma$, $\gamma > 0$, such that the mode is strongly damped. In light of our approximation for the magnetic field the actual pole should be at a location $\omega - (\Omega_{c1} - i\gamma) = \omega - \omega(1-z) + i\gamma = 0$, that is, at the location $z = -i\gamma/\omega$ which lies below the real axis rather than at $z = 0$. The potential, Q, then takes the form

$$Q = k_0^2 \left[1 - \frac{a}{z+i\gamma} \right] \qquad (5.57)$$

so that

$$J' = -k_0^2 a \left[2 - \frac{\gamma}{z^2+\gamma^2} \right] \psi\psi^* \qquad (5.58)$$

from which it is obvious that given an incident J at $\pm\infty$, that an amount of energy flow

$$\Delta = 2k_0^2 a \int \frac{\gamma}{z^2+\gamma^2} \psi\psi^* \qquad (5.59)$$

will be lost. That is $J^+ < J^-$ where the superscript refers to the value along the positive (negative) real axis. Then if there is no flux in or out on the positive real axis ($J^+ = 0$) there is a positive energy flow from the left ($J^- > 0$), which is absorbed. On the other hand, if there is no flux from the left ($J^- = 0$), then there is a negative flux from the right ($J^+ < 0$) sending wave energy, which is absorbed, into the system. The value of this energy loss clearly depends on the details of the boundary conditions in that the solution ψ must be known in order to calculate the energy loss. Physically, we may interpret this energy loss as resulting from resonant absorption at the gyrofrequency. Such absorption typically occurs because the cold plasma wave mode

converts into a thermal wave which is readily absorbed. Conversely, if the pole lies above the real axis, a similar procedure results in an energy gain which is not physical.

Budden recognized equation (5.52) to be of the form of a hypergeometric equation

$$w'' + \left[-\frac{1}{4} + \frac{\kappa}{\xi} + \frac{(1/4 - \mu^2)}{\xi^2} \right] w = 0 \qquad (5.60)$$

with the appropriate choices $\xi = iz/2k_0$, $\kappa = -ia/2$, and $\mu = 1/2$ [Abramowitz and Stegun, 1964]. Solutions to this equation are then expressible in terms of the confluent hypergeometric function. After an elaborate asymptotic expansion of these functions as $\xi \to \pm\infty$ Budden obtained the coefficients for various boundary conditions. From the form of the equation (5.52), it is clear that as $z \to \pm\infty$ the solutions of the differential equation are plane waves $e^{\pm ik_0 z}$ which correspond to upgoing and downgoing waves. Referring to the dispersion relation for the Budden problem in Figure 5.4, there are two possible situations. A wave may be incident from the right of the resonance so that it encounters the cutoff before the resonance. Presumably if the evanescent layer between the modes is large then all the wave power is reflected as at a cutoff. The other situation is that of incidence from the left in which case the resonance is encountered first. In this situation, if the "gap" is very large no wave power is expected to be transmitted. For incidence from the right, Budden [1965] found the coefficients to be of the form

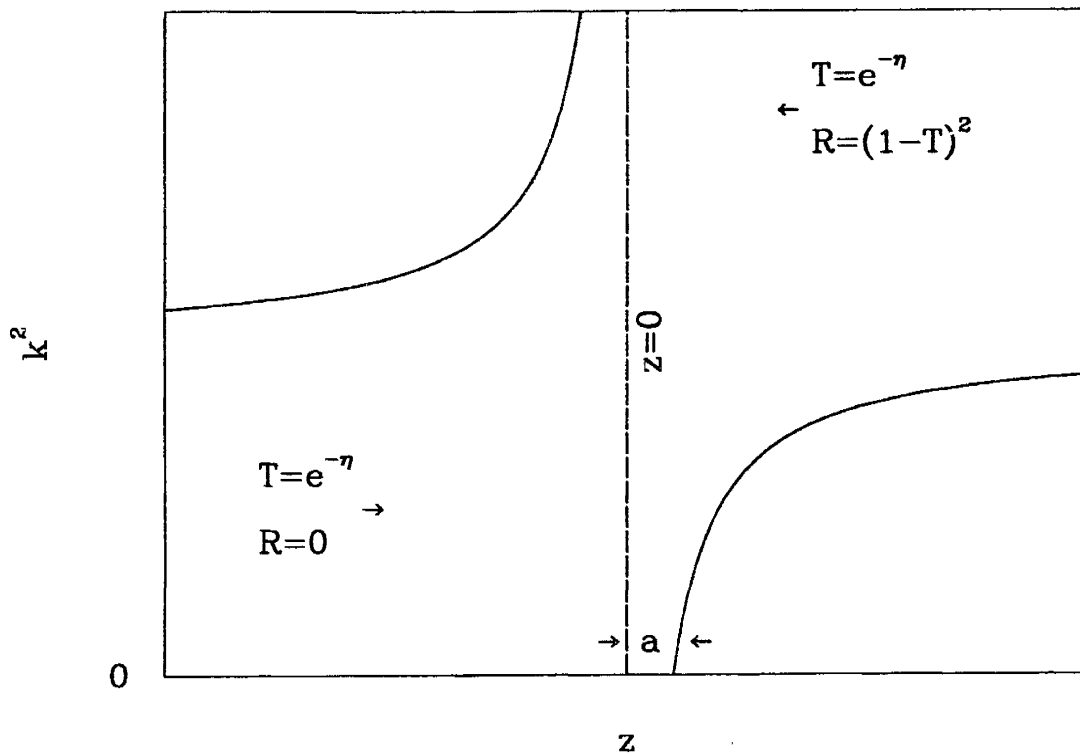$$T = e^{-\eta} \ , \ R = (1-T)^2 \qquad (5.61)$$

Figure 5.4. Dispersion relation for the Budden equation which illustrates the general feature of a cutoff-resonance pair. Waves are either incident from "above," (the right-hand side) or "below" (the left-hand side).

while for incidence from the left

$$T = e^{-\eta} \ , \ R = 0 \qquad (5.62)$$

with $\eta = \pi k_0 a$.

2. Phase integral Solution of Budden's Equation

Budden's solution of this equation is interesting; however, in general, it is not straightforward to obtain the exact solution of a differential equation, particularly if it is of fourth order. However, as we shall see, for this problem it is rather unnecessary to know the exact solution to the equation. The transmission coefficients follow

immediately from the consideration of asymptotic dominance, and consideration of the

conserved energy flow, J, leads immediately to a complete solution of the Budden

coefficients in which the work required is minimal.

For an equation of the form (5.10), the leading order WKB solutions are of the

form

$$\Theta^{\pm} = \exp\left[\pm ik_0\int_0^z Q^{1/2}ds\right] \qquad (5.63)$$

for the Budden potential, it is not difficult to integrate the potential to obtain

$$\int_a^z Q^{1/2}ds = \left[\sqrt{z(z-a)}-a\log\left[\sqrt{\frac{z}{a}}+\sqrt{\frac{z}{a}-1}\right]\right] \qquad (5.64)$$

from which it is clear that for $|z|\to\infty$ we recover the plane wave solutions as previ-

ously mentioned. For large z we see that the branch of the square roots are unimpor-

tant, but the branch of the logarithm characterizes the entire tunneling process. The

WKB solution contains much information. For example, the expansion of the WKB

solutions (5.64) about the cutoff, $z = a$, behaves like Airy functions (exponential

behavior as $z^{3/2}$) as is typical for wave solutions near a cutoff, while at the resonance,

$z = 0$, the solutions take the form of the Hankel function (exponential behavior as $z^{1/2}$)

which is characteristic of a resonance. The form (5.64) is reasonably cumbersome and

contains much more information than is necessary to compute the asymptotic proper-

ties of the solution to the Budden equation. Indeed, the function Q may simply be

expanded for large z, for which we find from equation (5.56)

$$Q^{1/2} \approx k_0 \left[1 - \frac{a}{2z} \right]$$ (5.65)

so that for large z, the WKB solutions are of the form

$$\Theta^{\pm} = e^{\pm ik_0(z - a \log(z)/2)}$$ (5.66)

From this form it is clear that the important branch is that of the logarithm, and it is convenient to take the branch cut along the branch cut of the multivalued solution to (5.52). We shall in the following sections take the branch cut to lie along the negative real axis, and it is to be noted that the solution to (5.52) is not continuous across the branch cut.

The general form of the solution, $\psi \equiv E_+$, of (5.52) along the positive real axis is given by

$$\psi = A \Theta^- + B \Theta^+ \quad , \quad Arg(z) = 0$$ (5.67)

The WKB approximations in the complex plane, however, are at best limited to validity within certain sectors due to the Stokes phenomenon which results from the fact that the exponential solutions are too simple to adequately describe the qualitative behavior of the actual functions [Heading, 1962]. Indeed, for z complex, one of the WKB solutions will, in fact, become dominant over the other WKB solution and hence dominate the behavior of ψ. From the form of the WKB solutions it is clear that the greatest dominance occurs for purely imaginary z so that Stokes lines occur at $Arg(z) = (n+1/2)\pi$. The Anti-Stokes lines correspond to the real axis along which both solutions are of equal dominance. Thus, we find that the asymptotic behavior of

the solution, ψ of the differential equation is given by

$$\psi \sim \Theta^- = e^{-ik_0(z - a \log(z)/2)} \quad , \quad Im(z) > 0 \tag{5.68}$$

$$\psi \sim \Theta^+ = e^{+ik_0(z - a \log(z)/2)} \quad , \quad Im(z) < 0 \tag{5.69}$$

in the various sectors of interest. It is clear that the coefficient of the dominant solution must remain the same throughout its region of dominance; however, the coefficient of the subdominant solution is liable to change. Moreover, on the grounds of continuity we expect that if the coefficient of the dominant solution is zero, the coefficient of the subdominant WKB solution must remain unchanged. To accommodate this phenomenon, we make a discontinuous adjustment of the subdominant term along the Stokes line where the subdominant term is least significant. The adjustment should be proportional to the amplitude of the dominant solution, so that it will vanish if the dominant solution vanishes. Thus we introduce the Stokes multiplier S, associated with a Stokes line such that the coefficient after crossing the Stokes line equals the coefficient of the subdominant term before crossing the Stokes line + S × the coefficient of the dominant term on the Stokes line.

Accordingly, suppose that the solution (5.67) describes the asymptotic behavior of the solution along the real axis for $z > 0$. Then, accordingly, the solution for $z < 0$ is given by

$$\psi = A \Theta^- + (B + AS_1)\Theta^+ \quad , \quad Arg(z) = \pi \tag{5.70}$$

according to the Stokes phenomenon. On the other hand, the solution may be contin-

ued through the lower half plane in which case the solution takes the form

$$\psi = (A - BS_2)\Theta^- + B\,\Theta^+ \quad , \quad Arg(z) = -\pi \qquad (5.71)$$

where the subscripts mean that the Stokes constants may not be the same although it turns out that $|S_1| = |S_2|$. (Heading has tabulated the values of the Stokes constants based upon the exact form of this differential equation [Heading, 1962]; however, for our purposes the only necessary information required is that the solutions undergo a Stokes phenomenon and the exact values are irrelevant.)

We may now solve the Budden problem. For a wave incident from "below" the resonance we require there to be no downward propagating wave at $z \to \infty$. This then means that the coefficient of Θ^- must be null, hence $A = 0$. This means that there is no reflected wave so that $R = 0$. We may then immediately read the Budden coefficient for transmission by comparing the values of J, which correspond to the Poynting fluxes, to be given by

$$T = \frac{|\Theta^+|^2_{Arg(z) = 0}}{|\Theta^+|^2_{Arg(z) = \pi}} \qquad (5.72)$$

We now see that the coefficients are in fact determined by the logarithmic behavior of the WKB solutions.

$$\Theta^{\pm}\big|_{\rho e^{i\theta}} = e^{\pm i k_0 (\rho e^{i\theta} - a\log(\rho)/2) \pm k_0 a\,\theta/2} \qquad (5.73)$$

So that we find immediately that

$$T = e^{-\eta} \quad , \quad \eta = \pi k_0 a \qquad (5.74)$$

which is identically the Budden result.

For a wave incident from "above" on the other hand, more information is required. Appropriate boundary conditions for this case require that no upgoing wave be found at $z \rightarrow -\infty$. This condition means that the coefficient of Θ^+ must be null at $Arg(z) = \pi$, hence $B = -AS_1$. In this case, the transmitted flux is given by

$$T = \frac{|\Theta^-|^2_{Arg(z) = \pi}}{|\Theta^-|^2_{Arg(z) = 0}} \tag{5.75}$$

whereas the reflected wave amplitude is given by

$$R = |S_1|^2 \frac{|\Theta^+|^2_{Arg(z) = 0}}{|\Theta^-|^2_{Arg(z) = 0}} = |S_1|^2 \tag{5.76}$$

Thus without further effort we may determine that

$$T = e^{-\eta} \tag{5.77}$$

as found by Budden. The reflection coefficient, however, requires more work.

If we refer to the conserved quantity J, we know that J is constant along the real axis. However, across the point $x=0$, J suffers a discontinuity. Let us consider how the quantity J changes across this discontinuity. Along the path $z = x \pm i\gamma$, J satisfies the differential equation (5.54) and undergoes the discontinuity

$$\Delta_\gamma = \pm 2k_0^2 a \int_{-\infty}^{+\infty} \frac{\gamma}{x^2 + \gamma^2} \psi \psi^* \tag{5.78}$$

The discontinuity for the differential equation under consideration then is

$$\lim_{\gamma \to 0} \Delta_\gamma = \mp 2\pi k_0^2 a \ |\psi|_{z=0}^2 \equiv \mp \Delta \quad , \quad \Delta > 0 \tag{5.79}$$

where we have recognized the form of the delta-function

$$\lim_{\gamma \to 0} \frac{\gamma}{x^2 + \gamma^2} = \pi \delta(x) \tag{5.80}$$

We should note that for small z the solutions of the differential equation are of the form

$$\psi \approx z^{1/2} \left[\alpha H_1^{(1)}(2\sqrt{z}) + \beta H_1^{(2)}(2\sqrt{z}) \right] \tag{5.81}$$

where $H^{(1)}$ and $H^{(2)}$ are the Hankel functions which take the limiting forms [Abramowitz and Stegun, 1964] for small z

$$H_1^{(1)}(2\sqrt{z}) \sim H_1^{(2)}(2\sqrt{z}) \sim \frac{-i}{\pi \sqrt{z}} \tag{5.82}$$

so that ψ is well defined at the origin. We find then that the discontinuity Δ depends upon which branch we continue the solution (i.e. whether $Arg(z) = \pm \pi$). However, if we take the boundary condition $B = 0$ and $A = 1$ in (5.70) and (5.71) we may express the value of J/k_0 to be

$$J/k_0 = \begin{cases} 1 & Arg(z) = 0 \\ e^\eta & Arg(z) = -\pi \\ e^{-\eta} - |S_1|^2 e^\eta & Arg(z) = \pi \end{cases} \tag{5.83}$$

But then we have

$$-\Delta = 1 - e^\eta = -1 + e^{-\eta} - |S_1|^2 e^\eta \tag{5.84}$$

so that

$$R = |S_1|^2 = (1-e^{-\eta})^2 \tag{5.85}$$

which is the reflection coefficient obtained by Budden.

3. Phase Integrals and the Fourth Order Equation

The method just presented may be applied in some limited sense to obtain information concerning the solutions of the fourth order equation under consideration. In particular, we shall find a close correlation between the transmission coefficients and the mode coupling previously considered. Moreover, when two of the modes are decaying or growing exponentials along the real axis, a case which occurs for large κ, the coefficients can be recovered unambiguously.

The coupled differential equation (5.2) is of the form

$$\Psi'' + M\Psi = 0 \tag{5.86}$$

where

$$M \equiv \begin{bmatrix} r - \dfrac{\kappa^2}{2} & \dfrac{\kappa^2}{2} \\[2mm] \dfrac{\kappa^2}{2} & 1 - \dfrac{\kappa^2}{2} \end{bmatrix} \tag{5.87}$$

and the vector Ψ consists of two components ψ and ϕ which correspond to the electric field amplitudes. From the adjoint of equation (5.86)

$$\Psi^{\dagger''} + \Psi^{\dagger}M^{\dagger} = 0 \tag{5.88}$$

we can form the analogous conserved quantity

$$J = i\,(\Psi^{\dagger\prime}\Psi - \Psi^{\dagger}\Psi')$$ (5.89)

which is conserved in space according to

$$J' = i\,\Psi^{\dagger}(M - M^{\dagger})\Psi$$ (5.90)

so that J, which corresponds to the Poynting flux along the z-axis, $\hat{z}\cdot(E\times B)$, is conserved along the real axis because the functions r and l are real. The function l, however is singular at the heavy ion gyrofrequency so that as for the previous Budden problem, we expect a discontinuous jump in the value of J across the singularity. The simplest model which approximates the functions r and l near the resonance and retains the essential characteristics of the dispersion relation is one in which

$$r \simeq k_r^2 \quad , \quad l \simeq k_l^2(1-a/z)$$ (5.91)

where the form of the magnetic field (5.51) has been used, with the expression for l the same as in (5.53), and r some suitable constant chosen to retain the location of the crossover frequency where $r = l$. Near the resonance, the behavior of J is completely dominated by the singularity in l so that higher order terms in z are unimportant for determining the jump in J across the cyclotron resonance. As for the Budden equation, we may determine the discontinuity across the resonance by considering the change in J along the path $z = x \pm i\gamma$. Then we find from equation (5.90) that the discontinuity is given by

$$\Delta_\gamma = \mp 2 k_l^2 a \int_{-\infty}^{+\infty} \frac{\gamma}{x^2+\gamma^2} \phi\phi^* \qquad (5.92)$$

where ϕ the lower component of Ψ. For small z ϕ behaves like the Hankel functions, which are regular [Abramowitz and Stegun, 1964], so that the discontinuity is as before

$$\lim_{\gamma \to 0} \Delta_\gamma = \mp 2\pi k_l^2 a \, |\phi|_{z=0}^2 \equiv \mp \Delta \quad , \quad \Delta > 0 \qquad (5.93)$$

As before, we see that energy flux is lost if we continue the solution above the branch point whereas energy would be gained if we were to continue the solution below the branch point.

We may also obtain a substantial amount of information concerning the asymptotic behavior of the solutions. The WKB solutions in this case are of the form

$$\Theta = \exp\left[\pm \frac{i}{\varepsilon} \int^{z} n_\pm ds \right] \qquad (5.94)$$

where the indices $n_\pm$ are the solutions to the dispersion relation (5.5). For large values of z the indices may be expanded using the approximation (5.91) to give

$$n_\pm \approx n_\pm^0 - \frac{k_l^2 a}{4z} \frac{\pm\delta + \sqrt{\delta^2 + \kappa^4/4}}{n_\pm^0 \sqrt{\delta^2 + \kappa^4/4}} \qquad (5.95)$$

where

$$n_\pm^0 = \left[\sigma - \frac{\kappa^2}{2} \pm \left[\delta^2 + \frac{\kappa^4}{4} \right]^{\frac{1}{2}} \right]^{1/2} \qquad (5.96)$$

and the zero order sum and difference functions are

$$\sigma = \frac{k_r^2 + k_l^2}{2} \quad , \quad \delta = \frac{k_l^2 - k_r^2}{2} > 0 \tag{5.97}$$

so that the four WKB solutions take the form

$$\Theta_+^{\pm} = e^{\pm i/\varepsilon(n_+ z - \beta_+ \log z/2)}$$
$$\Theta_-^{\pm} = e^{\pm i/\varepsilon(n_- z - \beta_- \log z/2)} \tag{5.98}$$

where

$$\beta_{\pm} \equiv \frac{k_l^2 a}{2} \frac{\pm \delta + \sqrt{\delta^2 + \kappa^4/4}}{n_{\pm}^0 \sqrt{\delta^2 + \kappa^4/4}} \tag{5.99}$$

so that once again the coupling is characterized by the multivalued nature of the logarithm.

From these expressions we can immediately determine the transmission coefficients for the case of incident magnetosonic waves or ion-cyclotron waves. We may once again extend the WKB solutions into the complex plane and use the dominance of the various solutions to determine transmission properties. The solutions on the positive real axis are of the form

$$\psi = A \Theta_+^- + B \Theta_-^- + C \Theta_-^+ + D \Theta_+^+ \quad , \quad Arg(z) = 0 \tag{5.100}$$

where we have written them in order of dominance in the upper half complex plane. The lower component of Ψ is of the same form with coefficients which are related to A, B, C, and D by the dispersion relation. The Stokes lines in this case are along the positive imaginary axis while the anti-Stokes lines are along the positive real axis.

According to the Stokes phenomenon we would then expect to find that on the positive

imaginary axis the solutions undergo a Stokes phenomenon and on the negative real

axis take the general form

$$
\psi = A\,\Theta_+^- + (B - AS_1)\Theta_-^- + (C - AS_2 - BS_3)\Theta_-^+
$$
$$
+ (D - AS_4 - BS_5 - CS_6)\Theta_+^+ \quad , \quad Arg(z) = \pi
$$

(5.101)

We have added Stokes constants across the region of least dominance according to a

reasonable prescription which retains the continuity of the equations in the absence of

the more dominant solutions. The boundary conditions for downgoing ion-cyclotron

waves are given by

$$
A = 1 \quad , \quad B = S_1 \quad , \quad C = D = 0
$$

(5.102)

while for downgoing magnetosonic waves the boundary conditions are

$$
A = 0 \quad , \quad B = 1 \quad , \quad C = D = 0
$$

(5.103)

We may immediately write down the asymptotic form of the transmission coefficients

in terms of the logarithmic singularity. The leading order coefficient for downgoing

ion-cyclotron waves is given by

$$
T_{IC} = \frac{|\Theta_+^-|^2_{Arg(z)=\pi}}{|\Theta_+^-|^2_{Arg(z)=0}}
$$

(5.104)

which is given immediately to be

$$
T_{IC} = e^{-\pi\beta_*/\varepsilon}
$$

(5.105)

whereas for downgoing magnetosonic waves in the absence of an incident ion-

cyclotron wave has no transmitted flux in the ion-cyclotron mode and transmission to the magnetosonic mode given by

$$T_{MS} = \frac{|\Theta_-^-|^2_{Arg(z) = \pi}}{|\Theta_-^-|^2_{Arg(z) = 0}} \tag{5.106}$$

which may be written in the form

$$T_{MS} = e^{-\pi\beta_-/\varepsilon} \tag{5.107}$$

We can make a number of observations concerning these two results. First, for $\kappa \ll \delta$, we find from equation (5.99) that T_{IC} is simply the Budden coefficient described previously. That is

$$\beta_+ = k_l a (1 - O(\kappa^4)) \tag{5.108}$$

which has little dependence on κ so that transmission for this mode may be considered to be essentially Budden tunneling and should have that character. With increasing κ, the tunneling diminishes. For large κ, we find that the coefficient approaches another constant, namely

$$\beta_+ = \frac{k_l^2 a}{2\sqrt{\sigma}} \tag{5.109}$$

indicative of Budden tunneling for nearly perpendicular propagation near the ion-ion hybrid frequency.

On the other hand, for the downgoing magnetosonic wave we find that for small κ equation (5.99) gives an intriguing result. The transmission coefficient then takes

the form

$$T_{MS} = e^{-\pi\beta_J/\varepsilon} \approx \exp\left[\frac{k_l^2 a}{\varepsilon 16 k_r \delta^2}\kappa^4\right]$$ (5.110)

We may relate this transmission coefficient to the coupling coefficient which we

obtained in section B. If we recognize that difference function is of the form

$$d = -\delta + \frac{k_l^2 a}{2z}$$ (5.111)

we find that

$$d_{cr}' = \frac{2\delta^2}{k_l^2 a}$$ (5.112)

which then demonstrates that the transmission coefficient is the same as the coupling

coefficient established in the section B, namely

$$T = \exp\left[-\frac{\pi}{8\varepsilon}\frac{\kappa^4}{d_{cr}'\sqrt{s_{cr}-\kappa^2/2}}\right]$$ (5.49)

We may make a physical interpretation of this result. For parallel propagation

transmission of the magnetosonic mode is complete $(T = 1)$. However, coupling

increases rapidly with larger values of κ, and we find that the transmission in the mag-

netosonic mode falls off substantially.

The values of the Stokes constants may not be unambiguously determined using

the methods of the previous section although a number of relationships between the

amplitudes of the various waves may be determined. For the case of a "large" gap, however, we may actually determine the coefficients unambiguously. In the case of a large gap, the WKB solution, Θ_+^- has negligible amplitude at $-\infty$, i.e. $\beta_+ \to \infty$ so that there will be no transmission in that mode. Furthermore, the restriction that no upgoing ion-cyclotron wave, Θ_+^+, be found at $-\infty$ implies that $\Delta \to 0$ so that no absorption occurs. In this case, after substantial and lengthy algebra detailed in Appendix A, it is possible to show that in the limit of a large "gap" the transmission and reflection coefficients, as defined in the appendix to be the ratio of the Poynting flux of a particular wave to that of the incident wave, are given by

$$C_{IC}^T = 1 - e^{-\pi\beta_-/\varepsilon} = 1 - C \tag{5.113}$$

$$R_{IC} = e^{-2\pi\beta_-/\varepsilon} = C^2 \tag{5.114}$$

$$C_{IC}^R = e^{-\pi\beta_-/\varepsilon}(1 - e^{-\pi\beta_-/\varepsilon}) = C(1-C) \tag{5.115}$$

where the meaning of the coefficients are illustrated in Figure 5.5. For a magnetosonic wave incident from above we find that

$$T_{MS} = e^{-\pi\beta_-/\varepsilon} = C \tag{5.116}$$

as before and

$$R_{MS} = (1 - e^{-\pi\beta_-/\varepsilon})^2 = (1-C)^2 \tag{5.117}$$

$$C_{MS}^R = e^{-\pi\beta_-/\varepsilon}(1 - e^{-\pi\beta_-/\varepsilon}) = C(1-C) \tag{5.118}$$

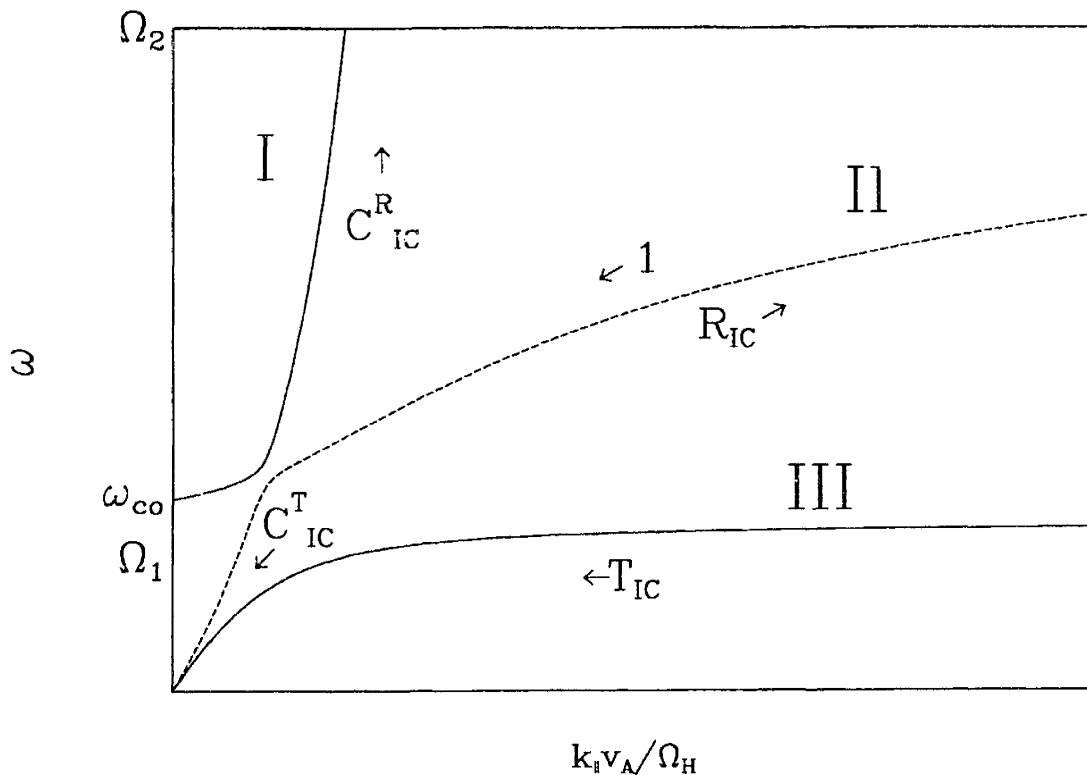This process is again illustrated in Figure 5.6.

Figure 5.5. Illustration of the meaning of the coefficients for a downgoing ion cyclotron wave. Waves are reflected back along the two upward propagating modes while a wave is transmitted on the downgoing magnetosonic branch.

As stated previously, in the case of large gap, wave propagation is entirely determined by the interaction at the crossover frequency which, as we have just shown, is characterized by the coefficient $C = e^{-\pi\beta_J/\varepsilon}$. In order to understand these results in an intuitive manner, consider the situation of Figure 5.5. A downgoing ion-cyclotron wave with unit flux encounters the crossover frequency at which point a fraction, C, is transferred from branch II to branch I. A fraction, $1-C$, continues down along mode II and is the coupled transmission coefficient C_{IC}^T. The wave which couples to branch I reflects at the cutoff frequency and once again encounters the crossover frequency as an upgoing wave. This reflected wave has amplitude C. Upon coupling, a fraction, C,
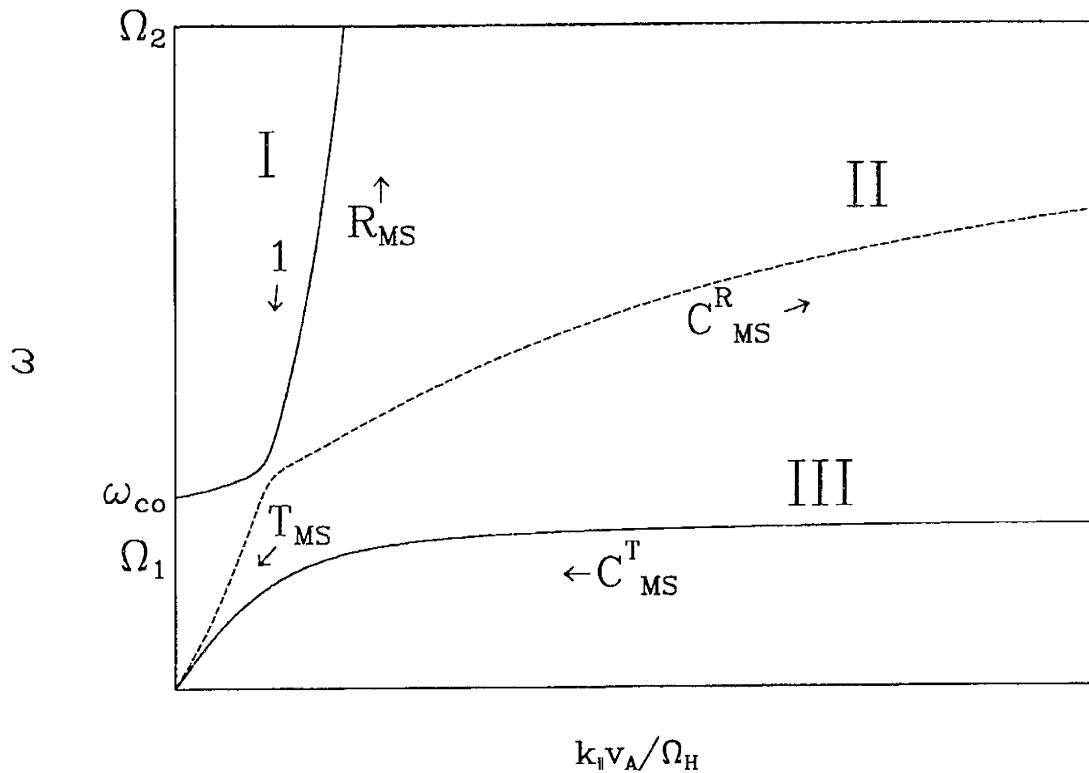
Figure 5.6. Illustration of the meaning of the coefficients for a downgoing magnetosonic wave. Waves are reflected back along the two upward propagating modes while a wave is transmitted on the downgoing magnetosonic branch.

of this reflected wave flux is coupled to branch II comprising the reflection coefficient $R_{IC} = C^2$. The fraction, $1-C$, remains on branch I and is the coupled reflected wave $C_{IC}^R = C(1-C)$. Although in the limit of a small "gap" the transmission coefficient T_{IC} is a Budden tunneling term, in the limit of a large "gap" T_{IC} vanishes.

The case of an incident magnetosonic wave is illustrated in Figure 5.6. In this case, a magnetosonic wave of unit amplitude is incident along branch I. Coupling occurs at the crossover frequency and a fraction, C, of the incident wave is coupled to branch II and comprises the transmission coefficient, $T_{MS} = C$. The fraction, $1-C$, remains on branch I, is reflected at the cutoff frequency, and again encounters the

crossover frequency as an upgoing wave. The amplitude of this reflected wave is $1-C$.
Again coupling occurs at the crossover frequency and a fraction, C, of the reflected
wave is coupled onto mode II giving the coupled reflected wave $C_{MS}^{R} = C(1-C)$, and
the remaining wave power, $R_{MS} = (1-C)^2$ is reflected along branch I. There is no cou-
pled mode C_{MS}^{T} in the limit of large "gap." As one can see, for the case of a large
frequency gap, the coefficients are well described in terms of the coupling at the cross-
over frequency.

In the case of a small "gap" it is not possible to determine the Stokes parame-
ters unambiguously although a number of relationships between them may be derived
using symmetry properties. In the following chapter we will determine the coefficients
numerically. The results which we have obtained, however, are useful in that they
provide both physical insight and a check of our numerical procedure. The method
which we have used for the Budden equation is, however, sufficient to determine the
coefficients for large κ in which case only one mode propagates at $\pm\infty$.

4. Phase Integral Solution for Large κ—Two Propagating Modes

As one can see from equation (5.95), for large enough κ, $\sigma < \kappa^2$, so that two of
the solutions become complex. That is, we find that n_+ is real and n_- is imaginary.
This means that two of the asymptotic solutions are growing along the real axis (a not-
ably unphysical situation). When this is the case, the positive and negative real axes
become Stokes lines for two of the solutions while the positive and negative imaginary
axes remain the Stokes lines for the other two solutions. The anti-Stokes lines are to

be found asymptotically along the rays

$$n_+^0 x = \pm n_-^0 y \qquad\qquad (5.119)$$

where $z = x + iy$ is the complex coordinate. This situation is easier to evaluate because each solution is dominant in one of four sectors in the complex plane.

At this point, we need to consider the concept of Stokes phenomena in somewhat more detail. Tracing Stokes coefficients in reality is only valid in the sense that in the region of maximum dominance, the coefficient of the exponential term must agree with the exact solution in an asymptotic sense. As will become clear, however, we actually require further information concerning the asymptotic behavior of the subdominant terms in order to extract the reflection and transmission coefficients. This information is important because we must determine the value of the oscillatory solutions along the real axis in the presence of an unphysical growing mode.

The WKB solutions which we have obtained are, in fact, only the terms of leading order in an asymptotic series. The concept of converging factors has lead to great improvement in accuracy of asymptotic expansions to such a degree that the subdominant series must be retained in order to obtain accurate solutions for finite values of argument. As a result, it has been determined that at least in the case of second-order equations that the changes in the coefficients take place at definite values of arg z [Heading, 1957 and references therein]. In the case of the Airy equation, for example, this change actually takes place in two definite jumps (much like a Fourier series across a discontinuity). In order to better understand this phenomena, consider the the

behavior of the asymptotic solutions to a simple parabolic cylinder equation

$$y'' + (1/2 - z^2/4)y = 0 \qquad (5.120)$$

for which the exact solutions

$$y_1 = e^{-z^2/4} \qquad (5.121)$$

and

$$y_2 = e^{-z^2/4} \int_0^z e^{\zeta^2/2} d\zeta \qquad (5.122)$$

may be obtained. The leading order WKB solutions are found to be

$$\phi_1 = e^{-z^2/4} \;,\; \phi_2 = \frac{e^{z^2/4}}{z} \qquad (5.123)$$

In the range $-\pi/4 < \arg z < \pi/4$, the asymptotic behavior for the exact solution is governed almost completely by the behavior of the descending series associated with ϕ_2. That is,

$$y_2 = \phi_2(1 + O(z^{-2})) \qquad (5.124)$$

and the coefficient multiplying the subdominant solution although nonzero (something of the order of $\frac{\sqrt{2}}{z}$), is asymptotically small (as opposed to being a Stokes constant) and for all practical computational purposes need not be considered. On the other hand, for $3\pi/4 > \arg z > \pi/4$, an abrupt change in the coefficient of ϕ_1 occurs as it becomes dominant across the ray $\arg z = \pi/4$. The contour of integration may then be taken up the positive imaginary axis and then back along a ray. That is

$$\int_0^z e^{\zeta^2/2} d\zeta \rightarrow \int_0^{i\infty} e^{\zeta^2/2} d\zeta + \int_\Gamma e^{\zeta^2/2} d\zeta + \int_{i\arg z \, \infty}^z e^{\zeta^2/2} d\zeta \qquad (5.125)$$

where the contour Γ is an arc at ∞ connecting the rays along the imaginary axis and

the ray arg z. This is practical because the integral taken along the contour, Γ, van-

ishes for $3\pi/4 > $ arg $z > \pi/4$. In this region it is not difficult to show that

$$y_2 = i\sqrt{2\pi}\phi_1 + \phi_2(1 + O(z^{-2})) \qquad (5.126)$$

The integral along the imaginary axis provides the first term whereas the subdominant

series arises from the integral along the ray arg z. It should be noted that the descend-

ing series for ϕ_2 is the same as for the region in which it is dominant, demonstrating

that no Stokes phenomena occurs for the asymptotic solution which is dominant along

the real axis. Moreover, at the anti-Stokes line the coefficient of ϕ_1 undergoes a

discontinuous increment of $i\sqrt{2\pi}$. This behavior arises because the contour between 0

and z is dominated by the behavior near the upper limit, z, for arg $z < \pi/4$, but is

dominanted by its behavior near the lower limit, 0, for $3\pi/4 > $ arg $z > \pi/4$. This fact

is manifest by the deformation of the contour along the imaginary axis (the arc at

infinity along Γ contributes nothing for arg $z > \pi/4$ but is exponentially large and not

useful for arg $z < \pi/4$). Similarly, another discontinuous jump in the coefficient occurs

for arg $z = -\pi/4$ so that in the range $-3\pi/4 < $ arg $z < -\pi/4$

$$y_2 = -i\sqrt{2\pi}\phi_1 + \phi_2(1 + O(z^{-2})) \qquad (5.127)$$

For this case the Stokes coefficient occurs as the result of two discontinuous jumps

along the anti-Stokes lines.

In Appendix B we demonstrate using an integral equation, that the Stokes coefficients for the asymptotic solutions of the fourth order equation which we are considering change abruptly at definite values of arg z in the region of maximum subdominance. It would appear that these jumps occur at three distinct values of arg z—along the Stokes lines and the bounding anti-Stokes lines of the maximally subdominant region. The change only occurs in the coefficient of the most subdominant solution. We may therefore determine the appropriate asymptotic behavior of the solution of interest if the relevant WKB solutions involved in the analysis are not maximally subdominant in the region where they must be evaluated. Because the solutions with growing (decaying) exponential behavior do not contribute to the Poynting flux on the real axis, we need only evaluate the coefficients of the oscillatory solutions in order to determine the transmission and reflection coefficients. The oscillatory solutions are not maximally subdominant along the real axis, and therefore, we may determine the coefficients unambiguously. In order to incorporate the Stokes phenomena we introduce the Stokes multipliers such that upon crossing a Stokes line on which a WKB solution is maximally subdominant the coefficient of that term equals the coefficient before crossing the Stokes lines + $\sum_{j} S_j \times$ the coefficients of the jth dominant term on the Stokes line.

Appropriate boundary conditions require that at $\pm\infty$ the exponentially growing modes be absent. In addition, appropriate boundary conditions require that no upgoing wave be found at $-\infty$. In order to satisfy these conditions, we assume along or above

the positive real axis that the solution takes the form

$$\psi = A\ \Theta_+^- + B\ \Theta_-^- + C\ \Theta_-^+ + D\ \Theta_+^+ \quad , \quad \text{Region II} \tag{5.128}$$

Using the rules stated above we may continue the solution into the following sectors illustrated in Figure 5.7.

$$\psi = A\ \Theta_+^- + B\ \Theta_-^- + C'\Theta_-^+ + D\ \Theta_+^+ \quad , \quad \text{Region III} \tag{5.129}$$

with

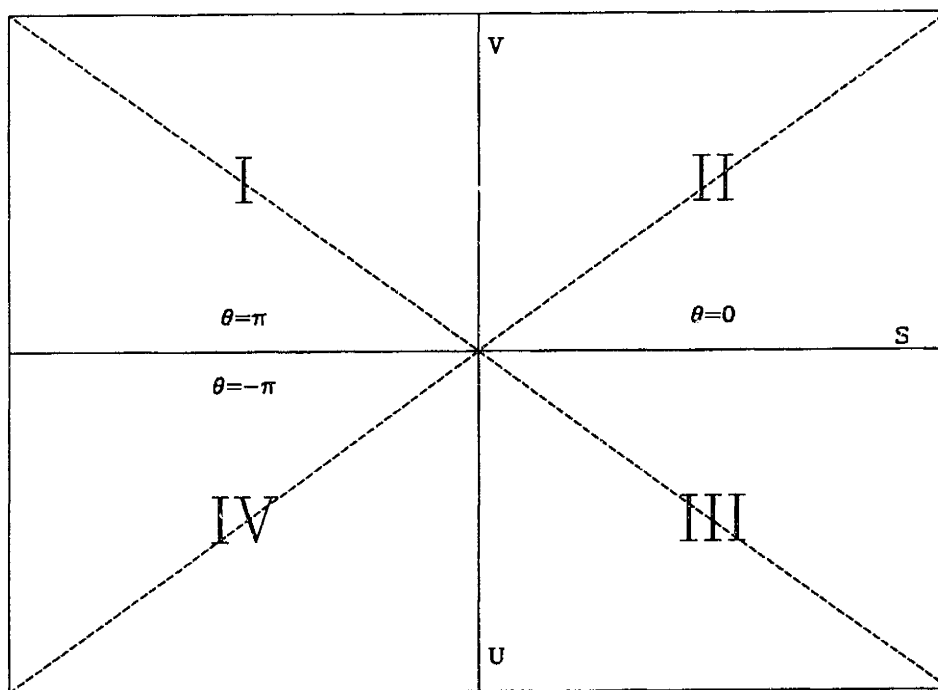$$C' = C - AS_1 - BS_2 - DS_4 \tag{5.130}$$

Figure 5.7. Sectors of the complex plane divided according to regions of dominance and subdominance of the asymptotic WKB solutions. The Stokes lines and anti-Stokes lines are solid and dashed respectively.

$$\psi = A'\Theta_+^- + B\,\Theta_-^- + C'\Theta_-^+ + D\,\Theta_+^+ \quad , \quad \text{Region IV} \tag{5.131}$$

with

$$A' = A - BU_2 - C'U_3 - DU_4 \tag{5.132}$$

and

$$\psi = A\,\Theta_+^- + B\,\Theta_-^- + C\,\Theta_-^+ + D'\Theta_+^+ \quad , \quad \text{Region I} \tag{5.133}$$

with

$$D' = D + AV_1 + BV_2 + CV_3 \tag{5.134}$$

where S, U, and V are Stokes constants. In order to satisfy the boundary conditions for downgoing waves, we require that

$$B = C = D' = 0 \; , \; A = 1 \tag{5.135}$$

Then we may immediately write down the transmission and reflection coefficients

$$T_{IC} = \frac{|\Theta_+^-|^2_{Arg(z)=\pi}}{|\Theta_+^-|^2_{Arg(z)=0}} \tag{5.136}$$

which as before takes the form

$$T_{IC} = e^{-\pi\beta_*/\varepsilon} \tag{5.137}$$

and

$$R_{IC} = \frac{|\Theta_+^+|^2_{Arg(z)=0}}{|\Theta_+^-|^2_{Arg(z)=0}}|V_1|^2 = |V_1|^2 \tag{5.138}$$

In order to determine the Stokes constant V_1 we may consider the situation with

$B = C = D = 0$, $A = 1$ from which we can compute the Stokes constant if we again

invoke the conservation law (7.89). As it turns out, on the real axis, the exponentially

growing solutions do not contribute to the Poynting flux so that the conserved quantity

J/n_+ is found to be

$$
J/n_+ = \begin{cases} 1 & Arg(z)=0 \\ e^{\pi \beta_-/\varepsilon} & Arg(z)=-\pi \\ e^{-\pi \beta_-/\varepsilon} - |V_1|^2 e^{\pi \beta_-/\varepsilon} & Arg(z)=\pi \end{cases} \qquad (5.139)
$$

Once again, from the energy discontinuity

$$
-\Delta = 1-e^{\pi \beta_-/\varepsilon} = -1+e^{-\pi \beta_-/\varepsilon} - |V_1|^2 e^{\pi \beta_-/\varepsilon} \qquad (5.140)
$$

we obtain the Budden-like reflection coefficient

$$
R_{IC} = |V_1|^2 = (1-T_{IC})^2 \qquad (5.141)
$$

D. Mode Coupling at Low Frequencies, Large κ

The result which we have just obtained for large values of κ does not depend

critically on the crossover frequency in that the factor β_+ depends weakly on the loca-

tion of the crossover frequency. From the analysis described in §5.III.A, we find that

for large values of κ, the saddle point associated with the crossover frequency is

located far from the real axis and is near the hydrogen cyclotron frequency. As a

result, coupling is not strongly dependent upon the location of the saddle point associ-

ated with the crossover frequency. However, in Figure 5.3, we find that the coupling

point associated with zero frequency at small κ, approaches the oxygen resonance for

large values of κ and is therefore of primary interest. As described previously, the transition from four propagating modes to two propagating modes occurs at a critical value of κ. Assuming that r and l take a simple form such as in equation (5.91), the cutoff condition (5.15) implies that

$$z_{co} = a\frac{1-\kappa^2/4k_r^2}{1-\sigma\kappa^2/k_r^2k_l^2} \tag{5.142}$$

We then find that the abrupt change in the behavior of the modes occurs at the critical value

$$\kappa^2 = \frac{k_r^2k_l^2}{\sigma} \tag{5.143}$$

For values smaller than this value of κ, the mode conversion processes are determined primarily from the coupling point associated with the crossover frequency. For intermediate values of κ, $\frac{k_r^2k_l^2}{\sigma}<\kappa^2<2k_r$, four modes propagate in the vicinity of the heavy ion resonance although the magnetosonic branch is cut off at some point below the gyrofrequency and does not propagate above the gyrofrequency. In this case, the dominant saddle point is that associated with zero frequency at small κ and the oxygen resonance at large κ. For larger κ, $\kappa^2>2k_r$, the downgoing ion-cyclotron wave is cutoff above the oxygen resonance at a frequency which approaches the ion-ion hybrid frequency and only two modes propagate. In this case the transmission properties may be obtained by expanding about the coupling point associated with the cutoff condition $rl-\kappa^2s = 0$. In the ensuing analysis we will follow the reasoning of Lashmore-Davies

et al. [1985] and Fuchs *et al.* [1981, 1985] as described in §5.III.A, and we will con-

sider the cases of intermediate and large κ separately.

The expression for the location of the saddle point in the complex plane is, as

before, given by the condition

$$d^2 + \frac{\kappa^4}{4} = 0 \tag{5.19}$$

As discussed in §5.III.A, the solutions to this condition are complex conjugate pairs

which satisfy a quartic equation as plotted in Figure 5.3. In this case the potential

again takes the form (5.41). The fact that the roots occur in complex conjugate pairs

means that the function, $d^2 + \kappa^4/4$, will have the form of a complex conjugate barrier

equation described by the Weber equation. It is once again both tractable and some-

what reasonable to assume the form of r and l as assumed in equation (5.91). In this

case, the potential takes the form

$$Q(\xi) = \frac{\delta^2 + \kappa^4/4}{4\xi^2(s - \kappa^2/2)} \left[(\xi - \xi_r)^2 + \xi_i^2 \right] \tag{5.144}$$

where

$$\xi = \xi_r \pm \xi_i = \frac{k_l^2 a}{2} \frac{\delta \pm i \, \kappa^2/2}{\delta^2 + \kappa^4/4} \tag{5.145}$$

is the location of the complex conjugate roots (for large κ the imaginary part dom-

inates as is the case for the actual solutions to the third order equation). Once again

the essential asymptotic features of the embedded dispersion relation are retained if we

evaluate the constant factor in equation (5.144) at some convenient point, such as the

real frequency above. If we then make the judicious choice for the variables

$$k_0^2 = \frac{\delta^2 + \kappa^4/4}{\xi_r^2(s_r - \kappa^2/2)}$$

(5.146)

and

$$\beta = \frac{\xi_i}{2} = \frac{k_l^2 a}{2(\delta^2 + \kappa^4/4)} \frac{\kappa^2}{4}$$

(5.147)

(where the index r indicates that the function is to be evaluated at ξ_r) then the embedded equation is of the form of the Weber equation (5.46) which has the transmission coefficient [Fuchs, et al., 1985; Lashmore Davies et al., 1985]

$$T = e^{-2\pi k_0 \beta^2/\varepsilon}$$

(5.148)

where the argument of the exponential takes the form

$$k_0\beta^2 = \frac{k_l^2 a}{8} \frac{\kappa^4/4\delta}{\sqrt{(\delta^2 + \kappa^4/4)(\kappa^4/4\delta + \kappa^2/2 - k_r^2)}}$$

(5.149)

Near the upper limit of validity, the two results have a reasonably simple limit. For $\kappa^2/2 = k_r^2$

$$\beta_+ = \frac{k_l^2 a}{2\sqrt{\delta^2 + k_r^4}}$$

(5.150)

whereas the equivalent coefficient from the saddle point becomes

$$2k_0\beta^2 = \beta_+ \frac{k_r^2}{2\sqrt{\delta}}$$

(5.151)

yielding roughly the same expression. Over the range of densities for which absorption is strong (0.5-5%), the ratio, $k_r^2/2\sqrt{\delta}$ takes values ranging from 1.3 to 0.6 depending on the density ratio and the two results are in reasonable agreement. Hence, we can understand that the coupling which arises at low frequencies results from coupling at the saddle point which occurs near the oxygen resonance for large values of κ.

The form of the reflection coefficient may be understood physically in the same manner that we understood coupling for smaller κ. In this case, coupling between the modes occurs below the heavy ion gyrofrequency. As illustrated in Figure 5.8, incident waves along mode II couple at the complex coupling point. A fraction,
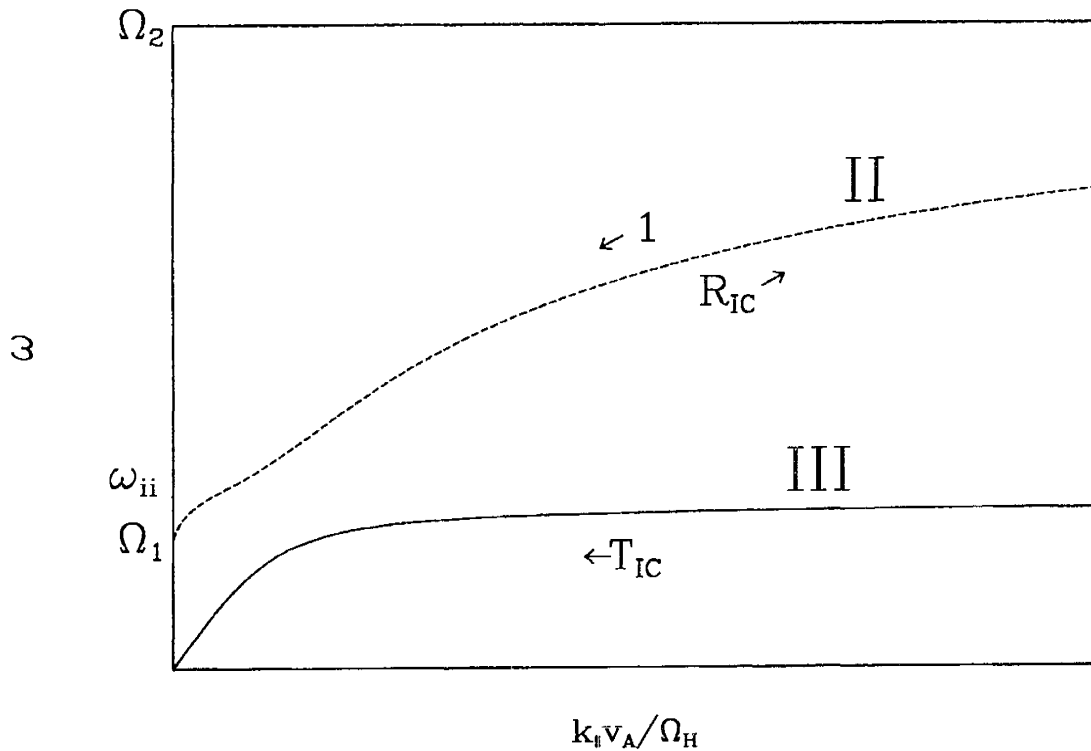

Figure 5.8. Illustration of the physical meaning of the coefficients for a downgoing ion-cyclotron wave for large angle of propagation. Waves are transmitted onto mode III and reflected back along mode II.

$T_{IC} = T = e^{-\pi\beta_+}$, is transferred to branch III. The remaining wave energy, $1-T$, continues along branch II, is reflected at the cutoff frequency for mode II and once again encounters the coupling point. The two waves couple again and a fraction, $1-T$, of the remaining wave power is found on branch II giving the reflection coefficient, $R_{IC} = (1-T)^2$. The rest of the wave power is absorbed at the resonance.

For larger values of κ we must expand about the cutoff-resonance pair which arises near the ion-ion hybrid frequency. In this case,

$$D(k_c,z) = rl - \kappa^2 s \qquad (5.152)$$

and

$$D_{kk}(k_c,z) = -2(r + l - \kappa^2) \qquad (5.153)$$

so that the coupling potential then takes the form

$$Q = \frac{rl - \kappa^2 s}{r + l - \kappa^2} \qquad (5.154)$$

Once again, the functions may be expanded about the gyrofrequency, $\Omega_{c1} = \omega(1-z)$, in which case the potential takes the form

$$Q = \frac{c + dz}{f + gz} \qquad (5.155)$$

where

$$c = v_{co}^2 - 1 - \kappa^2(v_{ii}^2 - 1)$$
$$d = 2(v_{co}^2 - v_{ii}^2 \kappa^2)$$
$$f = 2(v_{ii}^2 - 1) \tag{5.156}$$
$$g = 2((v_2^2 - 1)\kappa^2 + 2v_{ii}^2)$$

and

$$v_2 = \Omega_{c1}/\Omega_{c2} \quad , \quad v_{co} = \Omega_{c1}/\omega_{co} \quad , \quad v_{ii} = \Omega_{c1}/\omega_{ii}$$

are various mass and density ratios. We recognize this potential to be a Budden equation with a cutoff and resonance. With the appropriate change of variables

$$x = -(f + gz) \tag{5.157}$$

we recover the traditional form of the Budden equation (5.52) with

$$k_0^2 = d/g^3 \quad , \quad \alpha = cg/d - f \tag{5.158}$$

The transmission coefficients for the Budden equation are well known

$$T = e^{-\pi k_0 \alpha / \varepsilon} \quad , \quad R = (1-T)^2 \tag{5.159}$$

In the limit of large κ the potential takes the form

$$Q \approx s \sim -\frac{\Omega_{c1}^2 \Omega_{c2}^2}{\omega_{ii}^2} \frac{(\omega^2 - \omega_{ii}^2)}{(\omega^2 - \Omega_{c1}^2)(\omega^2 - \Omega_{c2}^2)} \tag{5.160}$$

which exhibits a cutoff at the ion-ion hybrid frequency and a resonance at the oxygen gyrofrequency. Expanding s about the gyrofrequency

$$s \approx \sigma(1 - k_l^2 a/2\sigma z) \tag{5.161}$$

we find that the coefficient takes the form

$$k_0\alpha = \beta_+ = \frac{k_l^2 a}{2\sqrt{\sigma}}$$

(5.162)

in agreement with (5.109) of the previous section.

Comparing both this result and the result for intermediate κ, we find that both

coefficients are of the Budden form with transmission and reflection coefficients given

by T and $(1-T)^2$ respectively. These results compare well with the form (5.137,

5.141) which we obtained using the phase-integral analysis. In this analysis, we have

three parameters: k_r, k_l and a. These three parameters are sufficient to retain the loca-

tion of the resonance (Ω_{c1}), crossover frequency (ω_{cr}), cutoff frequency (ω_{co}), and

ion-ion hybrid frequency (ω_{ii}). Thus, in some sense we can form a uniform approxi-

mation which retains the characteristics of the crossover and cutoff frequencies for

small κ but retains the characteristics of the ion-ion hybrid resonance for perpendicular

propagation. This linear approximation is good if the coupling is dominated by one or

the other of the two coupling points, but if both coupling points are of significant

importance, one suspects that the linear approximation will fail for the phase-integral

approach.

IV. Summary

In this chapter we have explored the analytic properties of the mode conversion

processes. We have found that near the crossover-cutoff-resonance triplet the pro-

pagating modes couple strongly, and substantial energy may be exchanged between

modes. For small values of κ, we have determined that the ion-cyclotron mode tunnels in a manner described by the Budden equation, and substantial wave power will be transmitted and absorbed for nearly parallel propagation. We have also shown that this tunneling factor drops off with larger κ, vanishing as κ becomes the order of 1 (in which case the approximation is not valid). For larger angles of propagation, this mode continues to be characterized by Budden tunneling; however, in this case, the mode does not interact with the nonpropagating magnetosonic wave. For large angles of propagation, the mode is described by a simple expression for tunneling at the ion-ion hybrid resonance. Because the "gap" which characterizes this tunneling is smaller than that for parallel propagation, we expect that the tunneling and absorption will be of the same order as for parallel propagation.

Incident magnetosonic waves are only of interest for reasonably small κ because for larger κ they do not propagate. For parallel propagation the coupling is negligible and the mode propagates without much interaction. However, the coupling increases rapidly as κ^4. For large κ the coupling is reasonably complete and all the wave power is reflected. The reflection occurs because the magnetosonic mode couples completely to the LHCP wave which is cutoff far above the oxygen resonance so that the tunneling barrier becomes insuperable.

In the next section, we will explore the numerical value of these coefficients. In particular, we will solve the differential equations numerically in the regimes where we have not obtained the coefficients. As we shall demonstrate, the basic features of the analytical results are retained.

CHAPTER 6

MODE CONVERSION—NUMERICAL CONSIDERATIONS

In the preceding chapter we have discussed the asymptotic behavior of the modes near the crossover-cutoff-resonance triplet of frequencies for the given model. We determined that the behavior of the modes across this region which corresponds to some localized region in spatial altitude would be characterized by various transmission and absorption coefficients. We have in all cases determined the primary transmission coefficient, and in the case of a large "gap," we have determined the reflection coefficients as well. For the case of large angle of propagation, we have also unambiguously determined the coefficients for the ion-cyclotron mode (the magnetosonic mode does not propagate in that regime). In all cases, the transmission was described by Budden-like transmission coefficients and a definite absorption characterized the transmission process. Ion heating (particularly of the cold bulk plasma population) may be inferred from the wave power which is absorbed. In addition, the thermal population should also damp on the transmitted ion-cyclotron wave providing an additional source for heating.

In order to expand upon the results which we have obtained analytically and to unambiguously determine the wave power associated with each mode, we will obtain a numerical solution to the differential equation associated with this problem. In particular, in the regime where the tunneling "gap" is small we can obtain the exact solu-

tions to the differential equation and from these extract coefficients. The advantages of a numerical solution are primarily that we can retain the presence of both resonances in the solution, and secondarily, we can model the variations in the magnetic field in a more realistic manner with a cubic dependence on altitude rather than a simple linear calculation. As we shall see, the presence of the extra terms does complicate the mode conversion process slightly. In addition, we shall see that at low altitudes the magnetosonic and ion-cyclotron branches couple strongly (this is the result of the coupling point at zero frequency described in the previous chapter) so that the transmitted wave amplitudes tend to be functions of altitude.

In the following sections we will develop and implement a reasonable procedure for extracting the values of the coefficients numerically. These coefficients can then be compared with the analytical results presented in the preceding chapter.

I. Numerical Procedure

A. Basic Equations

We wish to obtain numerical solutions to the fourth order coupled differential system (5.85) described in the preceding chapter, namely

$$\varepsilon^2 \psi'' + (r - \frac{\kappa^2}{2})\psi + \frac{\kappa^2}{2}\phi = 0$$

$$\varepsilon^2 \phi'' + (l - \frac{\kappa^2}{2})\phi + \frac{\kappa^2}{2}\psi = 0$$

(6.1)

with the small parameter ε and functions r and l as defined previously. If we assume a functional dependence of the magnetic field

$$\Omega_{c1} = \omega g(z)$$

(6.2)

then the functions r and l depend only on the function g and the various mass and density ratios. In particular, the rescaled Stix functions take the form

$$\frac{r}{l} = \pm \frac{v_{co} \pm g}{(1 \pm g)(v_2 \pm g)} \frac{g}{g_A}$$

(6.3)

where the constant ratios v are defined to be

$$v_2 = \Omega_{c1}/\Omega_{c2} \quad , \quad v_{co} = \Omega_{c1}/\omega_{co}$$

(6.4)

and the function g_A contains the dependence of the parameter ε along the field line, namely the dependence of k_A, which varies as the inverse of the Alfvèn velocity $(B^{-1} n^{1/2})$. For simplicity, we shall assume throughout the analysis that g_A remains constant (i.e. that the Alfvèn velocity remains fixed). Such an assumption is certainly reasonable if the region of coupling is localized. In addition, such an assumption also allows us to match the WKB solutions more easily in the region of high field (low altitude). A more realistic manner in which to incorporate the actual decrease in the Alfvèn velocity would be to incorporate mode solutions on the low altitude side of the resonance whose eigenvalues are determined by appropriate ionospheric boundary conditions [Lysak and Dum, 1983; Lysak, 1985]. Although perhaps slightly less realistic, our assumption, $g_A = 1$, should be sufficient to determine the coefficients to first order, and it is to be understood that inclusion of ionospheric boundary conditions is beyond the scope of the present work.

The function g contains all the essential information with regard to magnetic field variations. The most reasonable dependence for g on altitude would be that of a dipole field. We also require that $g = 1$ at the altitude at which the frequency of the wave matches the local oxygen gyrofrequency. Thus we expect that in physical coordinate r and scaled coordinate z the function f take the form

$$g = \frac{L_B^3}{r^3} = \frac{1}{z^3} \qquad (6.5)$$

where L_B is the factor which appears in ε. Then the proper choice for L_B in this instance is the altitude at which coupling occurs (the order of R_E).

Having thus relegated all functional dependence into the functions r and l through the function g we may solve the differential equation (6.1) numerically. However, as discussed at length in the preceding chapter, the differential equation has a regular singular point at the location of the plasma resonance, namely where $z = 1$. We have plotted the functions r and l in Figure 5.2 of the previous chapter. For large values of z we see that $l > r$, and at the local crossover frequency $r = l$. The function l is characterized by a zero at the local cutoff frequency and a pole at the heavy ion resonance. The solution to the differential equation (6.1) is multivalued and has a branch point at $z = 0$, so that as we have seen in the previous chapter, in order to retain the appropriate physical behavior, we must continue the solution above the pole which may be physically interpreted as damping. The differential equation (6.1) must therefore be suitably extended into the upper half of the complex plane so that the pole may be circumvented.

B. Numerical Technique

In order to solve the differential equation (6.1) numerically we solve the four

first order ODE's

$$Y' = MY \tag{6.6}$$

where

$$Y = \begin{bmatrix} \psi \\ \psi' \\ \phi \\ \phi' \end{bmatrix} \quad , \quad M = \begin{bmatrix} 0 & 1 & 0 & 0 \\ \dfrac{\kappa^2}{2} - r & 0 & -\dfrac{\kappa^2}{2} & 0 \\ 0 & 0 & 0 & 1 \\ -\dfrac{\kappa^2}{2} & 0 & \dfrac{\kappa^2}{2} - l & 0 \end{bmatrix} \tag{6.7}$$

This system of equations constitutes two fourth order equations for for the real and

imaginary part of Y. If we wish to solve this differential equation along some

parameterized path in the complex plane, $z(\tau)$, characterized by a real parameter τ, we

may change solution vectors according to the prescription

$$y_1 = \psi(z(\tau)) \quad , \quad y_2 = \frac{dy_1}{d\tau} = \psi' \frac{dz}{d\tau} \quad , \quad y_3 = \phi(z(\tau)) \quad , \quad y_4 = \phi' \frac{dz}{d\tau} \tag{6.8}$$

then the differential equation (A2) takes the form

$$\frac{dY}{d\tau} = M_1 Y + \left[\frac{dz}{d\tau} \right]^2 M_2 Y + \frac{d^2 z}{d\tau^2} M_3 Y \tag{6.9}$$

where the matrices, M_j, are

$$\mathbf{M}_1 = \begin{bmatrix} 0 & 1 & 0 & 0 \\ 0 & 0 & 0 & 0 \\ 0 & 0 & 0 & 1 \\ 0 & 0 & 0 & 0 \end{bmatrix} \ , \ \mathbf{M}_2 = \begin{bmatrix} 0 & 0 & 0 & 0 \\ \dfrac{\kappa^2}{2} - r & 0 & -\dfrac{\kappa^2}{2} & 0 \\ 0 & 0 & 0 & 0 \\ -\dfrac{\kappa^2}{2} & 0 & \dfrac{\kappa^2}{2} - l & 0 \end{bmatrix} \ , \ \mathbf{M}_3 = \begin{bmatrix} 0 & 0 & 0 & 0 \\ 0 & 1 & 0 & 0 \\ 0 & 0 & 0 & 0 \\ 0 & 0 & 0 & 1 \end{bmatrix} \quad (6.10)$$

Note that in the case that $\tau = z$ equation (6.9) reduces to equation (6.6). The differential equation (6.9) may then be integrated in the real variable, τ, by means of a well known integrating scheme such as the Runge-Kutta, Bulirsch-Stoer, or the predictor-corrector method. At some point, we may decide to make a discontinuous change in parameterized paths. That is, we may change from the solution, Y_1, along one parameterized path, $z_1(\tau)$, to the solution, Y_2, along another parameterized path, $z_2(\tau)$, such that $z_1(\tau_0) = z_2(\tau_0)$. In order that Y_1 and Y_2 describe the same solution, we must match the solutions according to the continuity of the analytic functions ψ and ϕ so that

$$\mathbf{N}_2 Y_1 = \mathbf{N}_1 Y_2 \ , \quad \tau = \tau_0 \qquad (6.11)$$

with

$$\mathbf{N}_j = \begin{bmatrix} 1 & 0 & 0 & 0 \\ 0 & \dfrac{dz_j}{d\tau} & 0 & 0 \\ 0 & 0 & 1 & 0 \\ 0 & 0 & 0 & \dfrac{dz_j}{d\tau} \end{bmatrix} \qquad (6.12)$$

In order to obtain the correct branch of the multivalued solution of the differential equation (6.9) we must solve the differential equation along a path which passes above the pole at $z = 0$ in the complex plane. Suppose that we know the solution, Y, at some point, z_0, along the negative real axis. In order to determine the value of the solution at some point, z, along the real axis, we may integrate the differential equation (6.9) along the parameterized path as illustrated in Figure 6.1
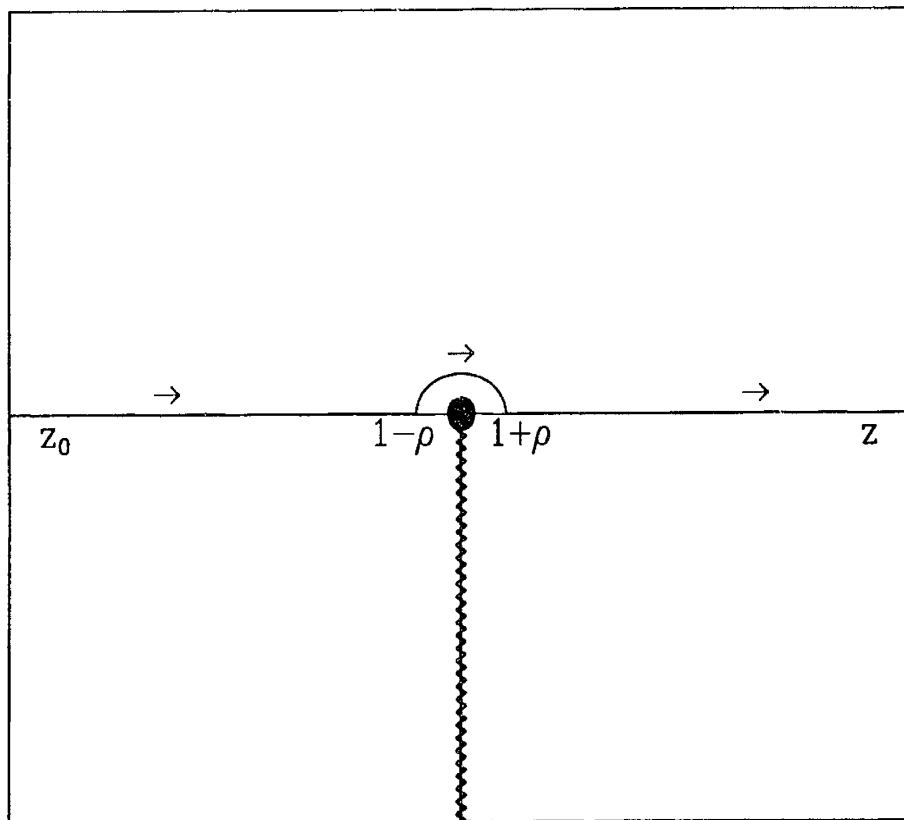

Figure 6.1. The parameterized path along which we solve the differential equation consists of three contours. The first integrates along the real axis to some point ρ. To continue the solution to the positive real axis, we take a contour along a circular arc above the pole. Finally the solution may be obtained by continuing the solution along the real axis.

$$z_1(\tau) = \tau \quad , \quad z_0 < \tau < 1-\rho$$

$$z_2(\tau) = \rho \exp\left[i\frac{\pi}{2}(1+\frac{1-\tau}{\rho})\right] \quad , \quad 1-\rho < \tau < 1+\rho \qquad (6.13)$$

$$z_3(\tau) = \tau \quad , \quad 1+\rho < \tau < z$$

which consists of integration along the real axis from z_0 to $1-\rho$ (recall that the pole is at $z = 1$) followed by integration along a circular arc above the pole to $1+\rho$ on the real axis. Finally, the solution at z may be obtained from further integration along the real axis. The solution must not depend on the choice of ρ or for that matter upon the choice of parameterized path. This requirement provides an additional check on the reliability of the procedure.

A general solution to the differential equation may then be obtained by taking four different initial conditions at the point z_0 which correspond to four linearly independent solutions. Once we have found a general solution to the differential equation we may decompose it into its constituent WKB solutions Θ as discussed in the previous chapter. Far from the coupling region, the WKB solutions are asymptotically close (in the parameter ε) to the actual solutions.

C. Extracting the Coefficients

In the region where the WKB approximation is valid, far from the coupling region, the solutions to the differential equation are asymptotically close to the set of basis functions

$$\Theta_1 = n_+^{-1/2} \exp\left[-\frac{i}{\varepsilon}\int^z n_+(z)\,dz\right]$$

$$\Theta_2 = n_+^{-1/2} \exp\left[+\frac{i}{\varepsilon}\int^z n_+(z)\,dz\right]$$

$$\Theta_3 = n_-^{-1/2} \exp\left[-\frac{i}{\varepsilon}\int^z n_-(z)\,dz\right] \tag{6.14}$$

$$\Theta_4 = n_-^{-1/2} \exp\left[+\frac{i}{\varepsilon}\int^z n_-(z)\,dz\right]$$

which are equivalent to the WKB solutions in the asymptotic regime (the WKB solutions are the same but have a common factor, $n_+^2 - n_-^2$, in the denominator). The functions $n_\pm$ have been defined previously in Chapter 3 and have nontrivial spatial dependence according to the function g. For parallel propagation these WKB solutions correspond to a downgoing LHCP wave, upgoing LHCP wave, downgoing RHCP wave, and an upgoing RHCP wave respectively. This set of WKB solutions provides a suitable set of basis functions in the asymptotic regime far away from the pole in the complex plane.

In some region far to the left of the coupling region along the negative real axis and far to the right along the positive real axis the WKB solutions are reasonable approximations to the actual solutions. In the region near the pole, we may obtain the exact solution numerically. The boundary conditions which we will impose on the exact solutions are related to the coefficients of the WKB solutions in the regions where they are valid. What we must do then is to patch together the two regions where the WKB solutions are valid using the exact solution as illustrated in Figure 6.2.
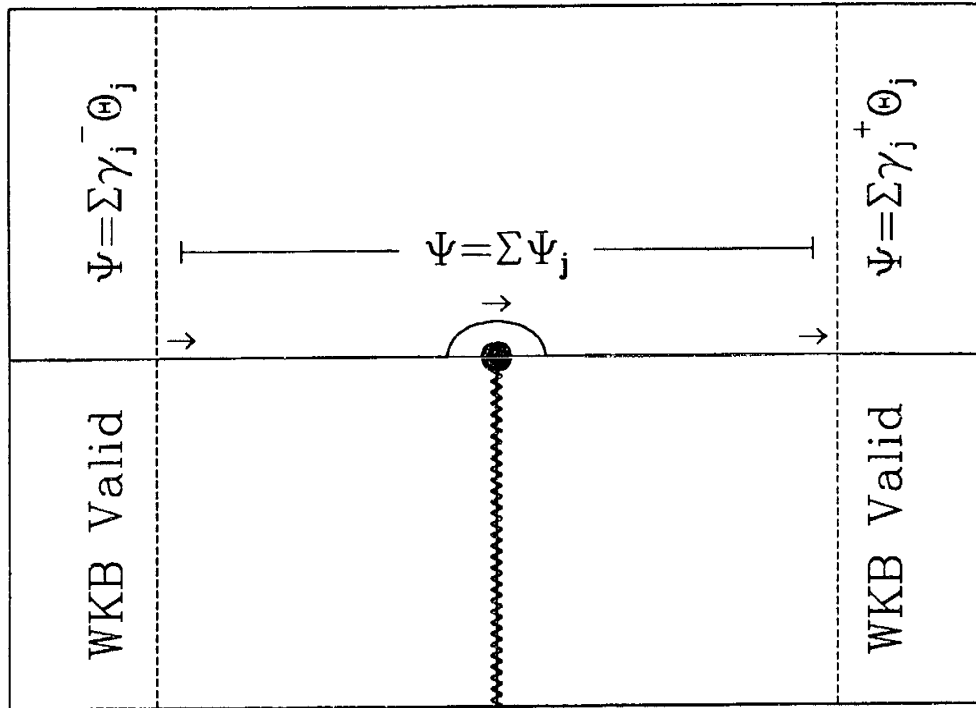
Figure 6.2. In regions far from the pole the WKB solutions are asymptotically valid. The numerical solution connects the regions in which the WKB solutions are accurate.

Suppose that we have obtained four linearly independent solutions, ψ_j, to the upper component of the differential equation (6.1) using the numerical techniques described in the previous chapter. Then we may construct a general solution

$$\psi = \sum_j \alpha_j \psi_j \qquad (6.15)$$

to the differential equation, where the coefficients, α_j, are chosen to satisfy the appropriate boundary conditions. In order to determine the α_j, we must decompose the solution ψ into the WKB solutions above and below the coupling region and impose the boundary conditions consonant with physical considerations. In other words

$$\psi = \sum_j \alpha_j \psi_j = \sum_l \gamma_l^{\pm} \Theta_l \quad , \quad z \to \pm\infty \tag{6.16}$$

where the decomposition will be different along the positive and negative real axis in light of the Stokes phenomena which we already discussed in Chapter 5.

The values of $\gamma^{\pm}$ must be consistent with the boundary conditions related to our problem. For a downgoing magnetosonic wave we require that

$$\gamma^+ = \begin{bmatrix} 0 \\ \tilde{C}_R \\ 1 \\ \tilde{R} \end{bmatrix} \quad , \quad \gamma^- = \begin{bmatrix} \tilde{C}_T \\ 0 \\ \tilde{T} \\ 0 \end{bmatrix} \tag{6.17}$$

Physically, these conditions correspond to no upgoing waves from below the coupling region, and above the coupling region, the only incident wave is the downcoming approximately RHCP mode. The coefficients refer to transmission in the incident mode, $\tilde{T}$; reflection in the incident mode, $\tilde{R}$; transmission in the coupled mode, $\tilde{C}_T$; and reflection in the coupled mode, $\tilde{C}_R$. For an incident ion-cyclotron wave, we require that the coefficients, γ, take the form

$$\gamma^+ = \begin{bmatrix} 1 \\ \tilde{R}' \\ 1 \\ \tilde{C}'_R \end{bmatrix} \quad , \quad \gamma^- = \begin{bmatrix} \tilde{T}' \\ 0 \\ \tilde{C}'_T \\ 0 \end{bmatrix} \tag{6.18}$$

consonant with the physical boundary conditions.

In order to determine the coefficients, α_j, we must decompose the linearly independent functions, ψ_j, into the constituent WKB solutions on both the positive and

negative imaginary axis. Again, in light of the Stokes phenomena, the expansions are

not the same. Then

$$\psi_j = \sum_k \beta_{jk}^{\pm} \Theta_k \ , \ z \rightarrow \pm\infty \tag{6.19}$$

which determines the relationship between the coefficients

$$\gamma_i^{\pm} = \sum_j \alpha_j \beta_{ji}^{\pm} \tag{6.20}$$

The equations (6.20) constitute a system of 8 complex equations in 8 unknown

complex variables. The variables which must be determined are the values of α_j and

the coefficients $\tilde{R}$, $\tilde{T}$, $\tilde{C}_R$, and $\tilde{C}_T$. The values of α are obtained from the four equa-

tions with definite boundary conditions. The values of the coefficients follow.

Once we have determined the coefficients for ψ we must obtain the conserved

quantity, J, as described in the previous chapter

$$J = i(\psi\psi'^* + \phi\phi'^* - \psi^*\psi' - \phi^*\phi') \tag{6.21}$$

which corresponds to the Poynting flux along the magnetic field. As before, ψ and ϕ

are the upper and lower components of equation (1). In the region where the WKB

solutions adequately describe the actual solutions, we find that the coefficients of the

WKB solutions ϕ and ψ are algebraicly related by equation (6.1). Then to first order

the Poynting flux above is proportional to

$$J^+ = -|\gamma_1^{\pm} f_+^+|^2 + |\gamma_2^{\pm} f_+^+|^2 - |\gamma_3^{\pm} f_-^{\pm}|^2 + |\gamma_4^{\pm} f_-^{\pm}|^2 \tag{6.22}$$

and the Poynting flux below is analogously

$$J^- = -|\gamma_1^- f_+^-|^2 + |\gamma_2^- f_+^-|^2 - |\gamma_3^- f_-^-|^2 + |\gamma_4^- f_-^-|^2 \tag{6.23}$$

where the factors f describe the relationship between ψ and ϕ. That is

$$f_\pm^j = 1 + \left[\frac{2}{\kappa^2}(n_\pm^2 - r + \kappa^2/2) \right]^2 \tag{6.24}$$

and the superscript j refers to the location at which this expression is to be evaluated, namely at the location where the $\beta^\pm$ have been determined.

Finally, we are able to determine the the appropriate values for the coefficients for an incident magnetosonic waves. Using the boundary conditions for a downcoming magnetosonic wave as found in equation (6.17), we find

$$\begin{aligned}
T_{MS} &\equiv |\tilde{T} f_-^-/f_-^+|^2 \\
R_{MS} &\equiv |\tilde{R}|^2 \\
C_{MS}^T &\equiv |\tilde{C}_T f_+^-/f_-^+|^2 \\
C_{MS}^R &\equiv |\tilde{C}_R f_+^+/f_-^+|^2
\end{aligned} \tag{6.26}$$

Using the boundary conditions for a downcoming ion-cyclotron wave as in equation (6.18) we find

$$\begin{aligned}
T_{IC} &\equiv |\tilde{T}' f_+^-/f_+^+|^2 \\
R_{IC} &\equiv |\tilde{R}'|^2 \\
C_{IC}^T &\equiv |\tilde{C}'_T f_-^-/f_+^+|^2 \\
C_{IC}^R &\equiv |\tilde{C}'_R f_-^+/f_+^+|^2
\end{aligned} \tag{6.27}$$

In either case, the absorption coefficient is of the form

$$A \equiv 1 - (T + R + C^R + C^T) \tag{6.28}$$

for either case.

II. Numerical Complications

In studying the ideal system of equations (6.1) with the well approximated spatial dependence on the magnetic field, it is important for us to address some basic limitations in the numerical analysis. Numerically, the equations are sufficiently tractable that the exact solution to the well approximated differential equation (6.1) may be determined to arbitrary accuracy (within the limits of computer accuracy). We can make a statement such as this for a number of reasons. We have solved the differential equation using three different techniques, Bulirsh-Stoer, Runge-Kutta and predictor-corrector [Press, et al., 1986]. All techniques produce the same results to within the limitations of double precision accuracy. Moreover, we have transformed the equations (6.1), using a Ricatti Transform, into a set of first order non-linear differential equations [Smith and Whitson, 1978]. (Such a transformation is particularly useful for suppressing exponentially growing solutions.) The numerical solution that we have obtained to the transformed Ricatti equation is again consistent with the numerical solution of (6.1) to arbitrary accuracy. In principle, then, the accuracy of the coefficients that we determine is limited to the accuracy of the imposed boundary conditions.

The boundary conditions which we impose upon the numerical solution are at best limited to the validity of the WKB solutions. That is, the accuracy of the coefficients is limited by the accuracy of $\beta_j^{\pm}$. Once a numerical solution ψ_j is

obtained, the most straightforward manner in which to determine the coefficients, $\beta_j^{\pm}$, is to compare the value of the numerical solution, ψ_j, with the four WKB solutions, Θ_j, at four different locations. Alternatively, we could match ψ_j and its derivatives at a single point with the Θ_j and their derivatives. More elaborate schemes are also conceivable in which ψ_j is matched in a number of locations and an average taken. Moreover, because we consider only the leading order WKB approximation, it is important that we match the numerical and WKB solutions in a region small compared to a typical wavelength. On the other hand, if this region is taken too small, then the values of Θ_j do not vary sufficiently to determine the coefficients $\beta_j^{\pm}$ to the required accuracy. Indeed, the quality of the matching is a basic limitation of our analysis. In the results which follow, we have matched the solutions in a region such that the WKB approximation is reasonably valid, and we have varied the width of the matching region and found that within the upper and lower limits mentioned above deviations from the presented results are not substantial.

For large values of κ, the RHCP magnetosonic mode has very small n_- so that matching to the WKB solutions becomes somewhat suspect. One should therefore question the exact manner in which the coefficients behave near the critical κ, which corresponds to the transition from four propagating WKB modes to two propagating modes, because the meaning of matching to WKB boundary conditions is questionable. However, we should point out that the coefficients do behave reasonably smoothly and it is not unreasonable to assume that the asymptotic solutions are reasonably accurate even when the WKB smallness parameter, ε, is of order 1 [Bender and Orszag, 1978].

We should also mention the dependence of the solutions on the parameter, ρ, which was introduced to circumvent the pole at $z = 1$. The solutions ψ_j have virtually no dependence on the parameter ρ as long as ρ is taken sufficiently small. In the case of very large ρ, the exponentially growing solution in the upper half plane dominates the subdominant solution to the machine precision in which case an inaccurate numerical solution is obtained. For all results presented, the value of ρ is taken sufficiently small so that numerical stability is retained.

Finally, as $z \rightarrow 0$ so that $g \rightarrow \infty$ we find that $r = l$ which corresponds to the lower crossover frequency. Coupling associated with this crossover frequency occurs between $z = 0$ and $z = 1$. Moreover, the strong dependence of the magnetic field on z^{-3} means that this coupling occurs over an extended range of z ($r \simeq l$ over a large range). As a result, the numerical values of the coupling coefficients are functions of altitude. However, the physical boundary conditions which we impose on the upgoing waves below the heavy ion resonance are independent of the location at which we match the solutions. Then it turns out that the reflection and absorption coefficients do not depend upon the location at which the solution is matched for $z < 1$; however, the relative value of the transmission coefficients will depend upon the location at which they are evaluated to a slight degree because the two downgoing Alfvèn modes couple at low altitudes. In the following analysis we match to the slowly varying WKB solutions at some point between $z = 0$ and $z = 1$. In all cases, we have chosen to evaluate the coefficients in a range over which the variation of the coupling coefficients with altitude is small. Indeed, this range is identically the altitude range over which the

boundary conditions may be optimally described in terms of the coefficients of the WKB solutions.

III. Results

A. Budden Equation

As a test of the reliability of our numerical procedure, we consider the coefficients of a well known equation, namely the Budden equation (5.52). In this case, we have a second order equation with coefficients determined from the two WKB solutions. A similar prescription to that described in section II, may be implemented to integrate the equation around the pole. As mentioned previously, we may obtain the numerical solution to arbitrary machine accuracy. In the case of the Budden equation, it is possible to specify the boundary conditions up to the specified accuracy, $O(z^{-2})$, where z is the location at which the WKB solutions are evaluated and matched to the numerical solution. In Figure 6.3 we plot the coefficients obtained from the numerical solution of the Budden equation for specific values of the parameter $\eta = k_0 a$. The analytical results are superimposed upon the numerical results. The curves are not distinguishable. Moreover, the results do not depend in any noticeable way upon the value of the numerical parameters which we have introduced into the problem such as the radius of the contour above the pole, ρ, or the relative location at which we match the WKB solutions to the numerical solutions.
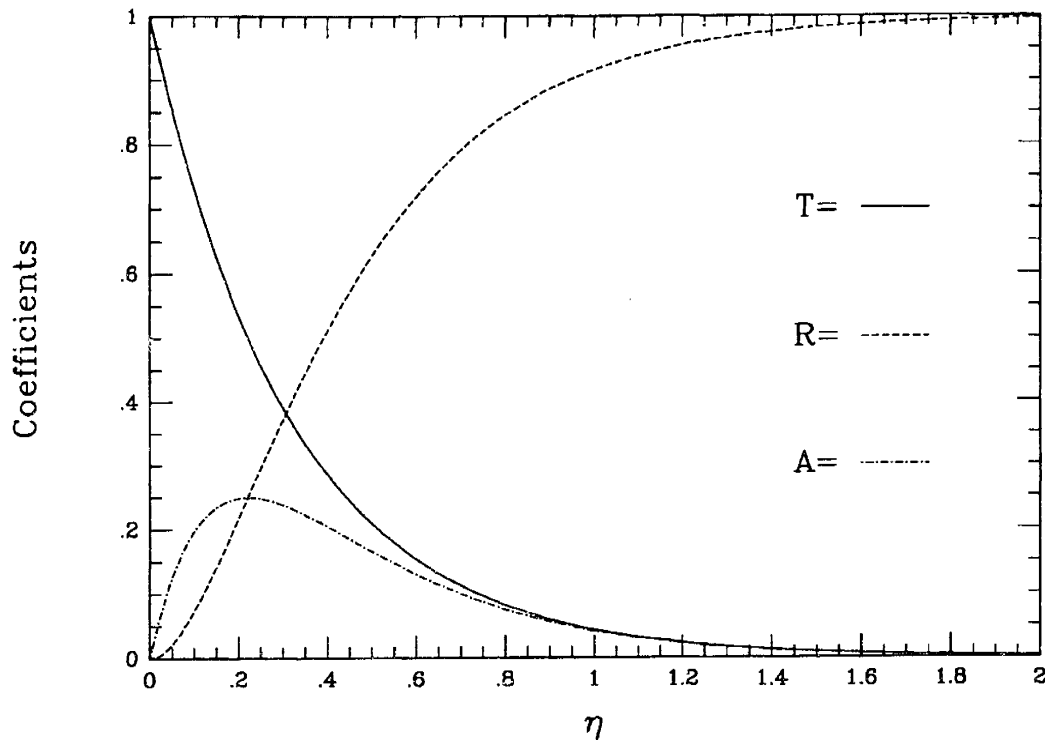
Figure 6.3. Budden coefficients for a downward propagating wave. The Transmission, Reflection, and Absorption coefficients have values of the parameter $\eta = k_0 a$.

B. Fourth Order Equation

1. Parameter Regime

In the following sections we determine the coefficients for several cases of incidence as described previously. The parameters which are of greatest interest are the magnetic field, magnetic field scale length, and the masses and densities of the various constituent ions. The masses are fixed parameters which we take to be hydrogen and oxygen (both singly ionized). The magnetic field and densities are embedded in the WKB parameter ε and the functions r and l depend only upon the density ratios. Hence a particular solution is determined from the specification of ε and the

concentration of the minority species η. Typical values for the parameter ε are

$$\varepsilon = \frac{1}{k_A L_B} \approx 0.5 r^{-1} \rho^{-1} \qquad (6.29)$$

where r is the scale length in earth radii ($\sim$ 1-3) and ρ is the mass density of ions ($\sim$ 1-100) [Moore et al., 1987 and references therein]. We will explore the parameter space for ε ranging from approximately 0.2 to 0.03. In this range, the WKB approximation is good and should provide reasonable matching conditions to the WKB solutions. We will in all cases concentrate on that range of oxygen concentration consistent with reasonable absorption levels. We have found this range to vary from 0.5 to 5 percent. In order to consider the limiting case of a large "gap" we will take ε to be small and η to be large.

2. Incident Magnetosonic Waves

For the results of this section, we impose the boundary conditions for downcoming magnetosonic waves and obtain the coefficients (6.26). In order to understand, the physical meaning of the coefficients, consider Figure 5.6 from Chapter 5. A wave is incident on the magnetosonic branch with unit flux. The fractions of wave flux T_{MS} and R_{MS} are transmitted and reflected on the magnetosonic branch while the fractions C_{MS}^R and C_{MS}^T are transmitted and reflected along the ion-cyclotron branches as indicated.

We have obtained full analytical solutions for the limit of a large "gap." In Figure 6.4 we show the numerical solutions to the differential equation. Superimposed

on the graph we have shown the analytical results (5.116-118) which we have

obtained from a phase integral analysis consistent with a large "gap" for which there

is no absorption. The results are in very good agreement. The most striking

difference is that the coefficient C_{MS}^T is non-zero in contrast to the analytic situation.

However, the analytical results only incorporate the existence of the coupling point

near the crossover frequency. As discussed in the last chapter, coupling between the

two Alfvèn waves can be very strong at frequencies below the heavy ion-cyclotron fre-
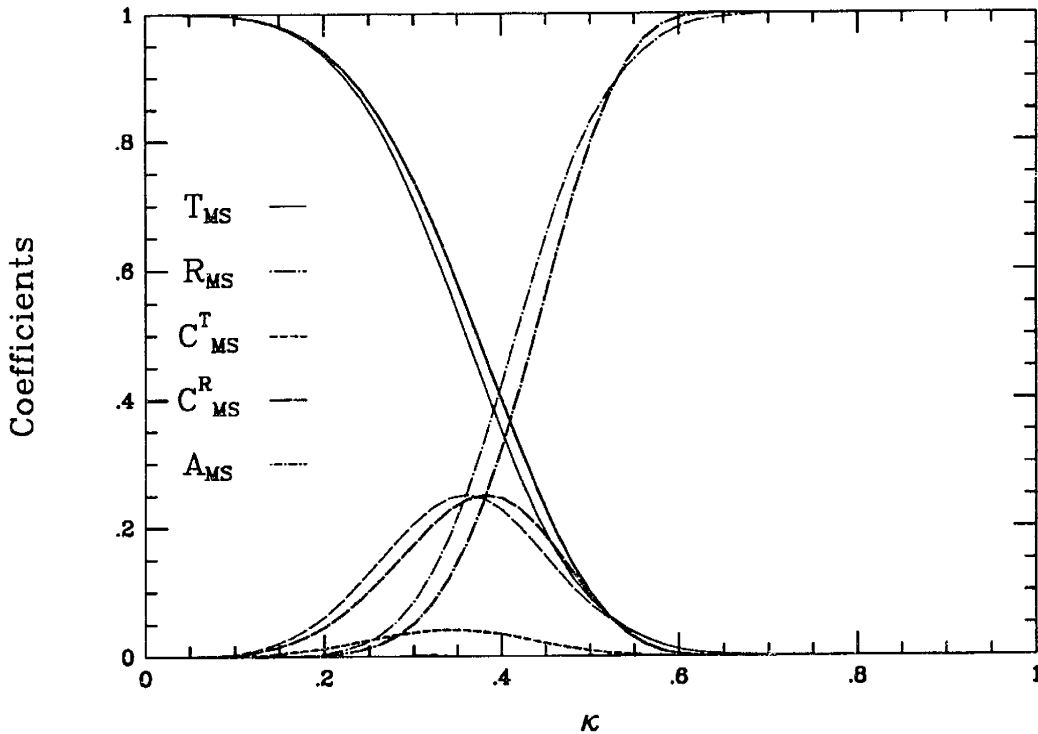
Figure 6.4. For the limit of large "gap" the numerical solutions and the analytical results are in reasonable agreement. We have taken $\varepsilon=0.03$ and $\eta=5\%$ for which there is no absorption. The numerical solutions are plotted in heavy set type and the analytical results are indicated in light type. Note that for the numerical results the coefficient $\exp(-\pi\beta_i/\varepsilon)$ although small is nonzero in contrast to the analytical results. This behavior is the result of coupling between the two Alfvèn waves below the ion resonance corresponding to the coupling point at zero frequency.

quency. It is this coupling which gives rise to the wave power found on the ion cyclo-tron branch.

In Figure 6.5 we compare the numerical transmission coefficient for a small "gap" with the analytical result (5.107). We have plotted the numerical transmission coefficient in heavy solid and the analytical coefficient in light solid. The analytical results predict no coupled wave C_{MS}^T. However, coupling between the two modes does occur below the heavy ion resonance. Because this coupling does not involve reflection one might expect the total transmission $T_{MS}+C_{MS}^T$ to match the analytical transmission coefficient. We have plotted this sum as a dashed line. Indeed the sum
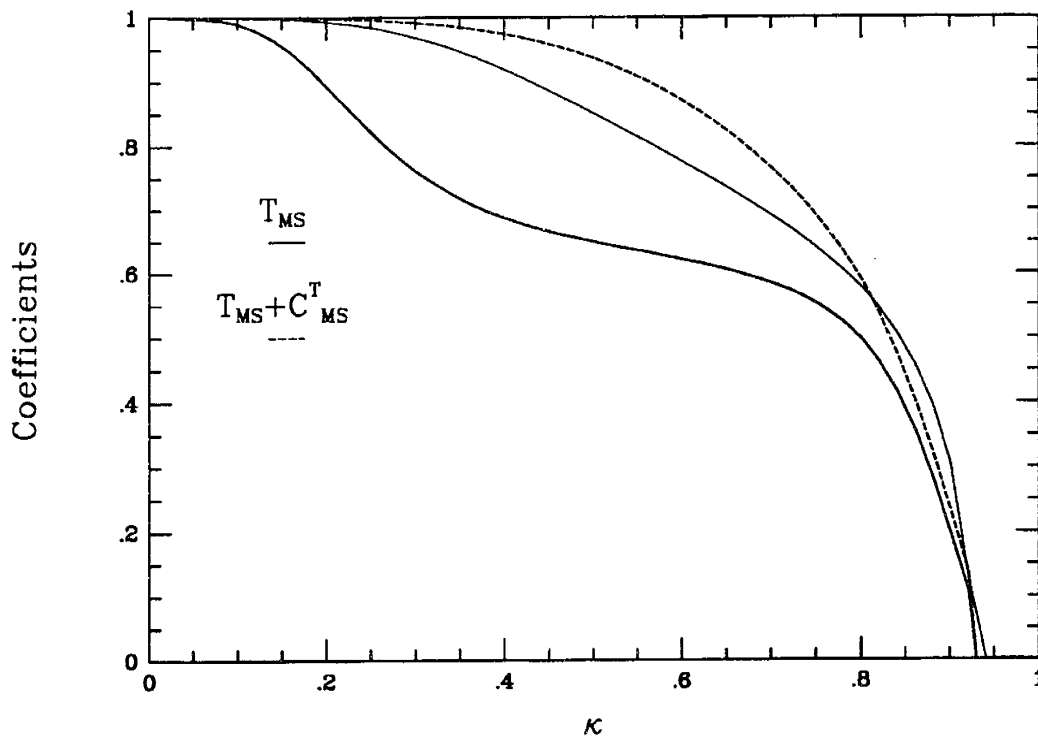
Figure 6.5. Transmission coefficient for the magnetosonic wave in the limit of small "gap" with $\varepsilon=0.2$ and $\eta=1\%$. Note that the total transmission is in good agreement with analytical result.

compares well with the analytical results.

In the regime which corresponds to a large "gap" our numerical results are in good agreement with the analytical results. Moreover, even in the limit of a small "gap," the analytical results are in reasonable agreement. Let us now explore the parameter space. In Figure 6.6 we have plotted the coefficients for the case $\varepsilon = 0.2$ and $\eta = 1\%$. For parallel propagation, no coupling occurs. As the κ increases strong coupling between the two transmitted Alfvèn waves occurs, and the sum of of those coefficients reproduces the analytical transmission coefficient found in the last chapter. For large κ waves are reflected in the two upward propagating modes. The cutoff frequency increases substantially for large enough κ and the "gap" becomes too large to
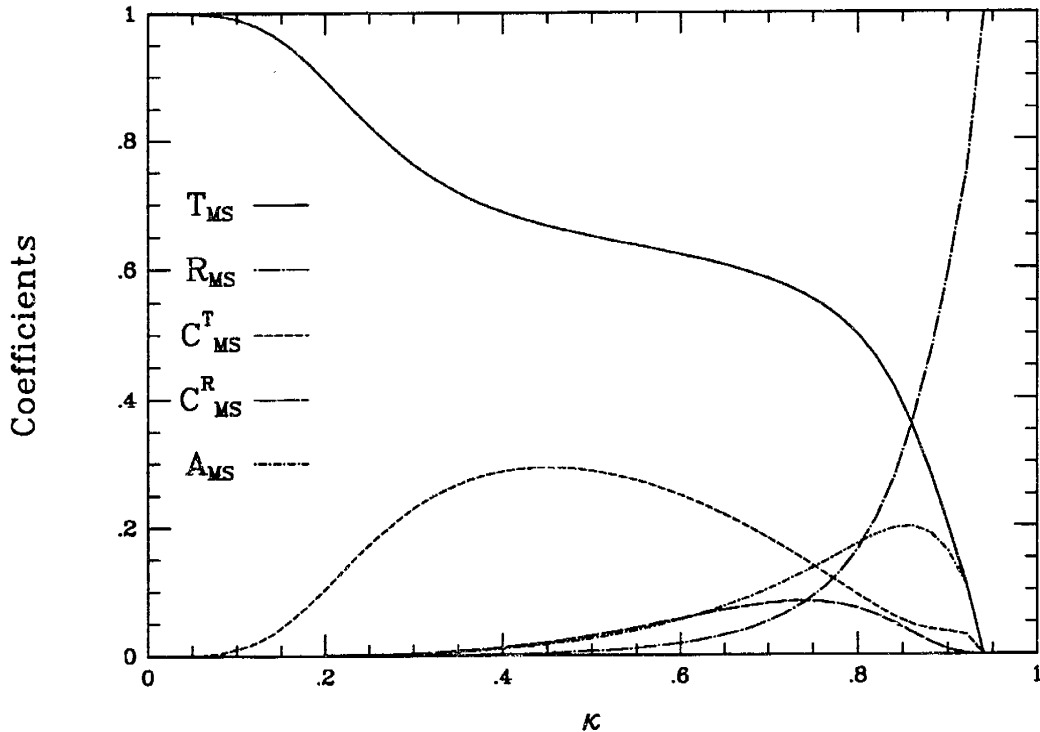
Figure 6.6. Coefficients for the case $\varepsilon=0.2$ and $\eta=1\%$.

penetrate (see for example the sequence of dispersion relations discussed in chapter 3). In this case the reflection coefficient grows rapidly, and for $\kappa \simeq 0.95$ the magnetosonic wave no longer propagates (the wave is reflected at the lower hybrid frequency well above the hydrogen gyrofrequency). For a substantial range of κ strong absorption occurs peaking at 20% for large κ.

For smaller densities, the absorption increases to about 25% although it tends to sharpen and occur mostly at large κ. Indeed, as the minority species density tends to zero, the transmission coefficient, T_{MS}, is approximately 1 and all other coefficients vanish. This means in effect that for very small oxygen densities the waves propagate as if there were no oxygen present.

For larger densities ($\eta=5\%$), as illustrated in Figure 6.7, we find that the absorption diminishes rapidly although the waves still couple at low altitude. In addition, we find that total reflection occurs at a much smaller value for κ. Absorption appears to be very small. However, one should keep in mind that in the case of a large gap all power upcoming in the LHCP mode will be absorbed. If perfect reflection were to occur at ionospheric altitudes, it is conceivable that a substantial portion of C_{MS}^{T} would also be absorbed.

For smaller values of ε (=0.08), as illustrated in Figure 6.8, we find that less coupling occurs between the two downgoing transmitted waves. In addition, reflection is much stronger at intermediate values of κ. This is because the "gap" contains more wavelengths and transmission is substantially diminished. Reasonably strong
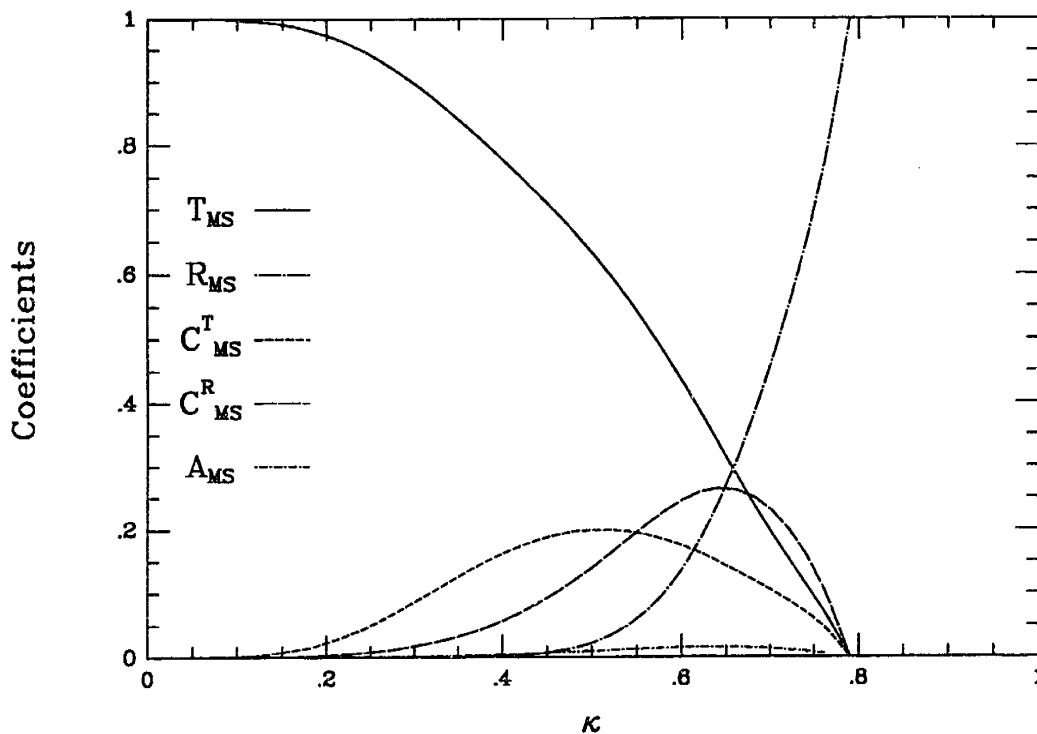
Figure 6.7. Coefficients for the case $\varepsilon=0.2$ and $\eta=5\%$.

absorption still occurs over a vast range of κ and is typically about 7 percent. It should also be noted that a substantial portion of the reflected wave C_{MS}^T can also contribute to heating upon reflection. For even smaller values of the parameter ε ($=0.03$) we find that the absorption becomes negligible for $\eta >1\%$, however, the absorption remains reasonably significant for $\eta = 0.5\%$.

In summary, we have found that incident magnetosonic waves couple strongly near the crossover frequency for reasonable values of the minority species density. For larger values of κ the waves are completely reflected, and strong absorption occurs over a substantial range of κ.
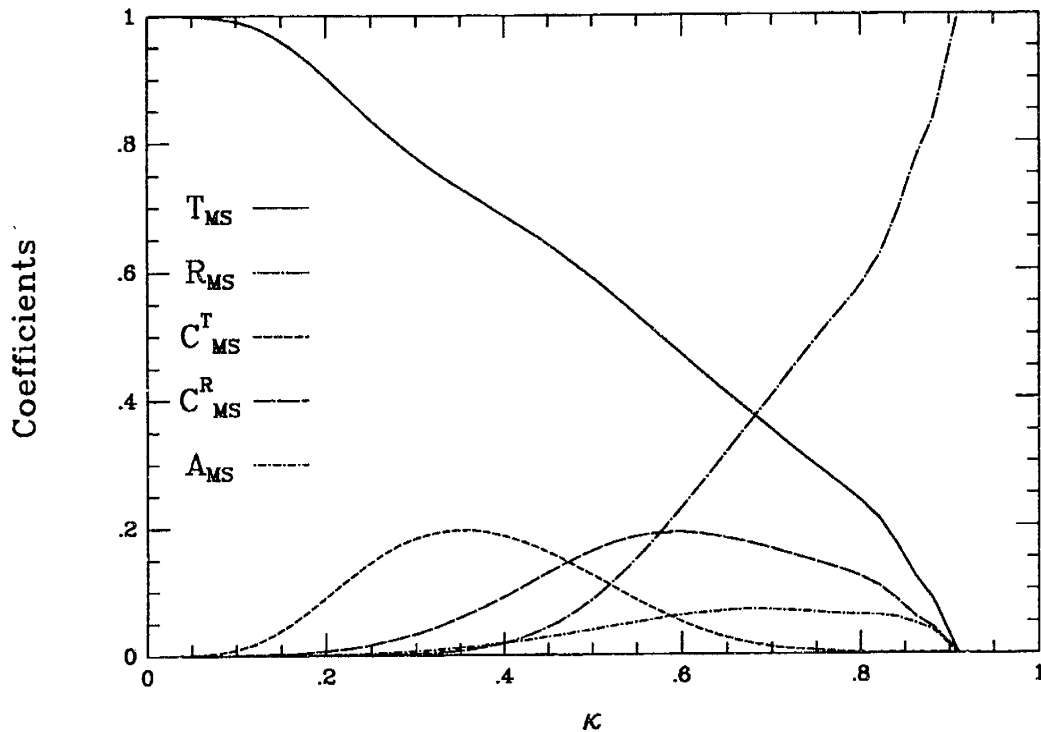
Figure 6.8. Coefficients for the case $\varepsilon=0.08$ and $\eta=1\%$.

3. Incident Ion-Cyclotron Waves

For the results of this section, we impose the boundary conditions for downcoming magnetosonic waves and obtain the coefficients (6.27). For values of κ smaller than the critical κ for which the magnetosonic mode is cut off we determine these values numerically. For larger values of κ we use the analytical results obtained in the previous chapter. Numerical extraction of the coefficients in the case of large κ involves substantial complications. In this section we will obtain correct estimates of the absorption for both small and large values of κ, and we will discuss the meaning and correctness of evaluating the coefficients for intermediate κ.

First, let us consider the coefficients for values of κ smaller than the critical κ for which the magnetosonic mode is cut-off. In order to understand the meaning of these coefficients, consider Figure 5.5 from Chapter 5. A wave is incident on the ion-cyclotron branch with unit flux. The fractions of wave flux T_{IC} and R_{IC} are transmitted and reflected on the ion-cyclotron branches while the fractions C_{IC}^R and C_{IC}^T are transmitted and reflected along the magnetosonic branch as indicated.

We have obtained full analytical solutions for the limit of a large "gap." In Figure 6.9 we show the numerical solutions to the differential equation. Superimposed on the graph we have shown the analytical results (5.113-115) which we have obtained from a phase integral analysis consistent with a large "gap" for which there is no absorption. As for the case of an incident magnetosonic wave, the results are in very good agreement. Again a small amount of wave flux is found in the coupled transmitted wave.

In Figure 6.10 we compare the analytic solution for a small "gap" with the numerical calculation. Once again coupling between the two transmitted modes diminishes the power found on the transmitted ion-cyclotron mode. However, the results are certainly quantitatively correct for small values of κ in which case the low frequency coupling point does not enter into the calculation. For larger κ, the results are qualitatively correct and are good for an order of magnitude estimate; however, the existence of two **different** coupling points (low frequency and crossover—see Figure 5.3 from Chapter 5) cannot be incorporated into a linear model and the analytic results are most accurate when the coupling is dominated by one of the two coupling points.
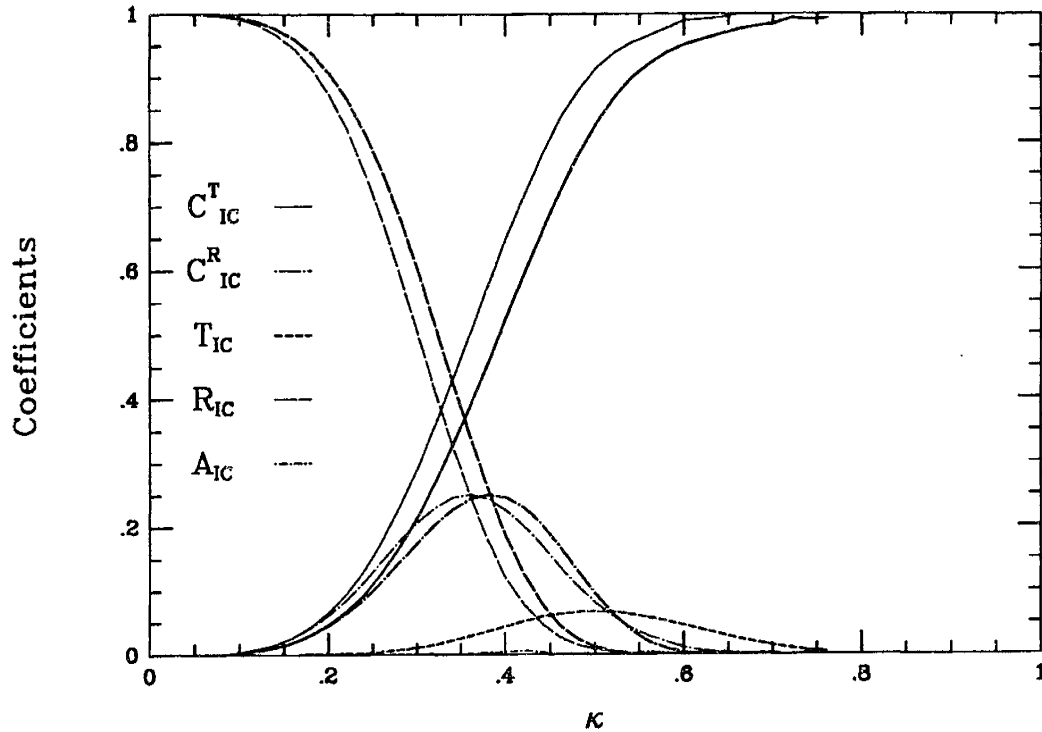
Figure 6.9. For the limit of large "gap" the numerical solutions and the analytical results are in reasonable agreement. We have taken $\varepsilon=0.03$ and $\eta=5\%$ for which there is no absorption. The numerical solutions are plotted in heavy set type and the analytical results are indicated in light type.

In Figure 6.11 we have plotted the coefficients for the case $\varepsilon = 0.2$ and $\eta = 1\%$. For parallel propagation, the problem is described as a Budden tunneling problem for the ion-cyclotron branch, and the ion-cyclotron and magnetosonic branches do not couple. For larger angles of propagation, the tunneling increases as, in fact, predicted by the analytical analysis in Figure 6.10. For larger values of κ, coupling between the downgoing modes occurs at the crossover frequency, and substantial wave energy is transferred to the coupled magnetosonic wave. Indeed, for the case of a small "gap" as in Figure 6.9, coupling to the coupled transmitted wave, C_{IC}^{T}, is complete for large values of κ. Substantial absorption occurs over a very large range of κ taking a value
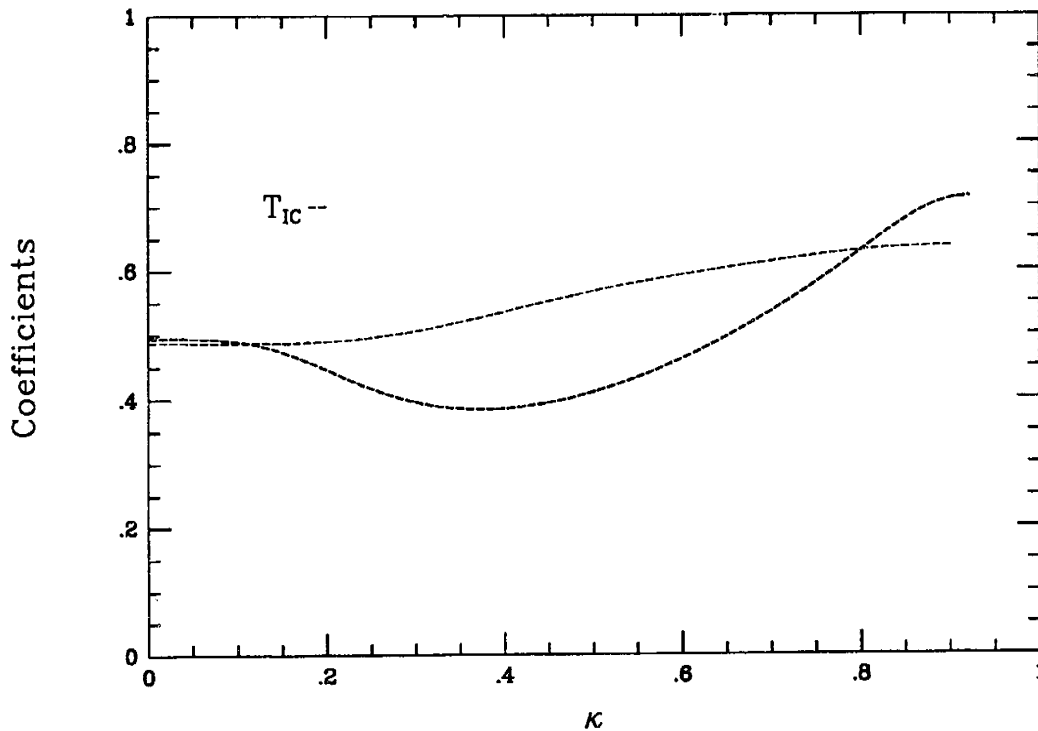
Figure 6.10. Transmission coefficient for the ion-cyclotron wave in the limit of small "gap" with $\varepsilon=0.2$ and $\eta=5\%$. Note that the transmission is in best agreement for small κ.

over 20% over most of the range. In Figure 6.12 we explore the transmission coefficients for parallel propagation for $\varepsilon = 0.2$ (for parallel propagation the two modes are uncoupled so that $C_{IC}^R = C_{IC}^T = 0$). As is clear, substantial absorption occurs over a large range of densities ranging from $\eta = 0.5\%$ to $\eta = 4\%$. For larger values of κ, the absorption remains essentially the same as for parallel propagation up to reasonably large values of κ.

As for the magnetosonic case, substantial absorption still occurs for $\varepsilon = 0.08$ as indicated in Figure 6.13. In this case, the "gap" is large so that most of the wave power is reflected at small angles of propagation rather than transmitted; however, for
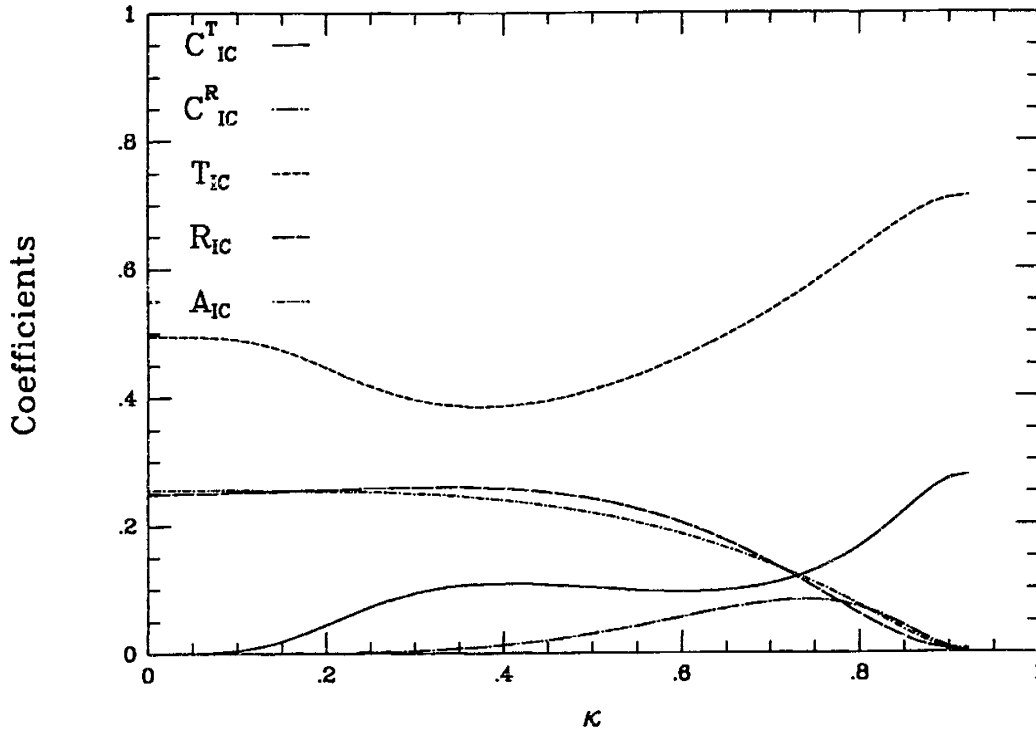
Figure 6.11. Coefficients for the case $\varepsilon=0.2$ and $\eta=1\%$.

larger angles of propagation, tunneling in both modes increases substantially until most

of the power is coupled into the magnetosonic branch. For the case of parallel propa-

gation with $\varepsilon = 0.08$, the peak absorption levels are skewed toward smaller values of

density ($\eta = 0.5\%$). For smaller values of ε the absorption is completely negligible

and the wave is completely reflected.

For large values of κ, we have shown using a variety of methods that the

transmission properties are described as a Budden tunneling problem at the ion-ion

hybrid frequency. Let us consider the analytical results. In Figure 6.14 we have plot-

ted in bold type the transmission factors found in equations (5.137, 5.141) along with

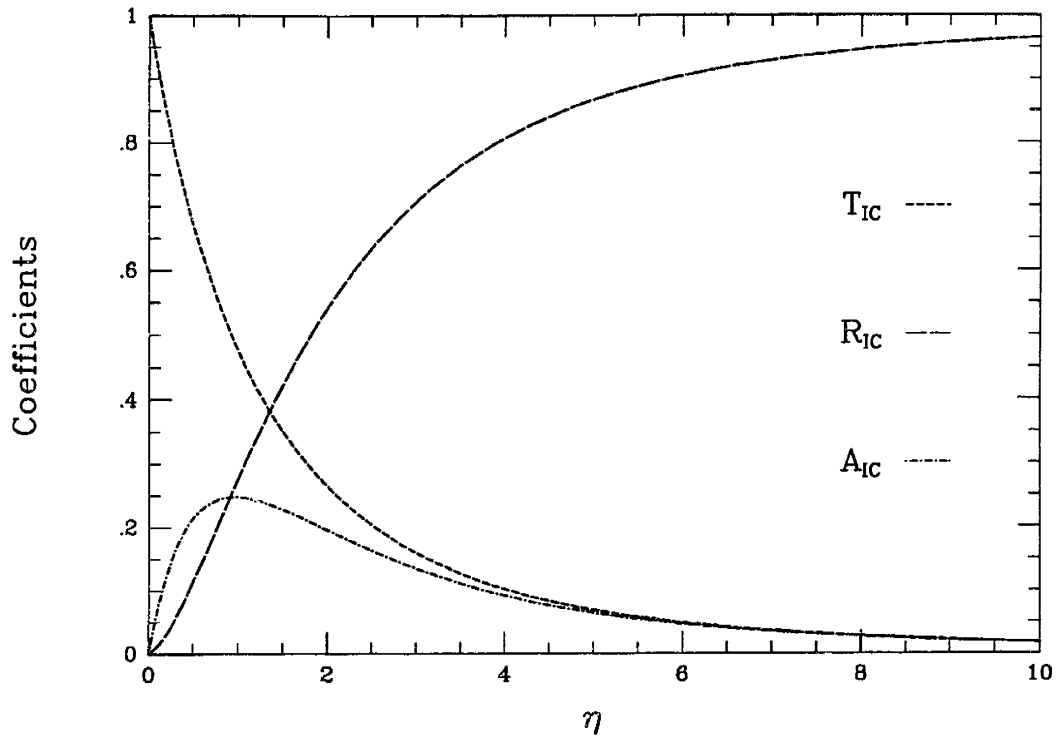the corresponding absorption factor. Physically, the coefficients correspond to Figure

Figure 6.12. Coefficients for parallel propagation with ε=0.2. Strong absorption occurs for 0.5%<η<4%.

5.8 from Chapter 5. In light type we have plotted the transmission factors obtained from the embedded differential equation (5.160). They are in good agreement in the regime in which they are both valid. It is to be noted that there is reasonable agreement between the transmission factor, T_{IC}, near the upper bound of the numerical solution of Figure 6.11 and the large κ solutions of Figure 6.14. The absorption and reflection coefficients do not match well. While it is to be expected that the dominant WKB solution would be continuous in κ it is not necessarily expected that the coefficient of the subdominant solutions would remain continuous.
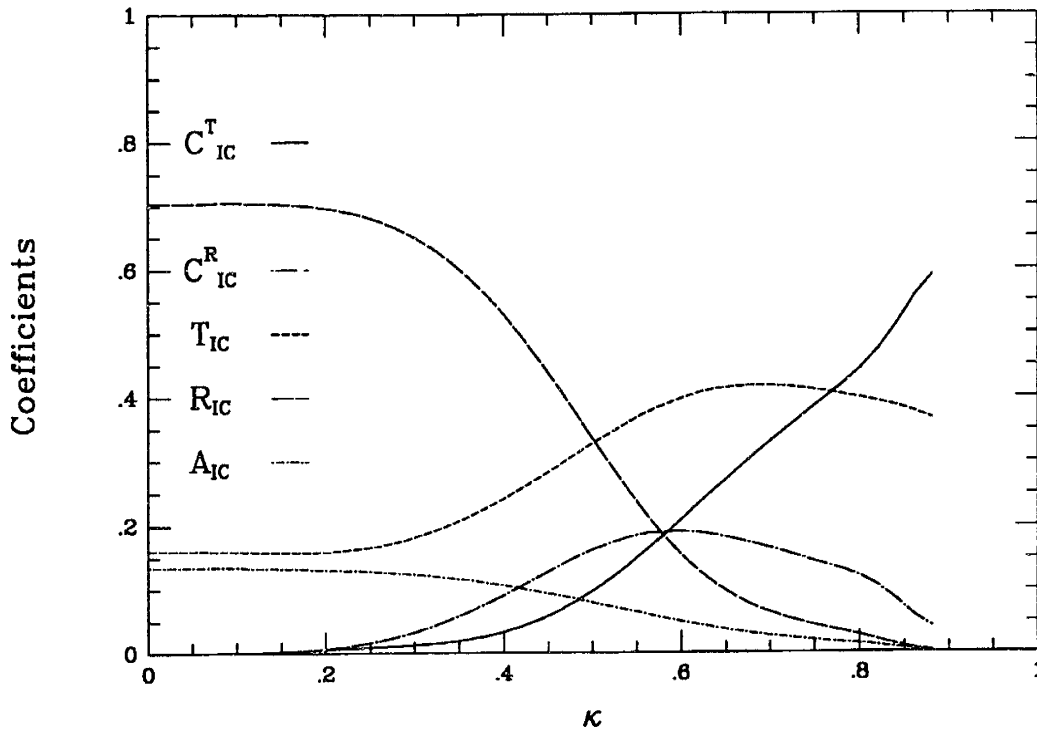
Figure 6.13. Coefficients for the case ε=0.08 and η=1%.

For large κ the transmission coefficients approach a constant value determined from Budden tunneling at the ion-ion hybrid frequency. In Figure 6.15 we plot the coefficients against the concentration of oxygen. As for the case of parallel propagation strong absorption occurs for a large range of densities ranging from $\eta = 0.5\%$ to $\eta = 7\%$. In all cases the absorption remains essentially constant for $\kappa > 1$.

For smaller values of ε the absorption still remains very large for reasonable densities. As illustrated in Figure 6.16 although the reflection is now much larger than the transmission, the absorption remains over 20%. Moreover, the transmission factor, T_{IC}, again matches reasonably well with that coefficient for small κ (see Figure 6.13), but the other coefficients are again discontinuous. From Figure 6.17, it is clear why
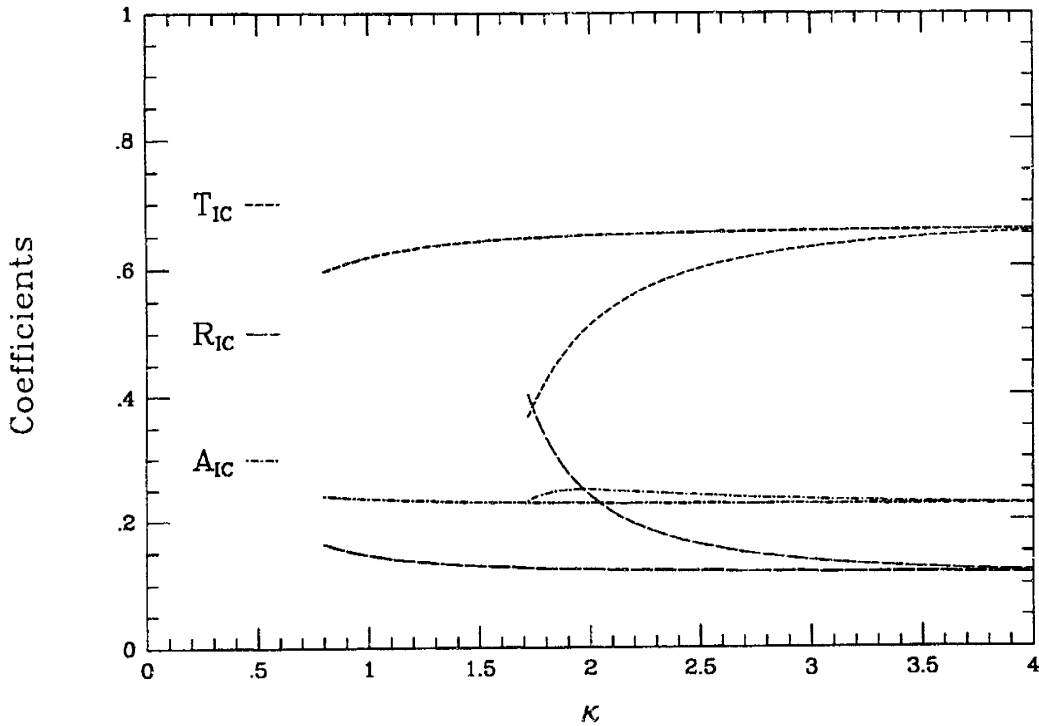
Figure 6.14. Analytical approximations for the transmission coefficients for $\varepsilon=0.2$ at large κ (which corresponds to large angles of propagation). We have plotted the coefficients related to the phase integral transmission, $\exp(-\pi\beta_*/\varepsilon)$, in dark type. The transmission coefficients found from the embedded Budden equation for tunneling through the "gap" are indicated in light type.

the transmission has not diminished from the case with $\varepsilon = 0.2$. The absorption is

strongly peaked around $\eta = 1$. For smaller values of ε the region of strong absorption

moves to very small (probably unphysical) values of η.

In summary, we have found that incident ion-cyclotron waves undergo Budden-

like tunneling at the cutoff frequency for nearly parallel propagation and at the ion-ion

hybrid frequency for nearly perpendicular propagation. The absorption is very strong

over a large range of κ and for a reasonable range of η. For intermediate values of κ,

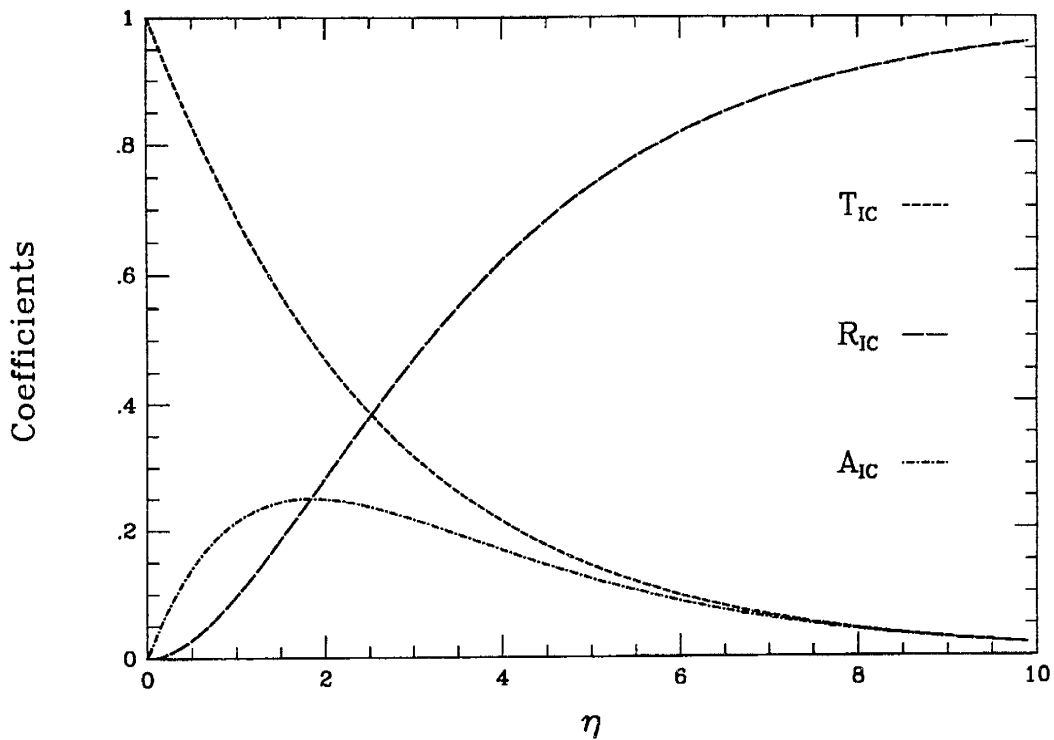coupling near the crossover frequency becomes important and a substantial amount of

Figure 6.15. Coefficients for large κ with $\varepsilon=0.2$. Strong absorption occurs for $0.5<\eta<6$.

wave power is transmitted in the magnetosonic mode. However, for large enough κ, the magnetosonic mode is cut-off and that wave power is reflected back into the system.

4. Physical Considerations

We have found that the analysis of an incident ion-cyclotron wave is somewhat more complicated than the magnetosonic case in that it involves an interesting change in the behavior for the coefficients for small and large κ. In particular, it is important to realize that the continuity of the the transmission properties for these waves is somewhat dependent upon the model from which boundary conditions are obtained.
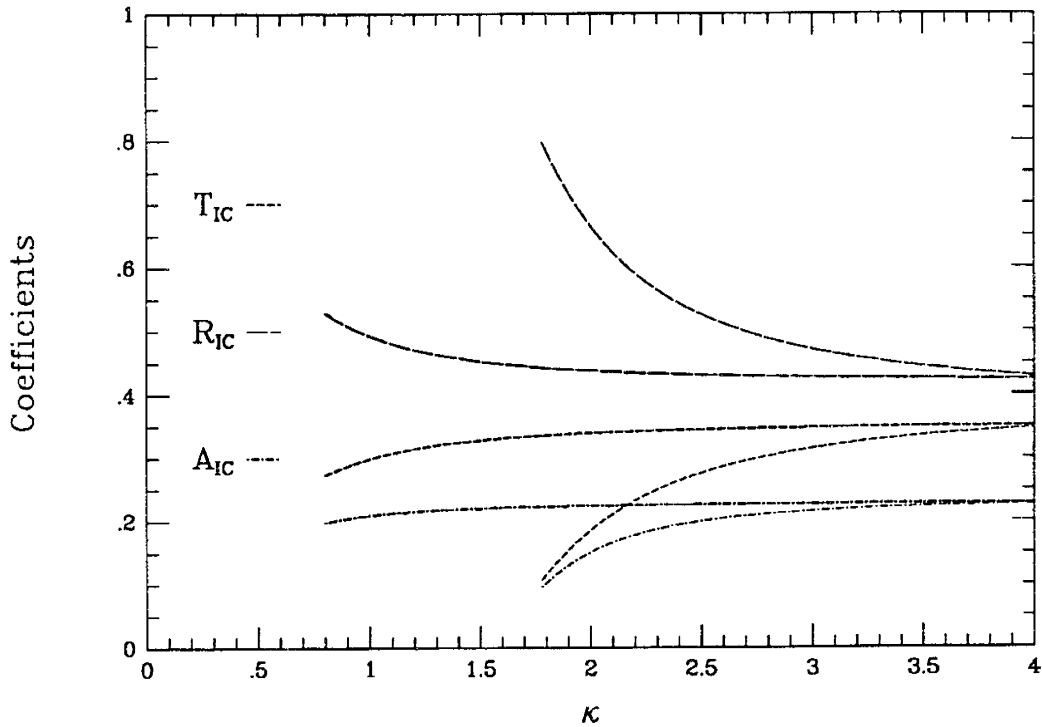
Figure 6.16. Analytical approximations for the transmission coefficients for ε=0.08 at large κ (which corresponds to large angles of propagation). We have plotted the coefficients related to the phase integral transmission, $\exp(-\pi\beta_+/\varepsilon)$, in dark type. The transmission coefficients found from the embedded Budden equation for tunneling through the "gap" are indicated in light type.

The fact that two different regimes exist for κ<1 and κ>1 is represented by the transition of the cutoff frequency as described in (5.142) where a cutoff appears below the ion-cyclotron frequency (instead of above). Then the boundary conditions at ±∞ are determined by two WKB solutions rather than four. One expects that such a sudden transition in the behavior of the modes is not physically meaningful although it is certainly mathematically feasible (recall the discussion of the sudden jump in the Stokes coefficients across a definite value for arg z).
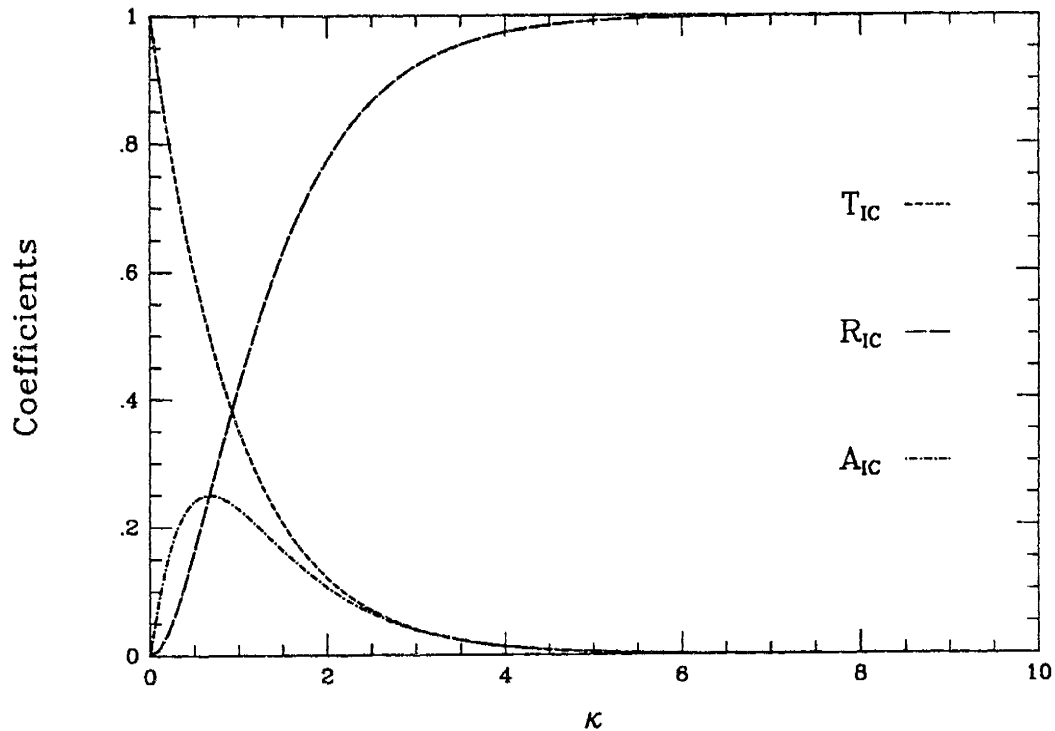
Figure 6.17. Coefficients for large κ with $\varepsilon=0.08$. Strong absorption is peaked about $\eta=1$.

In light of our present model, simply from physical considerations we would expect to find a discontinuous jump in the absorption coefficient as the cutoff moves from $+\infty$ to $-\infty$. If the magnetosonic mode propagates at $-\infty$ then one expects to find that all the wave power on the magnetosonic mode is transmitted; however, if that mode is reflected above the region where the coefficients are evaluated, then all of the wave power, C_{IC}^T, on that branch is reflected back into the system. Because C_{IC}^T increases substantially at large κ where coupling at the crossover frequency is most complete, this amount of reflected energy is substantial. Such reflection greatly modifies the reflection and absorption coefficients although it should not affect the transmission coefficient. As we have seen, the transmission coefficient actually

matches reasonably well across the critical κ.

Physically, we might expect more continuous behavior for the coefficients; however, producing a more continuous result does not mean solving the present equations more accurately. Rather, it means incorporating more physics into the boundary conditions of the model. For example, we have solved a problem in which the coefficients correspond to transmitted wave flux. However, when these waves reach ionospheric altitudes, they interact with a conducting ionosphere. Wave reflection, transmission, mode coupling and absorption at the magnetosphere-ionosphere boundary are at present a vigorous subject of active research. If, for example, the waves were completely reflected at that boundary, then a transition at a critical κ does not appear because waves are reflected at all κ and, hence, there is no discontinuous jump. If, on the other hand, the transmitted waves are absorbed, then we would expect an abrupt transition at some value of κ which corresponds to reflection at the altitude of the absorbing layer. Moreover, density gradients play a substantial role in determining the exact location of the reflection layer and thus of the exact behavior of the coefficients with κ.

As an example of the importance of boundary conditions, suppose we were to assume that waves incident on the ionosphere are completely reflected. Then from the phase integral analysis of the previous section, we find trivially that for an incident upgoing ion-cyclotron wave from below the ion-gyrofrequency the amount of wave flux $T_{IC} = \exp(-\pi\beta_{+}/\varepsilon)$ continues upward. Because this mode is completely subdominant, it couples to no other modes and hence, the remaining wave power is completely

absorbed. Thus, for example, in the case of Figure 6.7 where no absorption occurs, we would find that 60-70% of the flux transmitted on the coupled branch as C_{MS}^{T} would be reflected at the ionosphere and then absorbed at the oxygen resonance so that in actuality the coefficients which we have obtained serve as a lower bound.

In sum, our results provide insight with regard to a lower bound estimate of the absorption near the resonance-cutoff-crossover frequency triplet. The results will be somewhat modified if we include more physics into our analysis, but it is certainly clear that substantial wave power is available to heat minority species ions such as oxygen.

CHAPTER 7

CONCLUSIONS AND FUTURE DIRECTIONS

I. Conclusions

Ion heating associated with conic formation has provided perhaps the most strik-

ing example in space physics of a "theory that works." In the preceding chapters we

have investigated one of the most important aspects of the ion conic problem—namely,

the location of the source of energy that induces the ionospheric oxygen outflow and

whether such a source is consistent with the ion heating model described in the first

chapter. The strong theoretical correlation between the conics and a concomitant

broadband electromagnetic wave spectrum suggests that the wave energy is the source

of ion energization. Because there is apparently no local source for the waves, we

have constructed a global scenario in which waves are generated in a region where

free energy is available to excite waves. These waves then propagate into the region

where the conics are observed and provide the necessary energization.

The magnetosphere is a vast and varied object with many sources and sinks for

energy. Indeed, it is quite conceivable that the source of the broadband spectrum actu-

ally consists of a collage of waves patched together from a number of source regions.

The equatorial region is one of the most prominent candidates to be a source of the

auroral turbulence. Thermal anisotropies and anomalously large loss cones provide a

substantial reservoir of free energy which excites waves in the two propagating low

frequency modes. These waves are observed to attain substantial amplitude in the equatorial region and have been correlated with ground based measurements.

Having identified a substantial source of wave activity, we investigated the evolution of these waves using a non-local model for wave propagation. We incorporated both a realistic magnetic field with curvature and a density profile which approximates the plasmapause boundary. Using typical values for the relevant parameters, we investigated ray paths in detail for waves in the two propagating low frequency modes. Ion-cyclotron were guided along field lines, and in all cases, waves generated in the equatorial region are found at lower altitudes virtually independent of the density profile. These waves provide a substantial fraction of the power observed at auroral altitudes. Moreover, magnetosonic waves, although not guided by the magnetic field may be guided much like a whistler wave in the presence of density gradients. The boundary of the plasmasphere provides such a guiding effect.

As these equatorial waves propagate to lower altitudes, the ray tracing equations do not adequately describe their behavior, and we must solve Maxwell's equations for the full wave solution. The behavior of the modes near the resonance-cutoff-crossover triplet of frequencies is the most critical aspect of our whole analysis in that this behavior determines the amount of wave power available to heat ions and specifies, in particular, the apportionment of wave flux above and below the heating region. Indeed, the transmission coefficients are the heart of the matter in our scenario.

Because parallel magnetic field gradients are more substantial than perpendicular gradients at auroral altitudes, we have simplified the relevant plasma equations and have extracted a fourth order equation which describes coupling between the two circularly polarized components of the electric field. We have studied these equations in detail and we have estimated and determined coefficients which relate the Poynting flux of the wave modes above and below the coupling region. We demonstrated analytically that the ion-cyclotron and magnetosonic modes couple strongly near the crossover frequency. This coupling is a strong function of the perpendicular wavevector. Using a phase integral analysis, we determined that downgoing ion-cyclotron waves tend to tunnel through a cutoff-resonance "gap" in a manner similar to that described by Budden. On the other hand, downgoing magnetosonic waves tend to propagate through the "gap" and strongly couple to the ion-cyclotron wave for large angles of propagation. In both cases, strong absorption is expected to occur over a range of angles of propagation. In the limit of a large "gap" this absorption becomes negligible and we determined the coefficients analytically without ambiguity.

In order to incorporate the presence of coupling both above and below the heavy ion gyrofrequency, check our analytical results, and extract the values of all coefficients, we have solved the system of coupled differential equations numerically. In order to integrate the equations around the singularity, we incorporated physical considerations into our analysis. This prescription involved continuing the multivalued solution to the differential equation "above" the pole. By imposing boundary conditions on the numerical solution consistent with downcoming waves in a particular

mode, we were able to determine the coefficients associated with wave propagation near the heavy ion gyrofrequency.

We found that our numerical solutions were in reasonable agreement with the analytical solutions that we obtained. Incident magnetosonic waves couple strongly near the crossover frequency for reasonable values of the minority species density, and for large angle of propagation the waves are completely reflected. Strong absorption (the order of 10–20%) occurs over a substantial portion of the spectrum peaking near perpendicular propagation. Ion-cyclotron waves, on the other hand, undergo Budden-like tunneling at the cutoff frequency for nearly parallel propagation and at the ion-ion hybrid frequency for nearly perpendicular propagation. The absorption is very strong (~ 20%) over most angles of propagation for reasonable values of the minority species concentration. In either case the absorption levels are consistent with the power required to heat ion conics.

In summary, the scenario which we have presented is quite plausible. Waves are generated in the equatorial region and then propagate Earthward along field lines. As they reach auroral altitudes, the two downward propagating modes undergo strong coupling near the heavy ion gyrofrequency, and substantial wave power is absorbed. The absorbed wave power is significant and energizes oxygen conics to magnetospheric energies.

II. Future Considerations

A. Thermal Effects

Our analysis has provided us with an estimate of absorption levels which occur in a multispecies plasma near the minority cyclotron frequency. Our analysis, however, remains somewhat inadequate in that the equations which we studied are singular at the resonance. Budden [1965] has suggested a number of interpretations of the absorption ranging from collisional absorption to ion-cyclotron damping. Swanson [1989] and Fuchs *et al.* [1985] have incorporated thermal effects into the Budden analysis, and they have shown that near the resonance, the Budden equation should actually be approximated by a fourth order equation which introduces two thermal modes in addition to the two cold plasma mode. They have demonstrated that the wave power rather than being mysteriously absorbed is mode converted to a thermal wave which strongly damps on the ions.

It is natural, then, to believe that the absorption processes which we have studied have their predication in mode conversion processes which involve thermal branches such as the various ion Bernstein modes. In order to understand the absorption physically, we must incorporate thermal effects into our analysis. In doing so, we will obtain a higher order system. Given that our original system is of fourth order, the physical resolution of the problem will involve at least a sixth order equation. Solving such an equation will be a formidable task. Moreover, it is conceivable that as the Bernstein modes are excited, nonlinear effects which couple the cyclotron harmonics

will become important. Thus, although our linear calculations have given us some physical insight and suggested a definite absorption, the final resolution of this problem will probably involve a full nonlinear analysis of mode conversion.

B. Ionospheric Boundary Conditions

As we have discussed at length, ionospheric boundary conditions can be an important aspect of the problem particularly for waves waves which encounter the oxygen resonance at very low altitudes. The strong coupling between the two Alfvèn waves is substantial at low altitudes, and most wave power reflected in the LHCP mode tends to be absorbed. Boundary conditions at ionospheric altitudes, however, are not trivial. Although the ionosphere is a good conductor, substantial currents flow along the surface of the ionosphere. The currents on the ionosphere, however, are related to currents in the magnetosphere [Lysak and Dum, 1985; Lotko et al., 1987]. Waves in the ionosphere couple to waves in the magnetosphere [Keskinen et al., 1988; Seyler, 1990]. A complete investigation of the effects of ionospheric-magnetospheric coupling is an enormous task which at present remains a field of active research.

Our model is a starting point for understanding wave processes in the magnetosphere. Imposing simplistic boundary conditions which specify the ionosphere as a conductor with imposed currents on that boundary would provide a first step toward understanding the effects of the ionospheric boundary conditions. More realistic boundary conditions must incorporate the circuit–like nature of the ionosphere in which height integrated conductivities relate currents in the ionosphere to the electric field.

Eventually, an ionospheric code which incorporates the dynamics of a collisionally dominated ionosphere should be combined with a magnetospheric code which is dominated by the behavior of the electromagnetic fields. Such a code would not only provide the solution to the specific problem involving ion heating, but would also substantially enhance the present understanding of coupling between the magnetosphere and ionosphere.

C. Nonlinear Effects

In its crudest form, ray tracing demonstrates whether wave power, generated in some region of the magnetosphere, might propagate into another region where it may be observed. Ray-tracing is, of course, founded upon the assumption that a small wave packet behaves linearly and moves about as a particle. On the other hand, the observed spectrum is somewhat suggestive of turbulence in that it is very broadband in nature. The waves generated in the equatorial region tend to be excited in narrow bands of frequency. Nevertheless, the observed spectrum is somewhat broadband. We have already alluded to the fact that the focusing geometry of the Earth's magnetic field might lead to a smearing of the generated spectrum, but it is also reasonable that the waves which are generated reach sufficiently large amplitudes for nonlinear effects to couple the modes, thus leading to a broadband spectrum. Indeed, the suggestion that the waves bounce back and forth between conjugate points [Rauch and Roux, 1982] is suggestive of a driven oscillator and would suggest that at some point some of the waves may saturate. Moreover, some of the observations of waves generated

above the local hydrogen cyclotron frequency appeared to consist of not only waves generated at the harmonics of the proton cyclotron frequency, but also waves generated via harmonic-harmonic coupling. All this would suggest that there is a need to understand some of the nonlinear aspects of this problem.

The broadband nature of spectra has often led to the conclusion that the waves are in fact turbulence [Keskinen and Kintner, 1978; Keskinen, et al., 1988]. However, it is very difficult to compare present models of MHD turbulence with observation in that spatial structure is difficult if not impossible to resolve at the present time, and mapping frequency spectra into wavevector spectra seems somewhat inadequate [Labelle and Kintner, 1989]. If the waves, do indeed, interact nonlinearly in the region, then nonlinear parametric coupling might explain some of the spread in frequency that is observed. This topic is certainly of great interest and one which we should continue to explore.

D. Non-Resonant Heating

The relationship between low frequency turbulence and ion heating has been a confusing issue over the course of the last few years. The observation that wave spectra seem to peak at frequencies well below the ion gyrofrequency has led some to suggest that the random kicks associated with this enormous amount of field activity may indeed interact with the particles and, in fact, heat them in some non-resonant manner [Lundin and Hultqvist, 1989]. Simple plasma theory, on the other hand, suggests that particles are only adiabatically heated by the non-resonant wave activity and are

sloshed around by the waves with no net heating. Indeed, a careful calculation based on the modeling of ion heating in a "weakly turbulent" plasma demonstrates clearly that in the framework of a quasilinear model with stationary turbulence heating only results from the interaction of those waves which are in a frequency range which may resonant with particles [Ball et al., 1991]. On the other hand, it might be suggested that nonlinear coupling of waves at frequencies below the resonant frequency may indeed produce second order resonant heating of ions [Temerin and Roth, 1986]. Although such theories have some appeal in that they suggest that the large low frequency fields may heat ions, they are conspicuously deficient in that higher order resonant coupling involves higher order contributions in terms of the electric field spectral density which is small. We believe that careful scrutiny of the data precludes such mechanisms from efficiently energizing particles of ionospheric origin.

In the presence of gradients, however, we expect that the non-resonant sloshing of particles will no longer proceed in a adiabatic manner. Indeed, the gradients would act in such a manner as to push the more energetic particles to higher altitude in order to conserve the magnetic moment in the presence of a magnetic field gradient—much like water in a bucket sloshes over the rim if it is shaken. Moreover, the waves are observed all along the field lines so that we would expect this sloshing to have a cumulative effect and perhaps cause a net energization of ionospheric particles to magnetospheric energies. Once the ions have been drawn out of the ionosphere, to altitudes where their local gyrofrequency has sufficiently decreased so that they may interact resonantly with the waves, wave particle interactions will then be able to

dominate the energization process. Moreover, similar processes may draw ions out of the ionosphere into the boundary plasma sheet where resonant interaction with lower-hybrid waves accelerates the ions to magnetospheric energies [Chang and Coppi, 1981; Retterer et al., 1983,1986]. Although these resonant energization is reasonably well understood and the observations agree with well with theory, *the initial energization of ionospheric particles remains, at present, a mystery.*

It would be of interest to study the role of gradients in non-resonant "heating" processes to determine whether ions of ionospheric origin may, in fact, be drawn out of the ionosphere to altitudes where resonant interactions dominate. This process could be modeled using a Monte Carlo simulation to determine the evolution of ions immersed in a non-resonant electric field spectrum evolving spatially in a realistic magnetic field geometry. Because observational capacities at present limit our under-standing of the spatial character of the observed wave spectrum, we would need to explore a number of spatial models for the electromagnetic field quantities. In addi-tion, to unambiguously attribute any heating to non-resonant waves, we could filter out that part of the spectrum which may interact resonantly with the particles near their gyrofrequency. As we followed the evolution of the particles we could then determine the character of the outflow attributable to these low frequency waves.

E. Shear Instabilities

Transverse velocity shears associated with convective flows at lower altitudes appear to also be an attractive source for generating instabilities associated with ion

heating and conic formation. In particular, the kinetic instability studied by Ganguli *et al.* [1985a,b,1988] does generate a broadband of waves near the ion cyclotron frequencies with small wavelength. We believe that in this manner, energy may be extracted from bulk flow and transferred to ion thermal energy. Moreover, small scale shears in the electric field structure excite this instability in contrast to the large scale structure required to generate Alfvén waves which obviates one of the objections to a local source. Such waves would then be available to heat conics via a wave-particle interaction and thus provide an efficient preheating mechanism for extracting oxygen from the ionosphere.

Waves generated as the result of inhomogeneities in the ionospheric electric field should therefore be understood in detail. As a first step we could extend the nonlocal analysis of Ganguli *et al.* [1988] to include the presence of multiple ion species. Because such a mechanism is local in origin, the instability generates waves near the cyclotron resonance of the species which we are considering—in this case oxygen. In light of the previous work we expect such waves to arise in the region where oxygen is the dominant species, and it is not unlikely that such waves will also be generated at higher altitudes where oxygen becomes less dominant but is still appreciable. At lower altitudes, it is certainly conceivable that collisional effects might also play an important role with regard to the instability, and it would be important for us to eventually incorporate such effects into our model.

These kinetic ion-cyclotron modes were first understood in light of a simple top-hat potential which was later smoothed to allow direct comparison with the

Kelvin-Helmoltz instability. At this point, the theory was cast into the form of an integral equation. Such a formulation was important in that the fluid modes and the ion-cyclotron modes were described by two different limits of the same equation. Because many of the ion-cyclotron modes have wavelengths the order of or greater than the ion gyroradius, it is important to study this problem using the full integral equation rather than limits thereof. By solving the full integral equation, one would be able to elucidate the problem more completely than has been done before.

Once we demonstrate that waves could be generated near the oxygen gyrofrequency in a multispecies plasma and understand the characteristics of such waves, we could then calculate the heating of oxygen which results through wave-particle interaction. We believe that a heating rate based upon quasilinear theory would be adequate to explain how energy is transferred between waves and particles. In this manner, we could determine whether sheared electric fields in the ionosphere contribute ion preheating in the topside ionosphere.

F. Summary

In summary, there are a number of new and exciting directions which can be explored in light of this present work. The questions surrounding the physical interpretation of the absorption process may be resolved if we incorporate thermal effects into the analysis. Moreover, at lower altitudes, these results can be improved if we incorporate realistic ionospheric boundary conditions into the model. Finally, there are a number of other possible sources for the auroral turbulence which can and should

be studied in greater detail particularly with regard to the initial energization of oxy-

gen.

BIBLIOGRAPHY

[1] Abramowitz, M. and I. A. Stegun, *Handbook of Mathematical Functions with Formulas, Graphs, and Tables* (Dover Publications, Inc., New York, 1964), 1046 pp., §§9, 13.

[2] Al'pert, Y. L., *Space Plasma Volume I: Theory and Main Properties* (Cambridge University Press, 1990), 308 pp., Ch. 8.

[3] Andrè, Mats, G. B. Crew, W. K. Peterson, A. M. Persoon, C. J. Pollock, and M. J. Engebretson, Ion heating by broadband low-frequency waves in the cusp/cleft, J. Geophys. Res., **95**, pp. 20809–20823 (1990).

[4] Ashour-Abdalla, M. and S. W. H. Cowley, Wave-particle interactions near the geostationary orbit, in *Magnetospheric Physics*, B. M. McCormac ed., pp. 241–270 (D. Reidel, Hingham, MA, 1974).

[5] Ashour-Abdalla, M., H. Okuda, and C. Z. Cheng, Acceleration of heavy ions on auroral field lines, Geophys. Res. Lett., **8**, pp. 795–798 (1981).

[6] Ball, L., M. André, and J. R. Johnson, Wave observations and their relation to "nonresonant" ion heating in a "weakly turbulent" plasma model, Ann. Geophysicae, **9**, pp. 37–41 (1991).

[7] Bender, C. M. and S. A. Orszag, *Advanced Mathematical Methods for Scientists and Engineers* (McGraw-Hill, New York, 1978), 593 pp..

[8]   Budden, K. G., *The Propagation of Radio Waves* (Cambridge University Press, 1985), 669 pp., §§19.5, 19.6.

[9]   Burch, J. L., Energetic particles and currents: results from Dynamics Explorer, Rev. Geophys., **26**, pp. 215–228 (1988).

[10] Carpenter, D. L. and C. G. Park, On what ionospheric workers should know about the plasmapause-plasmasphere, Rev. Geophy. Space Sci., **11**, pp. 133–154 (1973).

[11] Chang, T. and B. Coppi, Lower hybrid acceleration and ion evolution in the suprauroral region, Geophys. Res. Lett., **8**, pp. 1253–1256 (1981).

[12] Chang, T., G. B. Crew, N. Hershkowitz, J. R. Jasperse, J. M. Retterer, and J. D. Winningham, Transverse acceleration of oxygen ions by electromagnetic ion cyclotron resonance with broad band left-hand polarized waves, Geophys. Res. Lett., **13**, pp. 636–639 (1986).

[13] Chang, T., G. B. Crew, and J. M. Retterer, Electromagnetic tornadoes in space, Computer Physics Communications, **49**, pp. 61–74 (1988).

[14] Crew, G. B. and Tom Chang, Path-integral formulation of ion conic heating, Phys. Fluids, **31**, pp. 3425–3439 (1988).

[15] Crew, G. B., Tom Chang, J. M. Retterer, W. K. Peterson, D. A. Gurnett, and R. L. Huff, Ion cyclotron resonance heated conics: theory and observations, J. Geophys. Res., **94**, p. 3959 (1990).

[16] Crew, G. B. and T. Chang, Particle acceleration by electromagnetic ion-cyclotron turbulence, in *Physics of Space Plasmas (1989), SPI Conference Proceedings and Reprint Series, Number 9*, T. Chang, G. B. Crew, and Jack Jasperse, eds., pp. 31–66 (Scientific Publishers, Inc., Cambridge, MA, 1990).

[17] Försterling, K., Uber die Ausbreitung elektromagnetischer Wellen in einem magnetisierten Medium bei senkrachter Incidenz, Hochfreq. Elek., **59**, pp. 10–22 (1942).

[18] Fuchs, V., A. Bers, and L. Harten, On the theory of pairwise coupling embedded in more general local dispersion relations, Phys. Fluids, **28**, pp. 177–189 (1985).

[19] Fuchs, V., K. Ko, and A. Bers, Theory of mode-conversion in weakly inhomogeneous plasma, Phys. Fluids, **24**, pp. 1251–1261 (1981).

[20] Ganguli, G., Y. C. Lee, and P. J. Palmadesso, Electrostatic ion cyclotron instability due to a nonuniform electric field perpendicular to the external magnetic field, Phys. Fluids, **28**, p. 761 (1985).

[21] Ganguli, G., P. J. Palmadesso, and Y. C. Lee, A new mechanism for excitation of electrostatic ion-cyclotron waves and associated perpendicular ion heating, Geophys. Res. Lett., **12**, pp. 643–646 (1985).

[22] Gurnett, D. A., R. L. Huff, J. D. Menietti, J. L. Burch, J. D. Winningham, and S. D. Shawhan, Correlated low-frequency electric and magnetic noise along the auroral field lines, J. Geophys. Res., **89**, pp. 8971–8985 (1984).

[23]   Gurnett, D. A., S. D. Shawhan, N. M. Brice, and R. L. Smith, Ion cyclotron whistlers, J. Geophys. Res., **70**, pp. 1665–1688 (1965).

[24]   Heading, J., The Stokes phenomenon and certain nth-order differential equations II. The Stokes Phenomenon, Proc. Cambridge Phil. Soc., **53**, pp. 419–441 (1957).

[25]   Heading, J., *An Introduction to Phase Integral Methods* (Wiley, 1962), 160 pp..

[26]   Heading, J., The Stokes phenomenon and the Whittaker function, J. London Math. Soc., **37**, pp. 195–208 (1962).

[27]   Helliwell, R. A., *Whistlers and Related Ionospheric Phenomena* (Stanford University Press, Stanford, CA, 1965).

[28]   Horne, R. B. and R. M. Thorne, Ion-cyclotron absorption at the second harmonic of the oxygen gyrofrequency, Geophys. Res. Lett., **17**, pp. 2225–2228 (1990).

[29]   Ichimaru, Setsuo, Theory of plasma heating by fluctuating electric fields—effects of correlation times, J. Phys. Soc. Japan, **39**, pp. 1373–1377 (1975).

[30]   Johnson, J. R., Tom Chang, G. B. Crew, and Mats Andre, in *Physics of Space Plasmas (1989), SPI Conference Proceedings and Reprint Series, Number 9*, T. Chang, G. B. Crew, and Jack Jasperse, eds., pp. 433–445 (Scientific Publishers, Inc., Cambridge, MA, 1990).

[31]   Johnson, J. R., T. Chang, and G. B. Crew, ULF wave propagation along closed field lines in the presence of parallel magnetic field gradients and density fluctuations, Eos, **71**, pp. 1537–1537 (1990).

[32] Johnson, J. R., T. Chang, G. B. Crew, and Mats Andre, ULF wave propagation along closed field lines in the presence of parallel magnetic field gradients and density fluctuations, Geophys. Res. Lett., 16, pp. 1469–1472 (1989).

[33] Kelley, M. C. and P. M. Kintner, Evidence for two-dimensional inertial turbulence in a cosmic-scale low β plasma, Astrophys. J., 220, pp. 339–345 (1978).

[34] Keskinen, M. and P. M. Kintner, Evidence for two-dimensional inertial turbulence in a cosmic-scale low β plasma, Astrophys. J., 220, pp. 339–345 (1978).

[35] Keskinen, M. J., H. G. Mitchell, J. A. Fedder, P. Satyanarayana, S. T. Zalesak, and J. D. Huba, Nonlinear evolution of the Kelvin-Helmholtz instability in the high latitude ionosphere, J. Geophys. Res., 93, pp. 137–152 (1988).

[36] Klumpar, D. M., A digest and comprehensive bibliography on transverse auroral ion acceleration, in *Ion Acceleration in the Magnetosphere and Ionosphere, Geophysical Monograph Series, Vol. 38*, Tom Chang, M. K. Hudson, J. R. Jasperse, R. G. Johnson, P. M. Kintner, M. Schulz, and G. B. Crew, eds., pp. 389–398 (American Geophysical Union, Washington D.C., 1986).

[37] Labelle, J. and P. M. Kintner, The measurement of wavelength in space plasmas, Rev. Geophys., 27, pp. 495–518 (1989).

[38] Lashmore-Davies, C. N., V. Fuchs, and R. A. Cairns, Ion-cyclotron resonance heating by means of the fast wave in a longitudinally inhomogeneous magnetic field, Phys. Fluids, 28, pp. 1791–1799 (1985).

[39] Lighthill, J., *Waves in Fluids* (Cambridge University Press, 1978), 504 pp., Ch. 4.

[40] Lotko, W., U. O. Sonnerup, and R. L. Lysak, Nonsteady boundary layer flow including ionospheric drag and parallel electric fields, J. Geophys. Res., 92, pp. 8635–8648 (1987).

[41] Lundin, Rickard and Bengt Hultqvist, Ionospheric plasma escape by high-altitude electric fields: magnetic moment "pumping", J. Geophys. Res., 94, pp. 6665–6680 (1989).

[42] Lysak, R. L., Auroral Electrodynamics with current and voltage generators, J. Geophys. Res., 90, pp. 4178–4190 (1985).

[43] Lysak, R. L., Ion acceleration by wave-particle interaction, in *Ion Acceleration in the Magnetosphere and Ionosphere, Geophysical Monograph Series* , Tom Chang, M. K. Hudson, J. R. Jasperse, R. G. Johnson, P. M. Kintner, M. Schulz, and G. B. Crew, eds., pp. 261–270 (American Geophysical Union, Washington D.C., 1986).

[44] Lysak, R. L. and C. T. Dum, Dynamics of magnetosphere-ionosphere coupling including turbulent transport, J. Geophys. Res., 88, pp. 365–380 (1983).

[45] Mead, G. D. and D. H. Fairfield, A quantitative magnetospheric model derived from spacecraft magnetometer data, J. Geophys. Res., 80, pp. 523–??? (1975).

[46] Mei, Y., R. M. Thorne, and R. B. Horne, Ion-cyclotron waves at Jupiter: possibility of detection by Ulysses, Geophys. Res. Lett., 19, pp. 629–623 (1992).

[47] Moore, T. E., D. L. Gallagher, J. L. Horwitz, and R. H. Comfort, MHD wave breaking in the outer plasmasphere, Geophys. Res. Lett., **14**, pp. 1007–1010 (1987).

[48] Olsen, R. C., S. D. Shawhan, D. L. Gallagher, J. L. Green, C. R. Chappell, and R. R. Anderson, Plasma observations at the Earth's magnetic equator, J. Geophys. Res., **92**, pp. 2385–2407 (1987).

[49] Oscarsson, T. and Mats André, Waves with frequencies below the proton gyrofrequency in a multicomponent plasma, Annales Geophysicae, **4**, pp. 319–326 (1986).

[50] Perraut, S., R. Gendrin, A. Roux, and C. de Villedary, Ion cyclotron waves: direct comparison between ground-based measurements and observations in the source region, J. Geophys. Res., **89**, pp. 195–202 (1984).

[51] Perraut, S., A. Roux, P. Robert, R. Gendrin, J. Sauvaud, J. Bosqued, G. Kremser, and A. Korth, A Systematic study of ULF waves above F_{H^+} from GEOS 1 and 2 measurements and their relationships with proton ring distributions, J. Geophys. Res., **87**, pp. 6219–6236 (1982).

[52] Press, W. H., B. P. Flannery, S. A. Teukolsky, and W. T. Vetterling, *Numerical Recipes* (Cambridge University Press, 1986), 818 pp., Ch. 15.

[53] Rauch, J. L. and A. Roux, Ray tracing of ULF waves in a multicomponent magnetospheric plasma: consequences for the generation mechanism of ion cyclotron waves, J. Geophys. Res., **87**, pp. 8191–8198 (1982).

[54] Retterer, John M., Tom Chang, G. B. Crew, J. R. Jasperse, and J. D. Winning-ham, Monte Carlo modeling of ionospheric oxygen acceleration by cyclotron resonance with broadband electromagnetic turbulence, Phys. Rev. Lett., **59**, pp. 148–151 (1987).

[55] Retterer, John M., Tom Chang, and J. R. Jasperse, Ion acceleration in the suprauroral region: A Monte Carlo model, Geophys. Rev. Lett., **10**, pp. 583–586 (1983).

[56] Retterer, John M., Tom Chang, and J. R. Jasperse, Ion acceleration by lower hybrid waves in the suprauroral region, J. Geophys. Res., **91**, pp. 1609–1618 (1986).

[57] Roux, A., S. Perraut, J. L. Rauch, C. de Villedary, G. Kremser, A. Korth, and D. T. Young, Wave-particle interactions near Ω_{He^+} observed on GEOS 1 and 2 2. generation of ion cyclotron waves and heating of He^+ ions, J. Geophys. Res., **87**, pp. 8174–8190 (1982).

[58] Rönnmark, K., "WHAMP—waves in homogeneous, anisotropic multicomponent plasmas," Rep 179, Kiruna Geophys. Inst., Umeå, Sweden (1982).

[59] Rönnmark, K., Computation of the dielectric tensor of a Maxwellian plasma, Plasma Phys., **25**, pp. 699–701 (1983).

[60] Rönnmark, K. and M. André, Convection of ion cyclotron waves to ion-heating regions, J. Geophys. Res., **10**, pp. 17,573–17,579 (1991).

[61] Sagdeev, R. Z. and A. A. Galeev, *Nonlinear Plasma Theory* (W. A. Benjamin, New York, 1969), pp. 54–55.

[62] Seyler, C. E., A mathematical model of the structure and evolution of small-scale discrete auroral arcs, J. Geophys. Res., **95**, pp. 17199–17215 (1990).

[63] Sibeck, D. G., R. W. McEntire, A. T. Y. Lui, R. E. Lopez, and S. M. Krimigis, Magnetic field drift shell splitting: cause of unusual dayside particle pitch angle distributions during storms and substorms, J. Geophys. Res., **92**, pp. 13,485–13,497 (1987).

[64] Smith, J. and J. C. Whitson, "A numerical study of the system of differential equations for the drift wave in tokomaks," Technical Report, Oak Ridge National Laboratory, Oak Ridge, TN (1978).

[65] Smith, R. L. and N. M. Brice, Propagation in multi-component plasmas, J. Geophys. Res., **69**, pp. 5029–5040 (1964).

[66] Stix, T. H., *The Theory of Plasma Waves* (McGraw-Hill, New York, 1962), §§2.5, 3.5.

[67] Strangeway, R. J. and S. M. Kaye , Quiet time mass composition at near-geosynchronous altitudes, J. Geophys. Res., **91**, p. 7105 (1986).

[68] Swanson, D. G., *Plasma Waves* (Academic Press, 1989), 669 pp., Ch. 6.

[69] Temerin, M. and I. Roth , Ion heating by waves with frequencies below the ion gyrofrequency, Geophys. Res. Lett., **13**, pp. 1109–1112 (1986).

[70] Weinberg, S., Eikonal method in magnetohydrodynamics, Phys. Rev., **126**, pp. 1899–1909 (1962).

[71] Winglee, R. M., M. Ashour-Abdalla, and R. D. Sydora, Heating of Ionospheric O^+ ions by shear Alfvèn waves, J. Geophys. Res., **92**, pp. 5911–5919 (1987).

[72] Young, D. T., S. Perraut, A. Roux, C. de Villedary, R. Gendrin, A. Korth, G. Kremser, and D. Jones, Wave-particle interactions near Ω_{He^+} observed on GEOS 1 and 2 1. propagation of ion cyclotron waves in He^+-rich plasma, J. Geophys. Res., **86**, pp. 6755–6772 (1981).

APPENDIX A

TUNNELING FOR A LARGE "GAP"

I. Approximation of a Large Gap

The differential equation

$$\Psi'' + M\Psi = 0 \tag{A.1}$$

where

$$M \equiv \begin{bmatrix} r - \dfrac{\kappa^2}{2} & \dfrac{\kappa^2}{2} \\ \dfrac{\kappa^2}{2} & l - \dfrac{\kappa^2}{2} \end{bmatrix} \tag{A.2}$$

determines wave propagation in a cold plasma. Near the oxygen gyrofrequency, it is reasonable expand the functions r and l in a Laurent series. The function, r, then takes the form

$$r = r_0 + r_1 z + \cdots \tag{A.3}$$

and the function, l, which exhibits a pole near the gyroresonance is of the form

$$l = l_{-1} z^{-1} + l_0 + l_1 z + \cdots \tag{A.4}$$

The upper component, ψ, of equation (A.1) then satisfies the equation

$$\varepsilon^4 \psi'''' - (\kappa^2 - r - l)\varepsilon^2 \psi'' + (rl - \kappa^2/2(r+l))\psi + 2\varepsilon r' \varepsilon \psi' + \varepsilon^2 r'' \psi = 0 \tag{A.5}$$

In light of the WKB approximation, the last two terms are asymptotically small and need not be considered in the asymptotic regime. The last two terms are also well behaved near the resonance where they remain small. Near the resonance, the differential equation is dominated by the behavior of l. A consideration of dominant balance yields the four linearly independent solutions. The first two terms balance to give

$$\varepsilon^2\psi'''' + \frac{l_{-1}}{z}\psi'' = 0 \tag{A.6}$$

The solutions to this equation are Hankel functions and contain the characteristics of the decaying exponentials in the "gap" region while exhibiting sinusoidal behavior below the resonance. That is

$$\psi'' \approx \alpha z^{1/2} H_1^{(1)}(2\sqrt{\mu z}) + \beta z^{1/2} H_1^{(2)}(2\sqrt{\mu z}) \tag{A.7}$$

where $\mu = l/\varepsilon^2$, and ψ is obtained by quadrature. These two solutions represent the ion-cyclotron branch near the origin in that this branch is "cut-off" above the resonance but propagates below which is the asymptotic behavior that the Hankel functions and the integrals of the Hankel function exhibit. The dominant balance of the second and third terms yields a second differential equation

$$\varepsilon^2\psi'' + (r_0 - \kappa^2/2)\psi = 0 \tag{A.8}$$

which provide the other two linearly independent solutions

$$\psi \approx e^{\pm i(r_0 - \kappa^2/2)z/\varepsilon} \tag{A.9}$$

These waves approximate the downcoming magnetosonic branch near the origin. Indeed, this is the first term in the WKB expansion for the magnetosonic branch near the origin. The behavior of the lower component, ϕ, may be determined from the upper component of equation (A.1)

$$\phi = -\frac{2}{\kappa^2}(\epsilon^2\psi'' + (r - \kappa^2/2)\psi) \tag{A.10}$$

Near the origin the leading behavior of ϕ is dominated by the behavior of the Hankel function solutions. If we substitute the solutions obtained for ψ into the above equation, we find that the magnetosonic like solutions are of first order in z vanishing at the origin. The leading behavior of ϕ is then dominated by the Hankel functions $H_1^{(1)}$ and $H_1^{(2)}$ and their integrals which are well behaved.

The asymptotic form of the Hankel function solutions is such that they describe the ion-cyclotron wave. In the limit of a large gap, the amplitude of the decaying exponential in the gap is vanishingly small. The further requirement requirement that no upgoing ion-cyclotron wave be found below the resonance (consistent with the boundary conditions for our solutions) specifies that the coefficients of the Hankel function solutions vanish. Because the other two solutions also vanish at the origin (they are of order z) we find that the energy loss Δ which is proportional to $\phi\phi^*|_z = 0$ must also vanish.

In the following sections, we will assume that as in chapter 5, the differential equation has the solutions

$$\Theta_+^{\pm} = e^{\pm i\,(n_+ z - \beta_+ \log z /2)/\varepsilon}$$
$$\Theta_-^{\pm} = e^{\pm i\,(n_- z - \beta_- \log z /2)/\varepsilon} \tag{A.11}$$

where the factors $n_{\pm}$ and $\beta_{\pm}$ have been defined in chapter 5. Along the negative real

axis the solution is of the form

$$\psi = A\,\Theta_+^- + B\,\Theta_-^- + C\,\Theta_-^+ + D\,\Theta_+^+ \tag{A.12}$$

The solution undergoes a Stokes phenomena so that the solution found on the positive

real axis is of the form

$$\psi = A\,\Theta_+^- + (B-AS_1)\Theta_-^- + (C-AS_2-BS_3)\Theta_-^+$$
$$+(D-AS_4-BS_5-CS_6)\Theta_+^+ \tag{A.13}$$

We may then proceed to calculate the appropriate Stokes constants for the case of a

large energy gap using the information that $\Delta = 0$ if the ion cyclotron wave is not

found below the coupling region. In the following sections we will make use of the

conserved quantity

$$J = i\,(\psi\psi^{*\prime} + \phi\phi^{*\prime} - \psi^*\psi^\prime - \phi^*\phi^\prime) \tag{A.14}$$

In the asymptotic regime along the negative real axis, the quantity J is of the form

$$f_+|A|^2 e^{-\eta_+} + f_-|B|^2 e^{-\eta_-} - f_-|C|^2 e^{\eta_-} - f_+|D|^2 e^{\eta_+} \tag{A.15}$$

while along the positive real axis, the solutions are of the form

$$f_+|A|^2 + f_-|B+S_1A|^2 - f_-|C+S_2A+S_3B|^2 -$$
$$f_+|D+S_4A+S_5B+S_6C|^2 \tag{A.16}$$

where the constants $f_{\pm}$ are factors which relate the lower and upper components, ψ

and ϕ, of the differential equation (A.1)

$$f_\pm = n_\pm \left[1+ \left[\frac{2}{\kappa^2}(n_\pm^2-r+\kappa^2/2) \right]^2 \right]$$

(A.17)

and

$$\eta_\pm = \pi\beta_\pm$$

(A.18)

is related to the change of the argument of the logarithm. In all subsequent sections, we shall assume that the factor η_+ is very large corresponding to a large "gap." This being the case, we shall assume that J is constant along the real axis.

II. Incident Magnetosonic Wave

For an incident magnetosonic wave, we may determine the coefficients from four initial conditions. The boundary conditions for downgoing magnetosonic waves are

$$A = 0 \ , \ B = 1 \ , \ C = 0 \ , \ D = 0$$

(A.19)

For which we find

$$J = \begin{cases} f_- - f_- |S_3|^2 - f_+ |S_5|^2 & Arg(z)=0 \\ f_- e^{-\eta_-} & Arg(z)=\pi \end{cases}$$

(A.20)

The ratios of these terms correspond to the coefficients. Thus

$$T_{MS} = e^{-\eta_-} \ , \ R_{MS} = |S_3|^2 \ , \ C_{MS}^R = \frac{f_+}{f_-}|S_5|^2$$

(A.21)

In order to determine the actual values of the Stokes constants we must consider three

other initial conditions.

$$A = 0 \quad , \quad B = 0 \quad , \quad C = 1 \quad , \quad D = 0 \tag{A.22}$$

for which

$$J = \begin{cases} -f_- - f_+ |S_6|^2 & Arg(z)=0 \\ -f_- e^{\eta_-} & Arg(z)=\pi \end{cases} \tag{A.23}$$

$$A = 0 \quad , \quad B = 1 \quad , \quad C = -S_3 \quad , \quad D = 0 \tag{A.24}$$

for which

$$J = \begin{cases} f_- - 4f_- |S_3|^2 - f_+ |S_5 - S_3 S_6|^2 & Arg(z)=0 \\ f_- e^{-\eta_-} - f_- |S_3|^2 e^{\eta_-} & Arg(z)=\pi \end{cases} \tag{A.25}$$

and

$$A = 0 \quad , \quad B = S_6 \quad , \quad C = S_5 \quad , \quad D = 0 \tag{A.26}$$

for which

$$J = \begin{cases} f_- |S_6|^2 - f_- |S_5 - S_3 S_6|^2 - 4f_+ |S_5|^2 |S_6|^2 & Arg(z)=0 \\ f_- |S_6|^2 e^{-\eta_-} - f_- |S_5|^2 e^{\eta_-} & Arg(z)=\pi \end{cases} \tag{A.27}$$

We may equate the coefficients on the positive and negative real axis in each case in which case we obtain four equations for four unknowns. Then after substantial algebra, we determine

$$|S_6|^2 = \frac{f_-}{f_+}(e^{\eta_-}-1)$$

$$|S_5|^2 = \frac{f_-}{f_+}e^{-\eta_-}(e^{-\eta_-}-1) \tag{A.28}$$

$$|S_3|^2 = (e^{-\eta_-}-1)^2$$

so that

$$T_{MS} = e^{-\eta_-} \quad , \quad R_{MS} = (1-e^{-\eta_-})^2 \quad , \quad C_{MS}^R = e^{-\eta_-}(1-e^{-\eta_-}) \tag{A.29}$$

III. Incident Ion-Cyclotron Wave

For the case of an incident ion-cyclotron wave, substantial more work is required. The boundary conditions for downgoing magnetosonic waves are

$$A = 1 \quad , \quad B = S_1 \quad , \quad C = 0 \quad , \quad D = 0 \tag{A.30}$$

for which we find

$$J = \begin{cases} f_+ - f_-|S_2 + S_1 S_3|^2 - f_+|S_4 + S_1 S_5|^2 & Arg(z)=0 \\ f_-|S_1|^2 e^{-\eta_-} & Arg(z)=\pi \end{cases} \tag{A.31}$$

where it is to be noted that we have ignored the term with the factor $e^{-\eta_+}$ along the negative real axis in that it is exponentially small. We may then identify the coefficients to be the ratios of the downgoing fluxes to the incident flux

$$C_{IC}^T = \frac{f_-}{f_+}|S_1|^2 e^{-\eta_-} \quad , \quad C_{IC}^R = \frac{f_-}{f_+}|S_2 + S_1 S_3|^2 \quad , \quad R_{IC} = |S_4 + S_1 S_5|^2 \tag{A.32}$$

It is possible to determine a relationship between the remaining Stokes constants, $|S_1|$,

$|S_2|$, and $|S_4|$ from three initial conditions

$$A = 1 \quad , \quad B = 0 \quad , \quad C = -S_2 \quad , \quad D = 0 \qquad (A.33)$$

for which we find

$$J = \begin{cases} f_+ + f_- |S_1|^2 - 4f_- |S_2|^2 - f_+ |S_4 - S_2 S_6|^2 & Arg\,(z) = 0 \\ -f_- |S_2|^2 e^{\eta-} & Arg\,(z) = \pi \end{cases} \qquad (A.34)$$

$$A = S_6 \quad , \quad B = 0 \quad , \quad C = S_4 \quad , \quad D = 0 \qquad (A.35)$$

for which we find

$$J = \begin{cases} f_+ |S_6|^2 + f_- |S_1|^2 |S_6|^2 - f_- |S_4 - S_2 S_6|^2 - 4f_+ |S_4|^2 |S_6|^2 & Arg\,(z) = 0 \\ -f_- |S_4|^2 e^{\eta-} & Arg\,(z) = \pi \end{cases} \qquad (A.36)$$

and

$$A = 1 \quad , \quad B = 0 \quad , \quad C = 0 \quad , \quad D = 0 \qquad (A.37)$$

for which we find

$$J = \begin{cases} f_+ + f_- |S_1|^2 - f_- |S_2|^2 - f_+ |S_4|^2 & Arg\,(z) = 0 \\ 0 & Arg\,(z) = \pi \end{cases} \qquad (A.38)$$

Equating the fluxes on both sides of the real axis, it is possible to determine the relationships

$$|S_2|^2 = \frac{f_+}{f_-}(e^{\eta_-}-1)|S_4|^2$$

$$|S_1|^2 = \frac{f_+}{f_-}(e^{\eta_-}|S_4|^2-1) \tag{A.39}$$

In order to make further progress, let us consider the case

$$A = 1 \quad , \quad B = S_1 \quad , \quad C = S_2+S_1S_3 \quad , \quad D = 0 \tag{A.40}$$

for which we find

$$J = \begin{cases} f_+-f_+|\chi|^2 & Arg(z)=0 \\ f_-|S_1|^2 e^{-\eta_-}-f_-|S_2+S_1S_3|^2 e^{\eta_-} & Arg(z)=\pi \end{cases} \tag{A.41}$$

where we have defined $\chi = S_4+S_1S_5+(S_2+S_1S_3)$. To extract the value of χ, we may

consider the case with $D = \chi$ and the preceding initial conditions with $A=1$, $B=S_1$,

and $C=S_2+S_1S_3$. Because Θ_+^- is maximally subdominant in the lower half plane we

may, in fact, determine the value of the solution at $Argz = -\pi$. The coefficient of the

maximally subdominant solution must remain unchanged in the absence of any of the

more dominant solutions so that we may determine

$$J = \begin{cases} f_+ & Arg(z)=0 \\ f_+e^{\eta_+} & Arg(z)=-\pi \\ f_+e^{-\eta_+}+f_-|S_1|^2 e^{-\eta_-} & Arg(z)=\pi \\ -f_-|S_2+S_1S_3|^2 e^{\eta_-}-f_+|\chi|^2 e^{\eta_+} & \end{cases} \tag{A.42}$$

where we have explicitly kept the dependence of η_+. Moreover, we realize that for

this situation Δ rather than vanishing takes a large value. For the case of non-zero Δ

the conservation law yields

$$\Delta = f_+(e^{\eta_+}-1) = f_+(1-e^{-\eta_+}+|\chi|^2 e^{\eta_+})+f_-(|S_2+S_1S_3|^2 e^{\eta_-}-|S_1|^2 e^{-\eta_-}) \quad \text{(A.43)}$$

In the limit of large η_+, we realize that the Stokes constants which appear in the equation are finite so that

$$|\chi|^2 = 1 \quad \text{(A.44)}$$

Then, we determine from equation (A.41) that

$$|S_2+S_1S_3|^2 = |S_1|^2 e^{-2\eta_-} \quad \text{(A.45)}$$

Finally, let us consider the two boundary conditions

$$A = S_5 \ , \ B = -S_4 \ , \ C = 0 \ , \ D = 0 \quad \text{(A.46)}$$

for which we find

$$J = \begin{cases} f_+|S_5|^2+f_-|S_4+S_1S_5|^2-f_-|S_2S_5-S_3S_4|^2 & Arg\,(z)=0 \\ f_-|S_4|^2 e^{-\eta_-} & Arg\,(z)=\pi \end{cases} \quad \text{(A.47)}$$

and

$$A = S_3 \ , \ B = -S_2 \ , \ C = 0 \ , \ D = 0 \quad \text{(A.48)}$$

for which we find

$$J = \begin{cases} f_+|S_3|^2+f_-|S_2+S_1S_3|^2-f_+|S_2S_5-S_3S_4|^2 & Arg\,(z)=0 \\ f_-|S_2|^2 e^{-\eta_-} & Arg\,(z)=\pi \end{cases} \quad \text{(A.49)}$$

These two equations may be combined to yield an equation relating $|S_2|$, $|S_4|$, $|S_3|$, $|S_5|$, $|S_2 + S_1 S_3|$, and $|S_4 + S_1 S_5|$. The coefficients $|S_3|$ and $|S_5|$ are known. The coefficients $|S_2|$, and $|S_2 + S_1 S_3|$ may be eliminated in favor of $|S_1|$. Then the above equation along with the physical equation (A.30) is sufficient to specify the coefficients. We find that

$$|S_1|^2 = |S_2|^2 = \frac{f_+}{f_-}(e^{\eta_-}-1)$$

$$|S_4|^2 = 1$$

$$|S_2+S_1S_3|^2 = \frac{f_+}{f_-}e^{-\eta_-}(1-e^{-\eta_-}) \qquad\qquad (A.50)$$

$$|S_4+S_1S_5|^2 = e^{-2\eta_-}$$

The coefficients may be immediately determined from equation (A.32)

$$C_{IC}^T = 1-e^{-\eta_-} \quad , \quad R_{IC} = e^{-2\eta_-} \quad , \quad C_{IC}^R = e^{-\eta_-}(1-e^{-\eta_-}) \qquad (A.51)$$

The physical interpretation of these results is discussed in chapter 5.

APPENDIX B

ADJUSTMENT OF STOKES MULTIPLIERS

I. Integral Equation

We consider the system of differential equations

$$\varepsilon^2 \psi'' + (r - \frac{\kappa^2}{2})\psi + \frac{\kappa^2}{2}\phi = 0$$

$$\varepsilon^2 \phi'' + (l - \frac{\kappa^2}{2})\phi + \frac{\kappa^2}{2}\psi = 0$$

(B.1)

Under the assumption that the reduced Stix functions take the well approximated form

$$r = k_r^2 \ , \quad l = k_l^2(1 - a/z)$$

we may cast the solutions into the form of an integral equation. Taking the Fourier transform of the equations (B.1), we find

$$-\varepsilon^2 k^2 \tilde{\psi} + (k_r^2 - \frac{\kappa^2}{2})\tilde{\psi} + \frac{\kappa^2}{2}\tilde{\phi} = 0$$

(B.2)

and

$$-\varepsilon^2 k^2 \tilde{\phi} + (k_l^2 - \frac{\kappa^2}{2})\tilde{\phi} + \frac{\kappa^2}{2}\tilde{\psi} = -ik_l^2 a \int \tilde{\phi} \, dk$$

(B.3)

where we have defined the Fourier transform of a function, f, to be $\tilde{f}$. We have assumed that the inverse transform

$$f = \int_C \tilde{f} \, e^{ikz} dk \tag{B.4}$$

is taken along a contour, C, which is either a closed contour or a contour for which the integrand vanishes at the endpoints.

The first equation (B.2) implies an algebraic relationship between $\tilde{\psi}$ and $\tilde{\phi}$, namely

$$\tilde{\psi} = \frac{\kappa^2}{2(k^2 - (k_r^2 - \kappa^2/2))} \tilde{\phi} \tag{B.5}$$

whereas the second equation (B.3) is a first order differential equation

$$\frac{dI}{dk} = -iak_l^2 \frac{k_r^2 - (k_r^2 - \kappa^2/2)}{(k+n_+^0)(k-n_+^0)(k+n_-^0)(k-n_-^0)} I \tag{B.6}$$

for the function $I = \int \tilde{\phi} \, dk$, and the functions $n_{\pm}^0$ are defined in (7.95). The first order differential equation for I is trivially solved by quadrature. From the derivative of I we find that

$$\tilde{\phi} = \frac{\kappa^2}{2(k+n_+^0)^{1+i\beta_+}(k-n_+^0)^{1-i\beta_+}(k+n_-^0)^{1+i\beta_-}(k-n_-^0)^{1-i\beta_-}} \tag{B.7}$$

where $\beta_{\pm}$ is defined in (7.98). The solution ϕ then takes the form

$$\phi = \frac{\kappa^2}{2} \int dk \, \frac{e^{ikz}}{(k+n_+^0)^{1+i\beta_+}(k-n_+^0)^{1-i\beta_+}(k+n_-^0)^{1+i\beta_-}(k-n_-^0)^{1-i\beta_-}} \tag{B.8}$$

and the contour is such that the integrand vanishes at the endpoints.

II. Relation of Asymptotic Behavior to Stokes Adjustment

Asymptotically, the branch points, $\pm n_\pm^0$, which appear in the integrand of equation (B.8) are related to the four WKB solutions. That is, the asymptotic expansion of a contour which encircles one of the branch points yields one of the WKB solutions which behaves as $\exp(\pm i n_\pm^0 z)$. The asymptotic expansion of the integral is found for a particular value of z by deforming the contour of integration to follow the path of steepest descent which has endpoints along the ray $\arg k = \dfrac{\pi}{2} - \arg z$ ensuring maximum convergence at large $|k|$. Paths which encircle each individual branch point correspond to one of the four linearly independent solutions. The paths of steepest descent descend from a branch point k_0 along the line, $\arg(k-k_0) = \dfrac{\pi}{2} - \arg z$. The branch points, $\pm n_+^0$, correspond to the waves $e^{\pm i n_+^0 z}$ whereas the branch points, $\pm n_-^0$, correspond to the waves $e^{\pm i n_-^0 z}$. If all four branch points are real then the asymptotic expansion of the integral corresponds to upgoing (downgoing) waves. On the other hand, if two of the branch points are imaginary, the branch points, $\pm n_+^0$, correspond to upward (downward) propagating waves along the real axis, and the imaginary branch points, $\pm n_-^0$, correspond to exponentially decaying (growing) solutions along the positive real axis.

In order to continue a solution from one value of $\arg z$ to another, the path must be continuously deformed such that endpoints remain along the path of steepest descent. From the topology of the branch points we find that as a contour is continuously deformed across the line which connects two branch points an additional contribution

Appendix B

to the asymptotic behavior of the more subdominant solution is obtained as in the example discussed in equation (7.119). To see this behavior, consider the the illustration of Figures B.1 and B.2. In this figure we indicate the manner in which a contour is deformed as the argument of z passes across a Stokes line. The contour to the left of the negative imaginary axis encircles only the upper, n_-^0, branch point descending the valley to the left of the branch point $-n_-^0$. The branch cut for the branch point n_-^0 is taken to lie between the two segments of the contour so that the path remains on the same Riemann sheet. The two segments of the contour differ in that along the ascend-
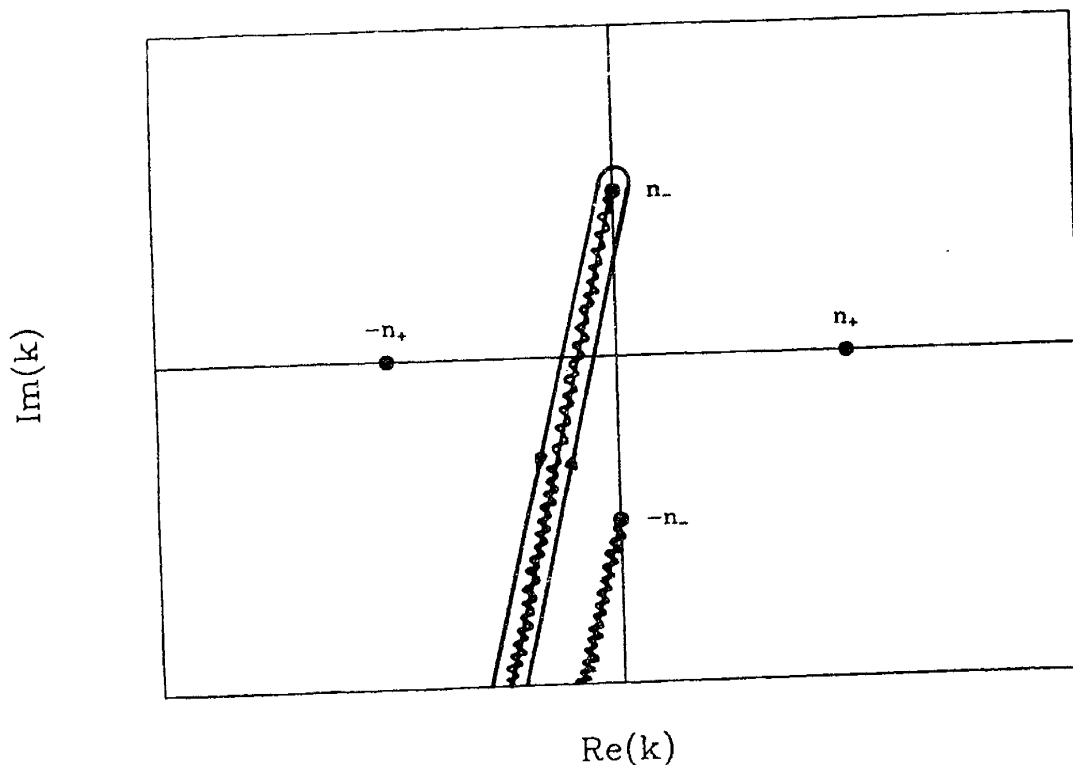
Figure B.1. A solution asymptotic to $\exp(in_+^0 z)$ is obtained from a contour which encircles the pole n_+^0. For $-\pi < \arg z < -3\pi/2$, the path of steepest descents follows a valley between the branch points $-n_+^0$ and $-n_-^0$ following the ray $\arg (k - n_+^0) = \pi/2 - \arg z$ as shown. The branch cut has been chosen to be along the path of steepest descent.

Re(k)
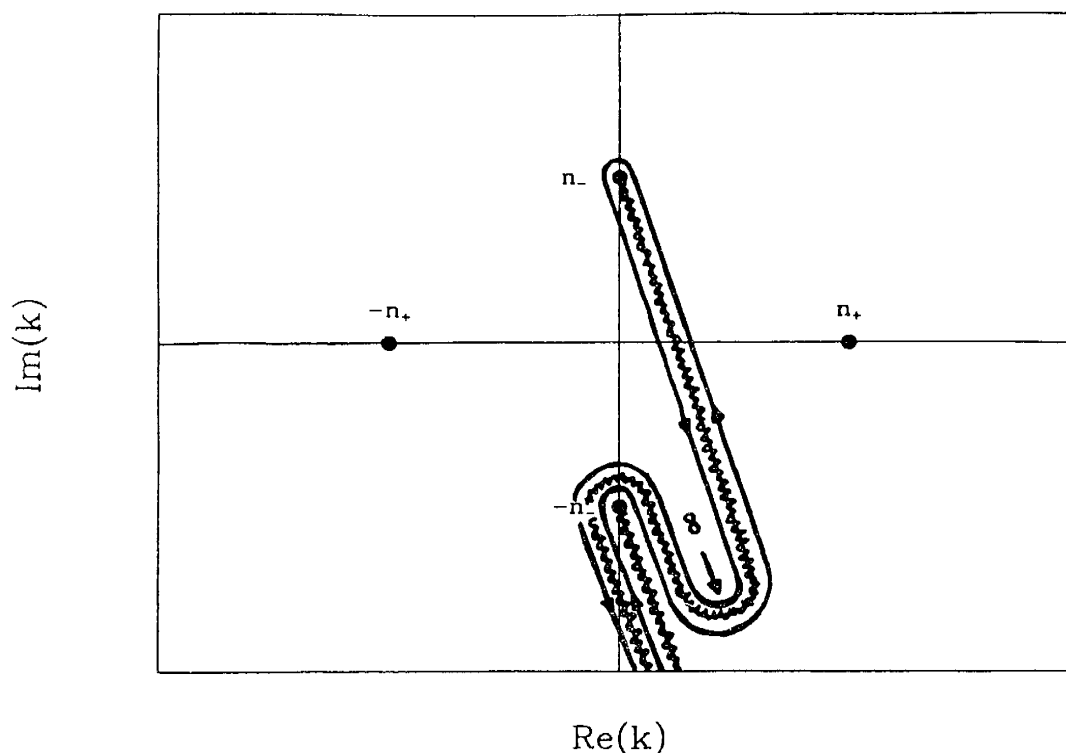
Figure B.2. As the solution is continued across arg $z = \pi$, the path of steepest descent now lies in a valley between the branch points $-n_+^0$ and n_-^0. However, the path must remain on the same Riemann sheet so that the branch point, $-n_+^0$, is now encircled as well. The path of steepest descent from $-n_+^0$ follows the ray arg $(k + n_+^0) = \pi/2 - $ arg z parallel to the path of steepest descent from n_+^0 as shown. Thus as the solution is continued across the ray, arg $z = \pi$, the coefficient of the subdominant solution changes discontinuously by a factor proportional to the amplitude of the dominant solution with branch point n_+^0.

ing and descending segments arg$(k - n_-^0)$ differs by 2π. As arg z passes through the Stokes line, the valley of steepest descent lies to the right of the imaginary axis and thus to the right of the branch point $-n_-^0$ rather than on the left as before. However, the topology of the branch points with respect to the contour must not change as the contour is continuously deformed. That is, the contours must remain on the same Riemann sheet, i.e. the branch cut cannot be deformed through the branch point at $-n_-^0$. Hence the contour wraps around the lower branch point at $-n_-^0$ and descends

along the path of steepest descent from there. Then in addition to the asymptotic expansion about the branch point at n_-^0, we find that upon traversing the Stokes line the coefficient of the subdominant solution undergoes an abrupt change proportional to the coefficient of the maximally dominant solution. Likewise, along the anti-Stokes lines, similar adjustments occur between the two dominant solutions and two subdominant solutions. Similar arguments apply to the case with four real values for $\pm n_\pm^0$ although in that case, all adjustments occur along the Stokes lines.

For the case of four real values of $n_\pm^0$ all branch points lie on the real axis. Then the lines which connect any two solutions are $\arg k = n\pi$. The discontinuous adjustments in the Stokes constants occur along the lines $\arg z = (n+1/2)\pi$, that is, along the Stokes lines.

On the other hand, for the case of two purely real and two purely imaginary roots, the discontinuous adjustments occur along the real axis ($\arg k = n\pi$) for interaction between $+n_+^0$ and $-n_+^0$ or along the imaginary axis ($\arg k = (n+1/2)\pi$) for interaction between $+n_-^0$ and $-n_-^0$. The mixed interactions between $\pm n_+^0$ and $\pm n_-^0$ occur along the lines $\arg k = \pm\tan^{-1}(n_-/n_+)+n\pi$. The Stokes adjustment between the asymptotic solutions represented by n_+^0 and $-n_+^0$ should be added to the subdominant solution along the lines $\arg z = (n+1/2)\pi$ i.e. along the Stokes line for which the WKB solution is maximally subdominant. Similarly, the adjustment between the asymptotic solutions represented by n_-^0 and $-n_-^0$ should be added along the lines $\arg z = n\pi$. That is, along the Stokes lines where one of the WKB solutions is maximally subdominant. The discontinuous adjustment between the asymptotic solutions represented by $\pm n_+$

and $\pm n_-$ occurs along the rays $\arg k = \pm\tan^{-1}(n_+^0/n_-^0) + n\pi$. That is, along the lines $n_+^0 x = \pm n_-^0 y$ ($z = x + iy$) which we have already identified as the anti-Stokes lines in equation (7.118).

In all cases adjustments between the maximally dominant solution and the maximally subdominant solution occurs along the Stokes lines. Along the anti-Stokes lines, one of the solutions asymptotic to $sxp(\pm n_+^0)$ and one of the solutions asymptotic to $\exp(\pm n_-^0)$ are equally dominant while the other two are equally subdominant. Along these lines a Stokes adjustment occurs between the two dominant solutions and the two subdominant solutions where the adjustment mixes the two modes represented by n_+^0 and n_-^0. The Stokes adjustments therefore only occur within or on the border of the region of maximum subdominance.

In Figure B.3 we illustrate the Stokes adjustment to a solution continued from the positive real axis to the negative real axis. The solution may be expressed in terms of the WKB solutions, $\Theta_\pm^\pm$, from equation (7.97). Along the positive real axis the solution is

$$\psi = A\,\Theta_+^- + B\,\Theta_-^- + C\,\Theta_-^+ + D\,\Theta_+^+ \ , \quad \text{Region IV} \tag{B.9}$$

as the anti-Stokes line is crossed into Region III, the coefficients of the two equally subdominant solutions, Θ_+^+ and Θ_-^+ change discontinuously so that in Region III

$$\psi = A'\Theta_+^- + B'\Theta_-^- + C'\Theta_-^+ + D'\Theta_+^+ \ , \quad \text{Region IV} \tag{B.10}$$
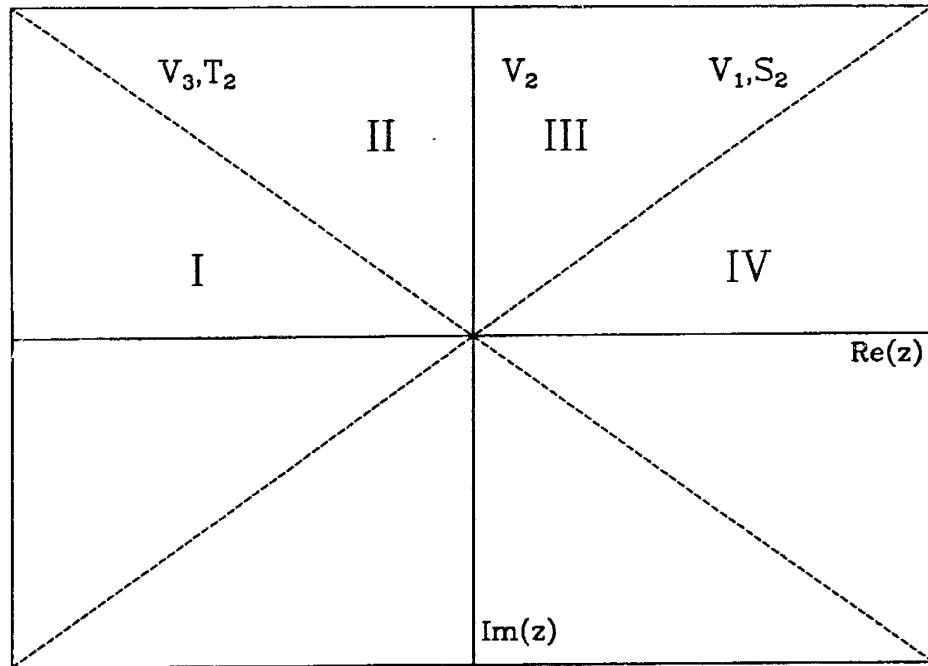
with

Figure B.3. Sectors of the complex plane. The WKB solutions are continued from Region IV along the positive real axis to region I along the negative real axis. Stokes lines are indicated in solid while the anti-Stokes lines are dashed.

$$D'=D+BV_2$$
$$C'=C+AS_1$$

(B.11)

Across the stokes line, the WKB solution, Θ_+^+, is maximally subdominant and its coefficient changes abruptly by an amount proportional to coefficient of the maximally dominant solution, Θ_+^-. In region II, the solution becomes

$$\psi = A\,\Theta_+^- + B\,\Theta_-^- + C'\,\Theta_-^+ + D''\,\Theta_+^+ \quad , \text{ Region II}$$

(B.12)

with

$$D'' = D' + AV_1$$

(B.13)

Across the next anti-Stokes line, the two subdominant solutions again undergo a

discontinuous change so that in Region I the solution is of the form

$$\psi = A\,'\Theta_+^-+B\,\Theta_-^-+C\,'\Theta_-^++D\,'''\Theta_+^+ \quad , \quad \text{Region I} \tag{B.14}$$

with

$$
\begin{aligned}
D\,''' &= D\,''+C\,'V_3 = D+AV_1+BV_2+C\,'V_3 \\
A\,' &= A+BT_2
\end{aligned}
\tag{B.15}
$$

At this point, we can note that if we were to continue the solution into the rest of the

plane, the coefficient of Θ_+^+ would not change. Hence, the Stokes phenomena may be

simply represented by a discontinuous adjustment in the coefficient of the maximally

subdominant solution in the region of maximum subdominance. Outside the region of

maximal subdominance, the coefficient of that WKB solution remains unaltered.

ACKNOWLEDGEMENTS

I want to express my deepest gratitude for the continuous academic and financial assistance provided by my advisor, Tom Chang, over the past 5 years. I also want to express my appreciation for the assistance of Geoff Crew in preparing this manuscript, particularly with respect to the obscure intricacies of *troff*. I also want to express my gratitude for his careful and critical reading of the manuscript which substantially improved the presentation of material.

The Center for Theoretical Geoplasma Research has been an excellent environment in which to explore exciting new areas of research. I have enjoyed the interactions that I have had with Fareed Yaseen, John Retterer, Peter Yoon, Sunny Tam, Chris Dum and a variety of other visiting scientists and graduate students. One of these visiting scientists, Jim Dungey, suggested the possibility that equatorially generated Pc waves might be a possible source for the waves associated with ion conics.

I want to particularly express my appreciation to John and Candy Hess with whom I have spent many days hiking, skiing, ice climbing, canoeing, and birdwatching in Vermont and the Adirondaks. Their continued interest in my work has been a continual source of inspiration, and their friendship has always been available whenever I have needed it.

I also want to express my deep gratitude to my parents for the desire for learning and understanding that they instilled in me as a child and their encouragement for me to pursue my dreams.